YAŞAR UNIVERSITY

GRADUATE SCHOOL

PHD THESIS

DESIGN AND ANALYSIS OF AN OPTIMAL DAY-AHEAD ENERGY MANAGEMENT SYSTEM BASED ON PV GENERATION AND BESS UNDER DISTRIBUTION GRID CONSTRAINTS

SEZAİ POLAT

THESIS ADVISOR: ASSIST. PROF. DR. HACER ŞEKERCİ

ELECTRICAL AND ELECTRONICS ENGINEERING

BORNOVA / İZMİR
August 2024

JURY APPROVAL PAGE

We certify that, as the jury, we have read this thesis and that in our opinion it is fully adequate, in scope and in quality, as a thesis for the degree of the Doctor of Philosophy.

Jury Members:	**Signature:**
Asst. Prof. (PhD) Hacer ŞEKERCİ Yaşar University	.....
Asst. Prof. (PhD) Erhan DEMİROK İzmir Katip Çelebi University	.....
Asst. Prof. (PhD) Emrah BIYIK Yaşar University	.....
Prof. (PhD) Müslüm Cengiz TAPLAMACIOĞLU Gazi University	.....
Asst. Prof. (PhD) Emin Selahattin UMDU Yaşar University	.....

Prof. (PhD) Yücel ÖZTÜRKOĞLU
Director of the Graduate School

ABSTRACT

DESIGN AND ANALYSIS OF AN OPTIMAL DAY-AHEAD ENERGY MANAGEMENT SYSTEM BASED ON PV GENERATION AND BESS UNDER DISTRIBUTION GRID CONSTRAINTS

POLAT, Sezai

PhD, Electrical and Electronics Engineering

Advisor: Assist. Prof. Dr. Hacer ŞEKERCİ

August 2024

The growing demand for energy has led to a surge in the utilization of renewable energy sources (RES). However, the intermittent nature of these renewable resources often results in challenges in maintaining a consistent energy supply. One of the key solutions to address these difficulties is the integration of battery energy storage system into the electrical grid. Recent technological advancements have significantly enhanced the capacity and cost-effectiveness of BESS, making them an increasingly viable option for both residential and grid-scale applications. These battery storage systems can provide various benefits to the electrical grid, such as voltage support, power support, and energy shifting. Nonetheless, optimizing the efficiency and reliability of the RES and BESS, while maximizing energy usage and ensuring a consistent energy supply, can be achieved through the implementation of an effective control strategy. The concept of an energy management system (EMS) has emerged as a viable approach for the technically feasible and cost-effective operation of grid-connected RES and BESS. An EMS can optimize the utilization of intermittent RES, forecast and manage energy storage, control loads, and plan the deployment of optimal resources by minimizing operating costs in a microgrid or distribution system with a structure that can provide technical criteria. With a day-ahead EMS, RES in the distribution system, system constraints, energy purchase and sale costs, and the aging costs of system equipment are all taken into consideration, and the system plans the most appropriate operational strategy.

This dissertation presents an optimization model for a grid-connected photovoltaic (PV) system and BESS aimed at minimizing operating costs under a dynamic

electricity price tariff. The model incorporates the reactive power support capabilities of the integrated inverters, utilizing a current-limiting approach rather than power limiting for power and energy balance calculations. This non-linear optimization problem also considers the previously neglected inverter losses and aging costs. Additionally, the dissertation introduces a dynamic thermal model for the distribution transformer at the grid connection point, enabling the transformer to operate at its rated power in accordance with industry standards. The resulting optimization model for a distribution network with PV and BESS allow the transformer to operate above full load, and various analyses were conducted using a day-ahead energy management system model. The advanced EMS model provides reactive power support through the current-limiting approach, accounts for inverter losses, and enables the system components to operate at their rated power due to the dynamic thermal model. The findings indicate that inverter losses are substantial and cannot be ignored, contributing to increased costs, and that the distribution transformer can safely operate with a lower capacity rating for short time period.

Keywords:

Day ahead energy management, inverter capability, reactive power capability, dynamic thermal model, transformer, load flow, load modelling

ÖZ

DAĞITIM ŞEBEKESİ KISITLAMALARI ALTINDA PV ÜRETİMİ VE BESS DAYALI OPTİMUM GÜN ÖNCESİ ENERJİ YÖNETİM SİSTEMİNİN TASARIMI VE ANALİZİ

POLAT, Sezai
Doktora Tezi, Elektrik ve Elektronik Mühendisliği
Danışman: Dr. Öğr. Üyesi Hacer Şekerci
Ağustos 2024

Artan enerji ihtiyacını karşılamak amacıyla, yenilebilir enerjinin kullanımı gün geçtikçe artmaktadır. Ancak yenilenebilir enerji kaynaklarının doğası kesintili olmasından dolayı, enerji temininde zorluklar meydana gelir. Bu zorlukları azaltmak için önde gelen çözümlerden biri, enerji depolama sistemlerinin elektrik şebekesine entegre edilmesidir. Son teknolojik gelişmeler, pil depolama sistemlerinin kapasitesinde önemli bir artışa ve maliyetlerinde düşüş sağlamış, böylece hem konut hem de şebeke ölçekli uygulamalar için giderek daha avantajlı bir çözüm haline gelmiştir. Batarya depolama sistemleri gerilim desteği, güç desteği ve enerji kaydırması dahil olmak üzere elektrik şebekesi için çeşitli faydalar sunabilmektedir. Ancak yenilebilir enerji kaynağı ve enerji depolama sisteminin etkinliği ve güvenilirliği, enerji kullanımını en üst düzeye çıkarmak ve tutarlı enerji tedarikini sağlamak iyi bir kontrol stratejisine ile mümkündür. Şebekeye bağlı yenilebilir enerji kaynağı ve batarya enerji depolama sistemlerini teknik olarak uygun ve düşük maliyetli çalıştırılması için enerji yönetim sistemi (EYS) kavramı ortaya çıkmıştır. Bir EYS, kesintili olan yenilebilir kaynakları optimize edebilir, tahmin edebilir, enerji depolamayı yönetebilir, yükleri kontrol edebilir, teknik kriterlerin sağlayabilir bir yapı ile bir mikro şebeke veya dağıtım sistemindeki işletme maliyetlerini en aza indirerek optimum kaynakları planlayabilir. Gün öncesi EYS ile dağıtım sistemindeki enerji kaynakları, sistem kısıtları ve enerji alış ve satış maliyetleri, sistem ekipmanlarının yaşlanma maliyetlerini göz önüne alarak, sistemin en uygun şekilde çalışmasını planlar.

Bu tezde, şebekeye bağlı bir dağıtım sistemine entegre fotovoltaik (FV) ve batarya depolama sisteminin (BDS), saatlik değişen elektrik fiyat tarifesi ile en düşük maliyetli çalışmasını amaçlayan bir optimizasyon modeli oluşturulmuştur. Bu model oluşturulurken gerçek sisteme yakın bir modelleme için, FV ve BDS ine entegre invertörlerin reaktif güç desteklerinden faydalanılmış, yeni bir bakış açısı ile, güç sınırı yerine akım sınırlayıcı bir yaklaşımla güç ve enerji dengesi hesaplamaları yapılarak, lineer olmayan bir optimizasyon problemi haline dönüştürülerek çözülmüştür. Ayrıca bir çok çalışmada göz ardı edilen, inverlerin kayıpları ve yaşlanma maliyetleri modele dahil edilmiştir. Bu tez kapmasında yapılan bir diğer bir yenilik ise, bir dağıtım sisteminin şebekeye bağlantı noktasındaki dağıtım transformatörünün, standartlarda verilen yükleme kılavuzları doğrulsunda anma gücü üzerinde çalıştırılabilmesi için gerekli dinamik termal model oluştulmuştur. Bu sayede dağıtım tranformatörü tam yükün üstünde bir yükle çalışmasına imkan sağlayan, FV ve BDS içeren bir dağıtım şebekesi için bir optimizasyon modeli oluşturularak, gün öncesi EYS modeli ile çeşitli analizler yapılmıştır. Sonuç olarak, içerisinde FV ve BDS olan bunlara entegre invertelerin akım sınırlama yaklaşımı ile reaktif güç desteği sağlayan, inverter kayıplarının göz önünde bulunurulduğu, dinamik termal model sayesinde anma gücü üzerinde çalışmasına imkan sağlayan gelişmiş bir EYS modeli oluşurularak çeşitli analizler gerçekleştirilmiştir. Böylece akım sınırlama yaklaşımı ile daha gerçekçi model sayesinde, inverter kayıplarının göz ardı edilmeyecek kadar yüksek ve maliyet artışına sebep olduğu, şebeke bağlantı noktasındaki dağıtım transformatörünün daha düşük güçlü seçilse bile kısa süreli de olsa güvenli bir şekilde çalışabileceği gözlenmiştir.

Anahtar Kelimeler: Gün öncesi enerji yönetimi, invertör kapasitesi, reaktif güç destek, dinamik termal model, trafo, transformatör, yük akışı, yük modelleme

ACKNOWLEDGEMENTS

I would like to extend my deepest gratitude to Dr. Hacer ŞEKERCİ for her exceptional guidance and mentorship throughout the course of this thesis. Her insightful advice, unwavering support, and invaluable feedback have been crucial in shaping the direction and quality of my work. She has been a constant source of encouragement and inspiration, always willing to share her knowledge and expertise. I am truly thankful for the time and effort she has dedicated to helping me succeed.

I would like to express my sincere gratitude to Dr. Emrah BIYIK, who has served as an invaluable guide and mentor throughout this dissertation. His insightful advice, encouragement, and constant support have been instrumental in shaping the direction of this study. He has always been available to provide guidance, offer constructive feedback, and inspire me to push the boundaries of my research. I am deeply appreciative of the time and effort he has dedicated to helping me succeed. Thank you for being a crucial part of this dissertation.

I would like to thank my thesis committee members, Dr. Erhan DEMİROK and Dr. Abdül BALIKÇI, for their useful suggestions and comments throughout my study.

I would also like to thank Prof. Dr. Müslüm Cengiz TAPLAMACIOĞLU and Dr. Emin Selahaddin UMDU for their interest in and time spent examining my thesis and for being part of my thesis jury.

I would like to extend my heartfelt thanks to my PhD companion, Irmak ÖNAL KORKUT, for her unwavering support and friendship throughout this journey.

My warm and sincere thanks go to my dear parents for their endless support and constant encouragement throughout my life. I would also like to extend my deepest gratitude to my mother-in-law for her unwavering support throughout this journey.

Finally, I would like to express my deepest gratitude to beloved wife Bengi and my dear son Tardu Eymen for their incredible patience and unwavering support

throughout this dissertation. Their love, understanding, and encouragement have been my greatest sources of strength, helping me persevere through the challenges of this process. I am truly thankful for their sacrifices and for always being there for me. Without their support, the completion of this thesis would not have been possible. Therefore, I am grateful for the opportunity to dedicate this thesis to them.

Sezai POLAT

İzmir, 2024

TEXT OF OATH

I declare and honestly confirm that my study, titled "DESIGN AND ANALYSIS OF AN OPTIMAL DAY-AHEAD ENERGY MANAGEMENT SYSTEM BASED ON PV GENERATION AND BESS UNDER DISTRIBUTION GRID CONSTRAINTS" and presented as a PhD Thesis, has been written without applying any assistance inconsistent with scientific ethics and traditions. I declare, to the best of my knowledge and belief, that all content and ideas drawn directly or indirectly from external sources are indicated in the text and listed in the list of references.

Sezai POLAT

27.08.2024

TABLE OF CONTENTS

LIST OF FIGURES

LIST OF TABLES

SYMBOLS AND ABBREVIATIONS

SYMBOLS:

i, j	: Bus indices
t	: Time
Z_i	: Impedance of branch *i*
$V_{(i),(t)}$	: Voltage magnitude of bus *i*, time *t*
$I_{(i),(t)}$	: Current magnitude of branch *i*, time *t*
$S_{(i),(t)}$	: Apparent power at bus *i*, time *t*
$P_{(i),(t)}$	: Active power at bus *i*, time t
$Q_{(i),(t)}$	: Reactive power at bus *i*, time *t*
Z_p, I_p, P_p	: ZIP Load modelling active power coefficients
$Z_{q,}\ I_q, P_q$	: ZIP Load modelling reactive power coefficients
α	: Active power exponent in voltage dependent load model
β	: Reactive power exponent in voltage dependent load model
V^{min}	: Lower operation voltage limit
V^{max}	: Upper operation voltage limit
B	: Vector of branch current B = $[B_{12}\ B_{23}\ B_{34}\ldots]'$
$P_{pv(t)}$	: Power generated by the PV system at time *t*
η_{Pv}	: Efficiency of the PV system

N_{Pv}	: Number of PV panel
W_{module}	: Module power of PV system
G	: Solar irradiation
T_{cell}	: The cell temperature of a PV panel
T_a	: Ambiente temperature
$P_{pv,real}$	: The panel output power
$P_{pv,STC}$	: The panel power at standard test conditions
η_{cell}	: Efficiency of the PV panel
$SoC_{(t)}^{BESS}$	: Battery state of charge at time *t*
η_{BC}, η_{BD}	: The charge and discharge efficiency of the BESS
$P_{(t)}^{BC}, P_{(t)}^{BD}$	: The charging and discharging power of BESS at time *t*
Δt	: Time interval
SoC_{min}, SoC_{max}	: The lower and upper limits of the SoC
$Q_{(t)}^{BC}, Q_{(t)}^{BD}$	: Reactive charging (absorbing), discharging (injecting) power of BESS at time *t*
S_{BESS}^{Rated}	: Apparent power of BESS
$C_{(t)}^{Q,LR}$	: Inverter lifetime reduction at time *t*
$C_{(t)}^{Q,invloss}$	: Inverter loss at time *t*
$Q_{(t)}^{Inverter}$	: Inverter reactive power at time *t*

$P_{(t)}^{Invloss}$	: Active power losses due to the reactive power at time *t*
c_{self}, c_v, c_R	: The power loss in the inverter coefficients
$\eta^{LR,0}, \eta^{LR,1}, \eta^{LR,2}, \eta^{LR,3}$	: Reduction in Inverter lifetime coefficients
$\theta_{h(t)}$	: The hot-spot temperature at time *t*
$\theta_{a(t)}$	: The temperature of the surrounding environment in transformer at time *t*
$\Delta\theta_{o(t)}$	: The increase in temperature of the oil at the top of the transformer at time *t*
$\Delta\theta_{ho(t)}$	: The hot-spot to top-oil gradient at time *t*
K	: The per unit loading factor
R	: The ratio of load losses at rated current to no-load losses
x	: The oil exponent
$\Delta\theta_{or}$	: The top-oil temperature rise in steady state at rated losses
k_{11}, k_{21}, k_{22}	: Thermal model constant of transfomer
τ_0	: Oil time constant
θ_0	: The top-oil temperature
y	: The winding exponent
$\Delta\theta_{hr}$	: The hot-spot-to-top-oil gradient at rated current
τ_w	: Winding time constant

D	: The variable difference operator
Re, Im	: Denotes the real and imaginary part of a complex-value
$I^{Load}_{Apparent(i),(t)}$	: Phasor current flowing along the line *i*, time *t*
$I_{Active(i),(t)}, I_{Real(i),(t)}$	: Real component of the current flowing along line *i*, time *t*
$I_{Reactive(i),(t)}, I_{Imaginary(i),(t)}$	: Imaginary component of the current flowing along line *i*, time *t*
$N^{Transformer}_{Ratio}$	: Transformer current ratio
$I^{Discharge}_{p(i),(t)}, I^{Charge}_{p(i),(t)}$	: Real component of the BESS discharge and charge current flowing along line *i*, time *t*
$I^{Inject}_{q(i),(t)}, I^{Absorb}_{q(i),(t)}$	: Imaginary component of the BESS inject and absorb current flowing along line *i*, time
θ_I, θ_V	: Phasor angle of Current and Voltage
$P^{Charge}_{BESS(i),(t)}, P^{Discharge}_{BESS(i),(t)}$	: The BESS charge and discharge power at bus *i*, time *t*
$Q^{Inject}_{BESS(i),(t)}, Q^{Absorb}_{BESS(i),(t)}$	: The BESS inject and absorb power at bus *i*, time *t*
$I^{Available}_{p(i),(t)}, I^{Curtail}_{p(i),(t)}$	: Real component of the PV available and curtail current flowing along line *i*, time *t*
$P_{PV(i),(t)}$	: The active power output of the PV system at bus *i*, time *t*
$Q_{PV(i),(t)}$	: The reactive power of the PV system at bus *i*, time *t*

$Q_{PV(i),(t)}^{Inject}, Q_{PV(i),(t)}^{Absorb}$	:The PV inject and absorb power at bus *i*, time *t*
$P_{PV(i),(t)}^{Net}, P_{PV(i),(t)}^{Curtail}$	: The active net output and curtail power of the PV system at bus *i*, time *t*
$P_{Inverter\ Loss(t)}^{BESS}, P_{Inverter\ Loss(t)}^{PV}$	: BESS and PV inverter active power losses at time *t*
$I_{invloss(t)}$	: Current due to BESS and PV inverter active power losses at time *t*
C_{Grid}^{Cost}	: Grid operational costs
$C_{BESS}^{DegraCost}$	: BESS degragation cost
$C_{BESS}^{Inverter\ Cost}, C_{PV}^{Inverter\ Cost}$	: BESS and PV inverter degragation cost
$C_{reactive\ power}^{Penalty\ Cost}$	: Reactive power penaly cost
$P_{(t)}^{GB}, P_{(t)}^{GS}$	: Active power bought from grid and power sold to grid at time *t*
$\lambda_{(t)}^{pp}, \lambda_{(t)}^{SP}$	: Buying and selling price electricity from to grid at time *t*
$P_{(t)}^{BC}, P_{(t)}^{BD}$	: The charged and discharged power of BESS at time *t*
β_{CC}, β_{DC}	: The charged and discharged degradation cost of BESS
a_1, a_2	: Fitting parameters for reactive power penalty function
K_{BESS}	: Number of BESS to be installed in the system
M_{PV}	: Number of PV system to be installed in the system

$TOT_{(t)}$: Top of the oil in transformer at time *t*

$HST_{(t)}$: Hot spot temperature in transformer at time *t*

$PUL_{(t)}$: Per unit loading of transformer at time *t*

ABBREVIATIONS:

AC-OPF	: Alternative Current Optimal Power Flow
BCBV	: Branch Current to Bus Voltage
BESS	: Battery Energy Storage System
BIBC	: Bus Incidence to Branch Current
CLM	: Classical Load Model
DBFS	: Direct Backward/Forward Sweep
DC	: Direct Current
DC-OPF	: Direct Current Optimal Power Flow
DLF	:Distribution Load Flow
DN	: Distribution Network
DSO	: Distribution System Operator
DTR	: Dynamic Thermal Rating
ELM	: Exponential Load Model
EMS	: Energy Management System
EPDK	: Energy Market Regulatory Authority
FIT	: Feed-in Tariff
HST	: Hot Spot Temperature
IEC	: International Electrotechnical Commission
IEEE	: The Institute of Electrical and Electronics Engineers
LCOE	: Levelized Cost of Electricity

LR : Lifetime Reduction

LV : Low Voltage

MILP : Mixed Integer Linear Programming

NLP : Nonlinear Programming

NOCT : Nominal Operating Cell Temperature

PCC : Point of Common Coupling

PFC : Power Flow Calculation

PUL : Per Unit Loading

PV : Photovoltaic

RDS : Radial Distribution System

RES : Renewable Energy Sources

SoC : State of Charge

STC : Standard Test Conditions

STR : Static Thermal Ratings

TOT : Top Oil Temperature

VV : Volt-VAR

ZIP : Impedance (Z), Current (I), Power (P)

1. CHAPTER: INTRODUCTION

1.1. Background

The increasing need for electricity generation, driven by a rising global population, has resulted in the overuse of fossil fuels in recent years (Liu et al., 2024). The use of fossil fuels for energy has detrimental environmental consequences, including ozone layer depletion and a rise in greenhouse gas emissions, posing a significant threat to the earth (J. Wang et al., 2024). This environmental impact has driven a worldwide transition towards lessening dependence on fossil fuels and migrating to renewable energy alternatives. Despite the cost-effective and environmentally friendly profile of renewable energy sources, their integration presents technical challenges due to the intermittent nature of their energy supply (Kiss et al., 2024). To address these challenges and ensure the efficient utilization of renewable energy, numerous methods and recommendations have been proposed, often involving the implementation of advanced system equipment (Notton et al., 2018). A leading solution for mitigating the challenges posed by the intermittent nature of renewable energy is the integration of energy storage systems into the power grid. Advances in technology have enabled a substantial growth in the storage capabilities of battery systems, coupled with a consistent reduction in their associated costs(Hu et al., 2022). These advancements make battery energy storage system (BESS) an increasingly attractive solution for both residential and grid-scale applications. The implementation of BESS offers a range of application opportunities within the power grid, including voltage support, power support, and energy shifting (Zhao et al., 2023).

The effectiveness and reliability of an energy storage system depend heavily on its control strategy, which is crucial for maximizing energy utilization and ensuring consistent energy supply. Developing a control strategy for BESS is inherently complex due to the unpredictable nature of renewable energy sources and the need to meet multiple objectives simultaneously. The implementation of an optimal control approach can substantially improve the performance and cost-efficiency of the entire

power system. When considering how BESS utilize energy, two primary management concepts arise. The first is rule-based energy management, which relies on straightforward logical or mathematical operations. This can involve calculating the remaining charge or initiating actions when the battery's charge level reaches a predetermined threshold (Ghorashi Khalil Abadi et al., 2021). The second concept is model-predictive energy management, which centers around optimization techniques. This approach focuses on determining the ideal trajectory for set point values by utilizing a defined objective function and a future-looking time window (Hartel et al., 2023).

Integrating BESS into distribution systems, along with renewable energy sources like photovoltaic systems, offers significant benefits in terms of reducing energy costs. However, while photovoltaic (PV) integration can lower expenses, it can also introduce technical challenges related to power quality. These challenges encompass reversed power flow, voltage fluctuations, and heightened power losses (Katiraei et al., 2011).

To address these challenges and ensure the cost-effective utilization of BESS while mitigating the issues associated with PV integration, the concept of an energy management system has emerged.

It's clear that expanding the scope of an Energy Management System (EMS) is key to unlocking its full potential in managing microgrids and small-scale distribution systems. An EMS can optimize, estimate intermittent resources, manage energy storage, control loads, and plan optimal resources to minimize operating costs, environmental pollution, and violations of technical criteria in a microgrid or distribution system (Fresia et al., 2024; Rafique et al., 2018)

Optimal power flow techniques employed in EMS can help minimize the primary issue of line losses in distribution networks operating at medium or low voltage levels.

The energy management system's effectiveness can be enhanced by accurately modeling and rapidly resolving the load flow problem associated with day-ahead energy scheduling.

Load flow analysis is employed to determine the voltage magnitudes of loads or buses connected to renewable energy sources in the distribution network, guaranteeing that the system remains within permissible voltage boundaries.

The primary determinant of bus voltage is the level of active power production or consumption. However, reactive power is another key factor. Accordingly, providing reactive power support at the bus can mitigate losses, enhance bus voltage profiles, and regulate voltage deviations (Wagle et al., 2024).

Power converters employed to integrate PV systems and BESS into the electricity grid have the ability to support reactive power. Inverters capable of providing reactive power compensation can mitigate losses in power distribution networks by reducing the reactive power drawn from the grid (Javid et al., 2024).

Its other capability is to absorb reactive power and prevent excessive voltage from occurring due to high RES penetration. This method helps avoid energy curtailment in renewable energy systems, which can result in increased economic benefits, in order to prevent voltage iraised caused by excessive generation (Fresia et al., 2024).

The transformer capacity at the grid interconnection or point of common coupling is one of the key factors that limits demand load or renewable energy generation within a distribution network (Javid et al., 2024).

The maximum demand load or generated energy must not surpass the transformer's rated power capacity. Nonetheless, transformers can operate temporarily beyond their nameplate rating (Z. Li et al., 2024). Owing to the transformer's capacity to function above its rated power, it is feasible not only to avoid curtailing the energy output of the RES, but also to install a lower-capacity transformer. The guidance provided in transformer loading manuals suggests how transformers can operate beyond their standard power limits.

1.2. Literature Review

The day-ahead EMS is a real and complex challenge that must be addressed from various objective function viewpoints and grid constraints. The academic literature extensively examines active power optimization within EMS, with a particular emphasis on minimizing costs through the application of diverse programming methodologies (Elsir et al., 2024; Nair et al., 2024; Tan et al., 2024; Q. Wang et al.,

2024). Researchers have utilized optimization techniques to simulate EMS in numerous studies for various objectives, such as minimizing pollutant emissions (Alavi et al., 2015; Kanchev et al., 2014; M. S. Taha et al., 2018) enhancing voltage profile stability (Chen et al., 2015), improving system reliability, and reducing outage duration.

The existing literature demonstrates that in a simple microgrid structure, daily energy costs can be minimized through day-ahead energy management systems that optimize only the battery energy storage system (Raghavan et al., 2020). However, other studies have explored the use of both photovoltaic systems and battery energy storage in simple microgrids, which are then optimized as a whole (Silva et al., 2020). A mixed-integer linear programming approach was employed by the authors to schedule BESS operations (Talluri et al., 2021).

EMS in simple distribution network configurations often do not account for power flow calculations. However, in buildings with installed RES system, it becomes necessary to analyze the effects of power flowing from the load to the grid through power flow analysis. Additionally, calculating the energy losses in distribution lines is crucial, and efforts should be made to minimize these losses.

Analyses of EMS that consider distribution line losses have been advancing to enable more realistic optimization models. Load flow calculations should be performed to determine line losses and bus voltage levels.

The authors evaluated three distinct approaches for calculating charge flow: direct current optimal power flow (DC-OPF), alternating current optimal power flow (AC-OPF) and a linearized AC-OPF model in (Soleimani et al., 2022).

In (Rigo-Mariani et al., 2022), the disflow method was used in the distribution system load flow calculation. This disflow method can be linearized for ease of calculation, which simplifies the complexity of the load flow analysis and enables faster computational performance.

Similarly, in (Z. Wang et al., 2015), the linearized load flow method was utilized in the distribution system load flow calculation. A backward/forward sweep algorithm for load flow calculation in the distribution network for EMS was proposed in (Chen et al., 2015).

A method derived from the backward/forward sweep algorithm distribution load flow (DLF) technique, which uses the Bus Incidence to Branch Current (BIBC) and Branch Current to Bus Voltage (BCBV) matrices (Ragab et al., 2023). Various test systems, such as the IEEE 9-bus in (J. Zhang et al., 2016), IEEE 30-bus (Surender Reddy et al., 2016), 33-bus in (Vardhan et al., 2022) and 69-bus in (Ahmed et al., 2022) distribution test systems, as well as the CIGRE medium voltage distribution network in (Chenier et al., 2024), are utilized to calculate load flow in power networks where EMS are implemented. Load flow calculations typically assume that demand loads maintain a constant power profile, which simplifies the computational requirements. In (Cortés-Caicedo et al., 2022), demand power is assumed that constant power in the load flow calculation, while in (Huaman-Rivera et al., 2024), the demand load is modeled as a voltage-dependent load. The existing literature contains limited empirical investigations examining load flow calculations that utilize voltage-dependent or ZIP load models. In contrast, load flow analyses employing alternative load modeling approaches, rather than the standard constant power assumption, have produced more realistic and precise outcomes.In order to make more accurate calculations closer to real life, more comprehensive modeling is required, especially for inverters used in BESS and PV.

In (Durán et al., 2024; El-Baz et al., 2018; Nair et al., 2024) their studies disregarded reactive power, assuming the PV inverter was capable of supplying only active power. Inverters can generate or consume reactive power, which allows them to offer reactive power support to the electrical distribution system, as illustrated in (Tziovani et al., 2022).

Many studies have examined that PV inverters can only provide active power, but the number of studies focusing on reactive power support capabilities within the EMS is insufficient. This gap in the literature highlights the need for further investigation into the reactive power support provided by PV inverters in EMS applications.

The many studies on inverters used in BESS contains a similar research gap. Many studies have omitted the consideration of reactive power support in their modeling approaches, assuming that BESS could only provide active power support.

The reactive power performance of a BESS integrated inverter is analogous to that of a PV integrated inverter. In contrast, the active power capability of a BESS inverter demonstrates bidirectional operation, similar to its reactive power features.

The existing literature has focused solely on the ability of BESS to provide active power support to the distribution system in Ref. (Akarne et al., 2024; Bahloul et al., 2024; Nguyen Hong et al., 2024; Xiong et al., 2024), while overlooking their potential for reactive power support in (Fresia et al., 2024; Saleem et al., 2024). Additionally, there is a scarcity of studies investigating the reactive power support provided by BESS and PV inverters. Consequently, there is a gap in the understanding of the role of BESS and PV systems in distribution network operations.

When the inverter provides reactive power support, an active power loss occurs. This active power loss depends on the apparent power, which is the vector sum of the active and reactive power supplied by the inverter. The reactive power support provided by the inverter can improve the overall power factor of the system, but it also leads to an active power loss that is proportional to the apparent power. This trade-off between reactive power support and active power loss must be carefully considered when designing and operating the inverter system.

The papers also experimentally demonstrated the active power losses that occur within the inverter in relation to the apparent power the inverter delivers to the electrical grid (Alramlawi, 2020; Braun, 2008; Brito et al., 2022; Gandhi et al., 2016).

These losses can be characterized using a quadratic function that captures the impacts of self-consumption, voltage drops in power semiconductors, and resistive losses in conductors (Gandhi et al., 2016; Grab et al., 2022). The DC capacitor link equipment employed by the inverter to produce reactive power has a finite lifespan, and consequently, this component is subject to deterioration and a reduction in its operational lifetime as a result of usage. In (Gandhi, Rodríguez-Gallegos, Reindl, et al., 2018; Gandhi et al., 2022) the authors have demonstrated that inverters incur a lifetime degradation cost associated with their reactive power generation. In summary, inverters experience degradation costs and consume active power during both operation and idle states due to self consumption.

The inverter loss cost is commonly calculated as the potential revenue lost from not selling the generated energy to the grid, or the cost incurred to purchase additional

energy from the grid to account for the losses (Gandhi, Rodríguez-Gallegos, Zhang, et al., 2018; Gandhi et al., 2019a). In the current literature, there is no research on modeling the effect of inverter power losses as electrical load and considering its effect on the bus voltage. This represents a gap in the current understanding of how inverter losses can affect overall voltage levels in an electrical system.

The distribution transformer is essential equipment within the distribution network. From an EMS perspective, the energy transfer between the distribution network and the grid is restricted by the power rating of the distribution transformer (Soares et al., 2013, 2016; Xu et al., 2023).

Transformers, the essential components of modern electrical power systems, are designed to operate within specific power ratings to ensure reliable and safe performance. However, in certain situations, such as during peak demand or emergency conditions, transformers may be temporarily required to operate at power levels above their rated capacity for short durations to preserve the stability and uninterrupted operation of the power distribution network (Arguence et al., 2020).

Transformers can operate short time at power levels beyond their rated capacity, a capability known as overload capacity. This feature allows power systems to adapt to sudden increases in demand or unexpected contingencies (Zenhom et al., 2024).

In (Daminov, Prokhorov, et al., 2021; Daminov, Rigo-Mariani, et al., 2021; Gamil et al., 2018; Taheri et al., 2012; C. Wang et al., 2016; E. Zhang et al., 2023), the researhers have demonstrated that through the use of dynamic thermal modeling, Transformer operation may be extended beyond the rated power specifications while preserving safe operating parameters, while remaining within the temperature limits specified by international standards IEC and IEEE. This safe operation means the transformers do not incur damage from overheating or accelerate the degradation of their lifespan.

There are many studies in the literature on the operation of transformers at beyond rated power. However, from the perspective of energy management systems (EMS), the literature lacks a comprehensive examination of transformers connected to distribution networks operating beyond their rated power levels.

A day-ahead EMS optimization was conducted through dynamic thermal modeling of a grid-connected power transformer in (Bagheri, 2024). However, this analysis was simulated for a transmission network. There is no study in the literature for day ahead EMS optimization of a transformer integrated into the distribution system.

The relevant literature and research content that define the scope of the dissertation are illustrated in Figure 1.

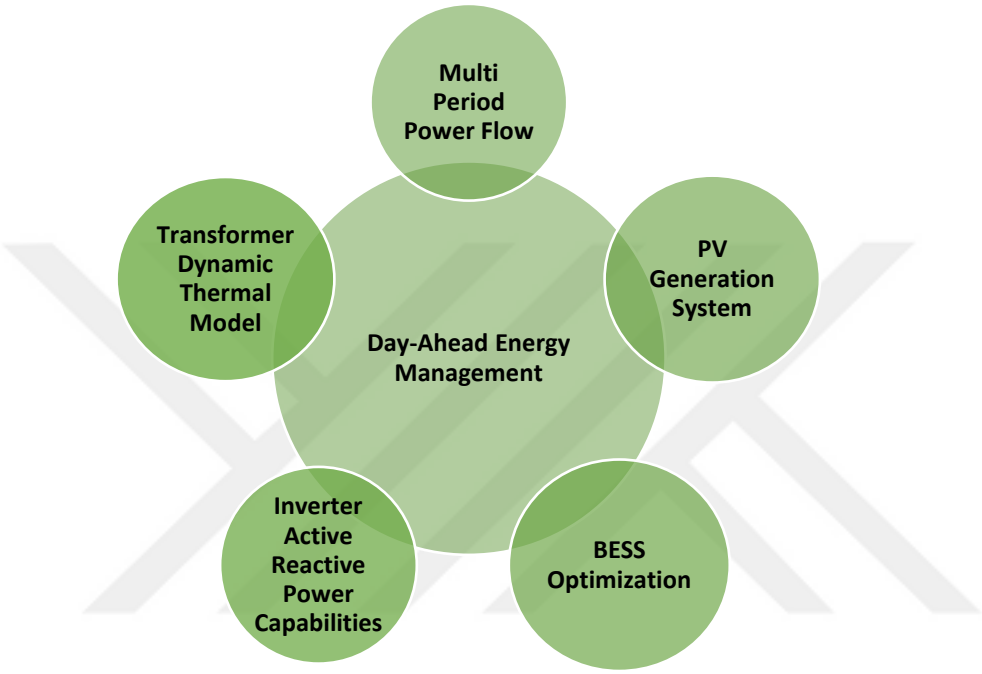

Figure 1. Scope of Dissertation: Literature Survey and Research Context

1.3. Research Gaps

Considering the literature discussed previously, the following gaps need to be filled when discussing on the day ahead EMS:

- Prior research has primarily examined the active power support capabilities of battery energy storage systems and photovoltaic systems within energy management systems for day-ahead operations. However, the inverters employed in BESS and PV systems can also provide reactive power support due to their reactive power capabilities. Therefore, it is necessary to consider the reactive power support of the inverter in the EMS.This aspect has not been thoroughly addressed in the existing literature. Incorporating the reactive power support of BESS and PV inverters can lead to improvements in bus

voltages, reductions in reactive power drawn from the grid, and decreases in PV generation curtailment.

- The literature contains a considerable number of studies that commonly assume the power flow calculation in day-ahead EMS analyses to be constant. Conversely, other load models, such as voltage-dependent and exponential load representations, have been infrequently explored in the literature. Day ahead EMS, voltage-dependent load model study contributes to filling the gap in this field.
- The existing research typically only considers the degradation costs associated with energy storage systems. However, few studies have been found in which the losses and degragation cost of BESS and PV inverters were optimized. In fact, losses are modeled only as energy costs.
- The current modeling approach typically represents losses solely as energy costs, failing to account for the impact of the active power required by inverters on bus voltages, as they effectively function as loads. Consequently, a more accurate modeling strategy would be to represent inverter losses as load, which topic has not been given sufficient attention in the existing literature.
- In studies optimizing BESS and PV inverters, the power limitation is often formulated in active and reactive power parameters However, the true limiting factor is the power semiconductor capacities within the inverters, which are defined by the maximum current. When inverters reach the maximum current specified by the manufacturer, they may be unable to deliver their maximum power output. Applying the maximum current to an inverter can result in power output variations depending on the bus voltage. Therefore, for a more realistic model, it would be more accurate to characterize the capacity limitation of BESS and PV inverters in terms of current rather than power. The existing literature has not adequately covered this particular aspect of EMS optimization.
- Optimizing the EMS for day-ahead operations can mitigate power congestion at the transformer connecting a distribution network to the grid. While previous studies have explored the operation of individual transformers beyond their rated capacity, there has been limited research integrating this approach into a distribution network with day-ahead EMS optimization. These methods can

facilitate the creation of an effective, resilient, and energy-saving EMS model that can adapt to fluctuations in demand, load, and renewable energy sources.

1.4. Specific Contributions

The thesis seeks to address gaps in existing research by developing a day-ahead energy planning model. In contrast to conventional approaches, the proposed model incorporates voltage-dependent load modeling, integrates the reactive power capabilities of BESS and PV inverters, realistically handles inverter power constraints, accounts for the degradation costs of BESS and inverters, models and optimizes inverter losses as loads, and can optimize and operate transformers while considering transformer winding insulation concerns and operation beyond rated power levels.

This thesis outlines the principal contributions provided herein:

- Optimizing day-ahead EMS energy costs through BESS and PV inverter modeling based on current capacities,
- Incorporating active power losses of inverters to enhance optimization in grid operations,
- Modeling inverter losses as load: implications for bus voltage,
- Incorporating the lifetime degradation costs of inverters into day-ahead energy management,
- Investigating the reactive power support provided by inverters: new perspective from the literature,
- Examining the modeling of overloading operations in distribution transformers located at the PCC within distribution network.

1.5. Paper Organisation

Chapter-1 introduces the recent advancements in a distribution network and the EMS perspective on these improvements. It presents applications aimed at reducing energy costs and discusses the existing literature, the research purpose, and the original contributions of the study. Chapter-2 describes the modeling approach used for the equipment in this research, which includes modeling the components of a distribution system and explaining their operation. Chapter-3 presents calculations related to reactive power capabilities, losses, and the lifetime cost of inverters. Chapter-4

showcases the dynamic thermal modeling of a distribution transformer, including a loading guide, and a simulation of the transformer's response to ambient temperature and loading. Chapter-5 provides data, features, and explanations of the calculation methods and concepts used in the modeling. Chapter-6 describes the mathematical model developed to optimize EMS in a distribution network that integrates BESS and PV system, including the specification of the objective function and constraints. Chapter-7 presents the simulation results and analysis. Chapter-8 concludes the dissertation and summarizes the key findings.

2. CHAPTER: MODELLING METHODOLOGY

2.1. Energy Management System

The day ahead energy management system (EMS) can be considered in terms of its various inputs and outputs, as depicted in Figure 2. To effectively manage the microgrid, the day-ahead EMS requires certain input data, which it uses to update its information on an hourly basis. This permits the EMS to render informed decisions and optimize the energy generation, dispatch and distribution within the distribution network.

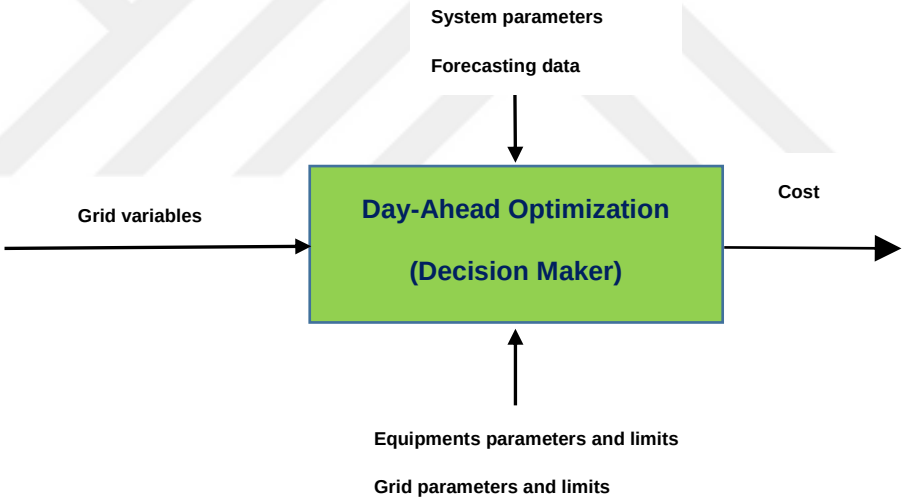

Figure 2. The Input and Output Scheme of Energy Management System

Accurate forecasting data inputs are essential for generating daily predictions of renewable energy source generation and demand profiles, which can be derived from historical data and weather forecasts. The Distribution System Operator (DSO) constraints represent the operational constraints of the distribution network determined through power flow analysis of the distribution network area.

The day-ahead EMS must incorporate distribution network configuration details, mathematical models of all distribution system components, the desired operational conditions, and an optimization methodology.

The input-output framework of the EMS calculates costs and optimizes the system, resulting in a near-optimal solution that determines the operating setup for the day-ahead EMS. This day-ahead EMS framework, as shown in Figure 2, defines the scope of the investigation.

2.2. Microgrid Modelling

2.2.1. Load Models

The distribution system has numerous load models which can generally be categorized into two primary groups: classical load models and voltage-dependent load models. Classical load models postulate a constant power, current, or impedance correlation between the load and the voltage. Conversely, voltage-dependent load models acknowledge the dependence of the load on the voltage magnitude. The mathematical representations for these different load models are provided in the sections below.

2.2.1.1 Classical Load Models (CLM)

This taxonomy of load models encapsulates the Constant Impedance (Z), Constant Current (I) and Constant Power (P) load categories (Satsangi et al., 2017). The mathematical formulations characterizing each of these load categories are presented in detail follow.

Constant Impedance Load (Z): The impedance is initially established through the application of an existing Eq. (1) and subsequently, the load current is calculated through the application of another relevant Eq. (2). It is crucial to note that although the values fluctuate with each iterative step, the impedance value computed by the initial Eq. (1) remains fixed (Satsangi et al., 2017).

$$Z_i = \frac{|V_n|^2}{S_i^*} \qquad \forall i \qquad (1)$$

$$I_{i,Load} = \frac{V_i}{Z_i} \qquad \forall i \qquad (2)$$

Constant Current Load (I): The current magnitude ($|I_{i,Load}|$) is initially calculated using Eq. (3) and is maintained at a steady level. Meanwhile, δ varies with changes in voltage during each iteration. As a result, the final load current angle ($\angle(\delta i - \theta i)$) adjusts according to Eq. (4), thereby maintaining a constant load power factor (Lim et al., 2000).

$$I_{Load(i)} = \left(\frac{S_{(i)}}{V_{(i)}}\right)^{*} \qquad \forall i \qquad (3)$$

$$I_{Load(i)} = \left|I_{Load(i)}\right| \angle(\delta i - \theta i) \qquad \forall i \qquad (4)$$

Constant Power Load (PQ): With the help of Eq. (3), the load current is calculated for a constant apparent power (S_i), where the V_i variable changes in each iteration of the calculation (Satsangi et al., 2017).

2.2.1.2 Voltage Dependent Load Models

Voltage-dependent load models can be classified into two distinct categories: the Exponential Load Model and the Polynomial Load Model, the latter of which is also known as the ZIP (constant impedance, constant current, and constant power) load model. The Exponential Load Model represents the load as an exponential function of the voltage, while the Polynomial Load Model, or ZIP load model, represents the load as a polynomial function of the voltage, with the coefficients corresponding to the constant impedance, constant current, and constant power components of the load. The mathematical representations for these two model types are as follows;

Exponential Load Model (ELM): This type of modeling allows the active power to be obtained using Eq. (5) and reactive power to be obtained using Eq. (6) (Maraaba et al., 2023).

$$P_i = P_0 \left(\frac{V_i}{V_0}\right)^{\alpha} \qquad \forall i \qquad (5)$$

$$Q_i = Q_0 \left(\frac{V_i}{V_0}\right)^{\beta} \qquad \forall i \qquad (6)$$

Table 1 presents examples of various load types paired with their respective coefficients (Zubair Iftikhar et al., 2024).

Table 1. Types of Load and Their Coefficient

Type of Load	α	β
Constant Power	0	0
Industrial	0.18	6
Residential	0.92	4.04
Commercial	1.51	3.4

Polynomial or ZIP Load Model (ZIP): Figure 3 presents a graphical depiction of the ZIP load model (Pacific Northwest National Laboratory et al., 2010).

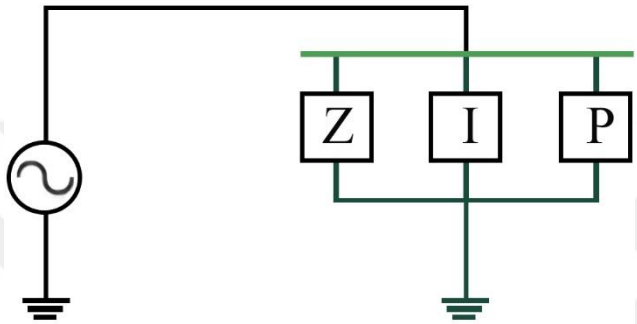

Figure 3. ZIP Load Model

The mathematical definitions of ZIP models are provided in Eq. (7) and Eq. (8) (Manikanta et al., 2024).

$$P_i = P_0 \left[Z_p \left(\frac{V_i}{V_0} \right)^2 + I_p \left(\frac{V_i}{V_0} \right) + P_p \right] \qquad \forall i \qquad (7)$$

$$Q_i = Q_0 \left[Z_q \left(\frac{V_i}{V_0} \right)^2 + I_q \left(\frac{V_i}{V_0} \right) + P_q \right] \qquad \forall i \qquad (8)$$

Equation (7) and (8) are valid provided $Z_p + I_p + P_p = 1$ and $Z_q + I_q + P_q = 1$.

Sample ZIP coefficients for different load characteristics are given in the Table 2 (Diaz-Aguilo et al., 2013).

Table 2. ZIP Coefficient for Different Load Characteristics

Load	Z_p	I_p	P_p	Z_q	I_q	P_q
Large Commercial	0.47	-0.53	1.06	5.3	-8.73	4.43
Small Commercial	0.43	-0.06	0.63	4.06	-6.65	3.59
Residential	0.85	-1.12	1.27	10.96	-18.73	8.77

2.2.2. Distribution Load Flow Method

Load flow analysis represents a key calculation for optimizing distribution systems. However, the high R/X ratio in distribution systems makes it impractical to employ commonly used load flow techniques such as Newton–Raphson, Gauss–Seidel, and Fast-Decoupled methods (Prakash et al., 2011).

It is reported in (Polat et al., 2023) that the recommended technique which distribution load flow (DLF) for analyzing power flow in radial distribution systems is to perform calculations by constructing BIBC and BCBV matrices.

The apparent power at a specific bus i is calculated at a particular time t using the appropriate Eq. (9) in the analysis of the distribution network.

$$S_{(i),(t)} = P_{(i),(t)} + jQ_{(i),(t)} \qquad \forall t, i \quad (9)$$

The active power, $P_{(i),(t)}$, and reactive power, $Q_{(i),(t)}$, at bus i at time t are defined. Given the known apparent power $S_{(i)}$ and voltage magnitude of bus $V_{(i)}$, the corresponding load currents $I_{(i)}$ can be determined by using Eq. (10).

$$I_{(i),(t)} = \left(\frac{S_{(i),(t)}}{V_{(i),(t)}}\right)^* \qquad \forall t, i \quad (10)$$

The 6-bus radial distrubution system (RDS) depicted in Figure 4 is analyzed using the recommended DLF technique, which is applied in the following steps (adapted from (Şeker et al., 2021)).

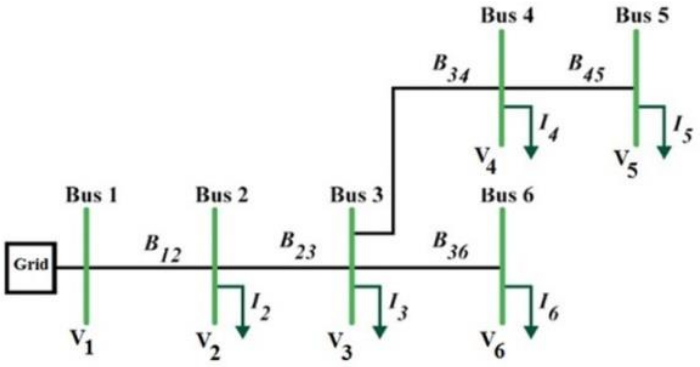

Figure 4. Example of an RDS with Six Buses

The branch currents can be represented in a matrix form, which allows for a compact and organized expression of the current values in the different branches of the bus.

$$\begin{bmatrix} B_{12} \\ B_{23} \\ B_{34} \\ B_{45} \\ B_{36} \end{bmatrix} = \begin{bmatrix} 1 & 1 & 1 & 1 & 1 \\ 0 & 1 & 1 & 1 & 1 \\ 0 & 0 & 1 & 1 & 0 \\ 0 & 0 & 0 & 1 & 0 \\ 0 & 0 & 0 & 0 & 1 \end{bmatrix} . \begin{bmatrix} I_2 \\ I_3 \\ I_4 \\ I_5 \\ I_6 \end{bmatrix} \tag{11}$$

$$[B] = [BIBC\,] . [I] \tag{12}$$

The voltage difference can be derived from the line currents.

$$\begin{bmatrix} V_1 \\ V_1 \\ V_1 \\ V_1 \\ V_1 \end{bmatrix} - \begin{bmatrix} V_2 \\ V_3 \\ V_4 \\ V_5 \\ V_6 \end{bmatrix} = \begin{bmatrix} Z_{12} & 0 & 0 & 0 & 0 \\ Z_{12} & Z_{23} & 0 & 0 & 0 \\ Z_{12} & Z_{23} & Z_{34} & 0 & 0 \\ Z_{12} & Z_{23} & Z_{34} & Z_{45} & 0 \\ Z_{12} & Z_{23} & 0 & 0 & Z_{36} \end{bmatrix} . \begin{bmatrix} B_{12} \\ B_{23} \\ B_{34} \\ B_{45} \\ B_{36} \end{bmatrix} \tag{13}$$

$$[\Delta V] = [BIBC] . [B] \tag{14}$$

$$[\Delta V] = [BCBV] . [BIBC] . [I] \tag{15}$$

$$[\Delta V] = [DLF] . [I] \tag{16}$$

The voltage differences between the primary bus and the remaining buses can be obtained from the DLF matrix, which is composed of the BIBC and BCBV matrices. An iterative process is then used to compute the voltage differences and magnitudes across all buses.

$$[\Delta V^{k+1}] = [DLF].[I^k] \tag{17}$$

$$[V^{k+1}] = V^0 - [\Delta V^{k+1}] \tag{18}$$

The Figure 5 gives the flow chart of power flow calculation (PFC) procedure (Polat et al., 2023).

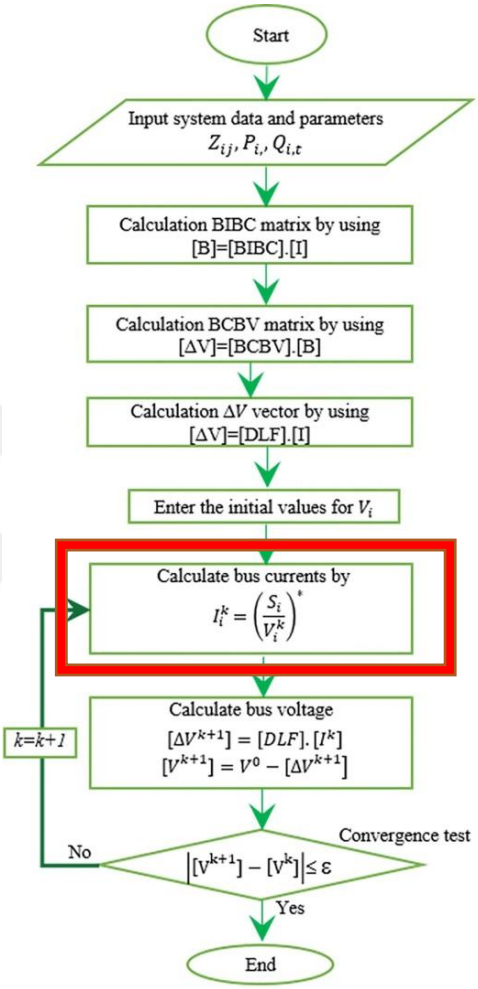

Figure 5. Simplified Flowchart of Power Flow

The recommended PFC approach is assessed utilizing the IEEE 33-bus test system, as depicted in Figure 6 (Baran et al., 1989). The examined system functions at a nominal voltage of 12.66 kV and has a combined load of 3.715 MW and 2.300 MVAr. The information about this test system can be found in (Vita, 2017) and Appendix.

Various power flow analysis techniques have been developed in the literature for radial distribution systems. In (Srinivasa Rao et al., 2011), the authors introduced new Analytical Methods for solving radial distribution networks. Additionally, the

backward-forward sweep approach described by in (Kirthiga et al., 2013) has been used to analyze radial distribution systems. Furthermore, in (Vasquez et al., 2016), the authors proposed a Dynamic Data Matrix technique to compute bus voltages. (Diaz et al., 2016) developed a direct backward/forward sweep (DBFS) approach to calculate power flow in radial networks

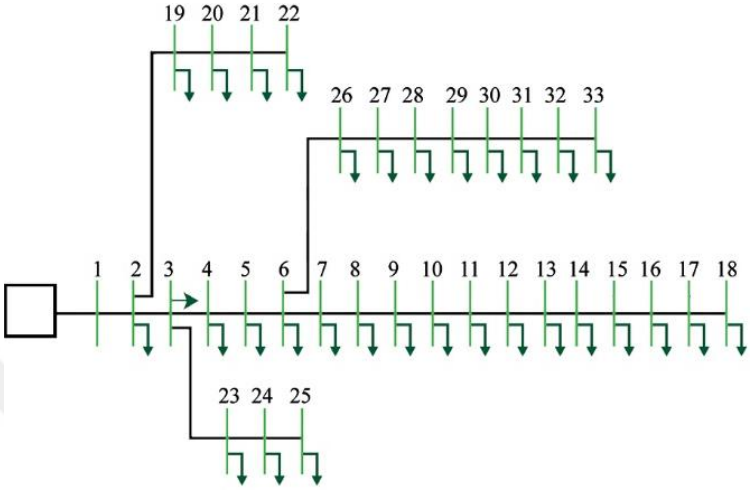

Figure 6. Structure of the IEEE 33 Test System

In Table 3, the power losses computed from the demand load and load flow analyses for the basic IEEE 33 test system are presented.

Table 3. Results of PF Calculation for Base IEEE 33 Bus Test System

	Active Power	**Reactive Power**
Peak Demand Load	3715.00 kW	2300.00 kVAr
Peak Power Loss	202.68 kW	18.90 kVAr
Total Demand Power	3917.68 kW	2318.90 kVAr
Demand Apparent Power	4552.53 kVA	

The comparison of the bus voltages obtained to validate the proposed methodology with the results obtained in the literature is provided in Table 4. The losses are shown in Table 5.

Table 4. Comparison of Bus Voltage Calculations Using the DLF and Other Power Flow Methods for the IEEE 33-Bus Test System

Bus No	DLF method (proposed)		Analytical Method Bus voltages (p.u.) (Srinivasa Rao et al., 2011)	Dynamic Data Matrix Method Bus voltages (p.u.) (Kirthiga et al., 2013)	Direct Backward/Forward Sweep Technique Bus voltages (p.u.)(Vasquez et al., 2016)
	Bus voltages (p.u.)	Bus Angles (degree)			
1	1.0000	0.0000	1.0000	1.0000	1.0000
2	0.9970	0.0145	0.9970	0.9970	0.9970
3	0.9829	0.0960	0.9829	0.9829	0.9829
4	0.9754	0.1617	0.9754	0.9755	0.9754
5	0.9680	0.2283	0.9680	0.9681	0.9679
6	0.9496	0.1339	0.9496	0.9497	0.9494
7	0.9461	- 0.0965	0.9461	0.9462	0.9459
8	0.9413	- 0.0604	0.9412	0.9413	0.9322
9	0.9350	- 0.1335	0.9350	0.9351	0.9259
10	0.9292	- 0.1960	0.9292	0.9292	0.9200
11	0.9283	- 0.1888	0.9283	0.9284	0.9192
12	0.9268	- 0.1773	0.9268	0.9269	0.9177
13	0.9207	- 0.2686	0.9207	0.9208	0.9115
14	0.9185	- 0.3473	0.9185	0.9185	0.9092
15	0.9170	- 0.3850	0.9171	0.9171	0.9078
16	0.9157	- 0.4082	0.9157	0.9157	0.9064
17	0.9136	- 0.4855	0.9137	0.9137	0.9043
18	0.9130	- 0.4951	0.9131	0.9131	0.9037
19	0.9965	0.0037	0.9965	0.9965	0.9964
20	0.9929	- 0.0633	0.9929	0.9929	0.9929
21	0.9922	- 0.0827	0.9922	0.9922	0.9922
22	0.9915	- 0.1030	0.9916	0.9916	0.9915
23	0.9793	0.0651	0.9793	0.9794	0.9792
24	0.9726	- 0.0237	0.9727	0.9727	0.9726
25	0.9693	- 0.0674	0.9693	0.9694	0.9692
26	0.9477	0.1733	0.9477	0.9477	0.9475
27	0.9451	0.2295	0.9451	0.9452	0.9449
28	0.9337	0.3124	0.9338	0.9337	0.9335
29	0.9255	0.3903	0.9256	0.9255	0.9253
30	0.9219	0.4956	0.9220	0.9220	0.9217
31	0.9177	0.4112	0.9178	0.9178	0.9175
32	0.9168	0.3881	0.9169	0.9169	0.9166
33	0.9165	0.3804	0.9166	0.9166	0.9163

Table 5. Power Loss Findings for Different Modeling Approaches

Method	Total Active Power Loss (kW)
DLF Method	202.677
The New Analytical Formulation (Srinivasa Rao et al., 2011)	202.771
Dynamic Data Matrix Method (Kirthiga et al., 2013)	202.700
The Direct Backward/Forward Sweep Technique (Vasquez et al., 2016)	211.000

A comparison of the bus voltage profiles obtained from various power flow solution methods is presented in Figure 7.

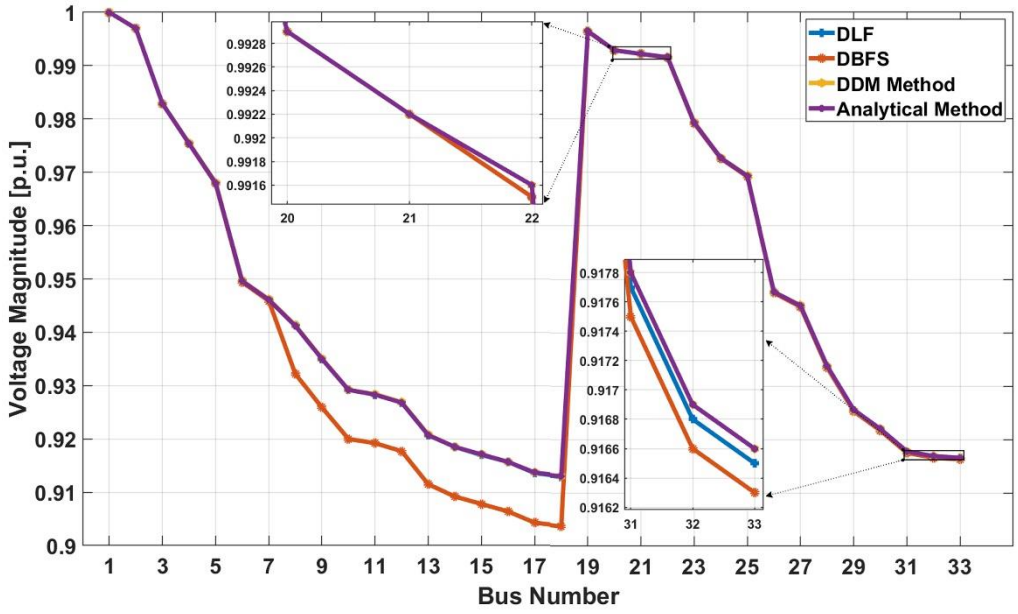

Figure 7. The Comparison of Voltages at Buses for Different Power Flow Methods

The proposed approach shows only a minor deviation from other well-established methodologies. The validity of the utilized technique is affirmed by its consistency with the findings of previous methods applied to the test system.

The proposed flowchart assumes a constant power load at the network bus. However, when alternative load modeling approaches are employed, particularly in the step accentuated by the red border in the flowchart of Figure 5, the currents for each load model are calculated iteratively using methods specific to that load model. For example, in the case of the Exponential Load Model, the apparent power (S) derived from the active-reactive power (P,Q) values is utilized in each iteration to compute a new apparent power (S) by using Eq. (5) and Eq. (6). This is followed by the determination of a new current value, and the iteration continues.

2.2.3. Load Flow Analysis For Different Load Model

The load flow model developed for the various load modeling approaches discussed in sections 2.2.1.1 and 2.2.1.2 was simulated using the IEEE 33 test system. The created models were utilized to analyze the bus loads of the test system in the provided case studies. The outcomes of the load flow analysis employing different load models, encompassing bus voltages and the total active and reactive power losses in the system, are depicted in Figure 8 and Figure 9.

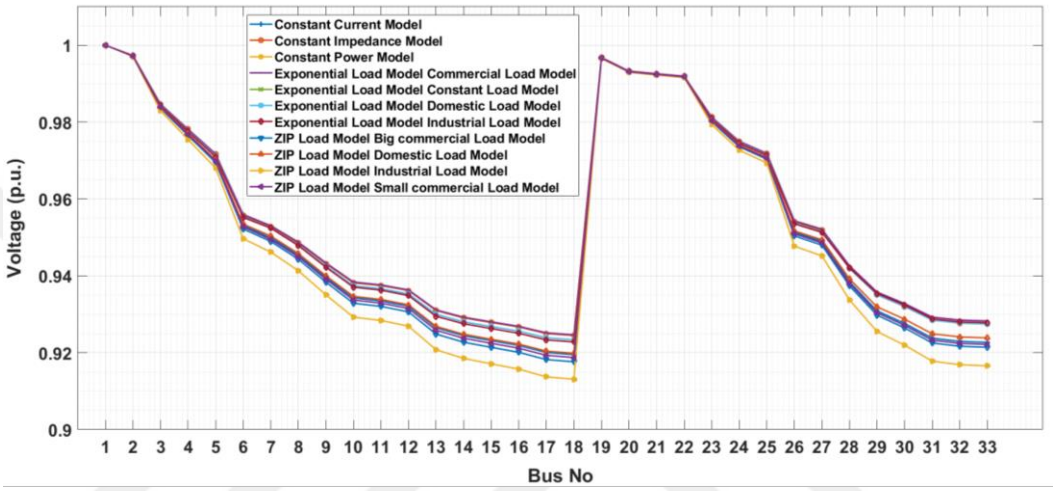

Figure 8. Buses Voltage According to Different Load Modelling

The Constant Power Model and ZIP Load Model for industrial load calculations have been shown to result in the most significant voltage drops at the system buses. Similarly, the highest active and reactive power losses were also obtained when the same method was used.

Figure 9. Comparison of Active and Reactive Power Losses for Various Load Modeling Methodologies

2.2.4. Photovoltaic System

Photovoltaic (PV) modules constitute the core power conversion components within a PV system. Configuring PV modules in series and parallel arrangements is crucial to regulate the voltage and current levels, thereby enabling the scaling of the PV array's output. Once the specific PV panel type to be employed in a PV system is identified, the calculation of the necessary number of PV panels to achieve the desired installed PV system power can be carried out Eq. (19).

$$\text{Number PV panel} = \frac{Desired\ PV\ system\ Power(W)}{Rated\ Power\ of\ PV\ module\ (W)} \tag{19}$$

The number of PV panels is calculated by rounding up to the nearest integer.

Various analytical approaches for estimating PV power output have been explored in the literature (Dolara et al., 2015). However, a particular Eq.(20) can be utilized for calculating PV power at a specific time due to its simplicity, low computational requirements, and faster execution (Basir Khan et al., 2016). The electricity generation of photovoltaic systems is directly proportional to the available global solar irradiance and the total surface area of the photovoltaic panels. The power generation can be computed using Eq. (20).

$$P_{pv(t)} = \eta_{Pv} \times N_{Pv} \times W_{module} \times G_{(t)} \qquad \forall t \quad (20)$$

P_{pv} is Output from the PV power generation system (W),

η_{Pv} is Efficiency of the PV system (%),

N_{Pv} is number of PV panel,

W_{modul} is module power (W),

G is Solar irradiation (W/m^2).

2.2.5. Investigating the Effect of Temperature on PV Panel Output

The cell temperature of a PV panel (T_{cell}) can be estimated from the ambiente temperature (T_a) and irradiance (G) using Eq. (21) (Appelbaum et al., 2020).

$$T_{cell} = T_a + \frac{G\left(\frac{W}{m^2}\right)}{800}(NOCT - 20) \qquad (21)$$

The panel's output power can be calculated using the measured ambiente temperature and the temperature dependence coefficient of the panel's power, as given by Eq. (22) (Hohne et al., 2020).

$$P_{pv,real} = P_{pv,STC}[\underbrace{1 - \alpha\,(T_{cell} - 25)}_{\eta_{cell}}] \qquad (22)$$

Where $P_{pv,STC}$ represents the panel power at standard test conditions (STC). In photovoltaic panels, the Nominal Operating Cell Temperature (NOCT) typically ranges between 43°C and 47°C (Osorio et al., 2024). This variability results in a 3.8 % to 4.5 % difference in panel power output, which is substantial given the temperature dependence coefficient, denoted as α, ranging from 0.38 % to 0.45 % per Kelvin (Boztepe, 2017). Therefore, when selecting photovoltaic panels, it is critical to consider both NOCT and the temperature dependence coefficient of power in order to identify panels least affected by temperature fluctuations and ensure optimal performance, especially under high-temperature conditions.

$$P_{pv(t)} = \eta_{cell\ (t)} \times \eta_{Pv} \times N_{Pv} \times W_{module} \times G_{(t)} \qquad \forall t \qquad (23)$$

The variations in the power output of a photovoltaic module within a photovoltaic system are shown to be affected by the ambient temperature and irradiance levels, as shown in Figure 10.

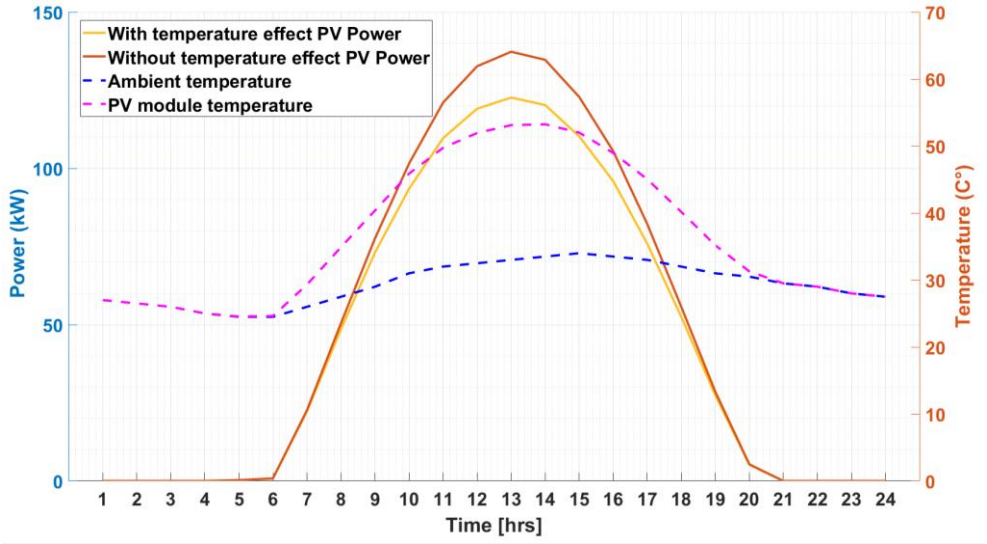

Figure 10. The Effect Temperature on PV Panel

Elevated ambient temperatures negatively impact the efficiency of PV modules. The light blue dashed line depicts the ambient temperature, while the dark red line represents the electricity generation corresponding to the hourly irradiance levels. However, fluctuations in ambient temperature and radiation values throughout the day cause variations in PV module temperatures, which in turn affect the output power, ultimately decreasing to the level shown in yellow. Elevated ambient temperatures are associated with diminished efficiency of photovoltaic modules, resulting in a decline in their power generation capacity.

Figure 10 shows a gradual increase in ambient temperature after 12:00. As a result, the temperature of the PV modules increased. As the temperature of the photovoltaic module increased, the discrepancy between the generated power and its impact on the output power expanded.

2.2.6. Battery Energy Storage System

Battery energy storage system (BESS) is widely employed in grids to offer various advantages, including power support, voltage support, frequency support, energy shifting, and energy shaving (Xavier et al., 2019).

Battery energy storage systems can offer voltage regulation support to mitigate voltage variations in low-voltage distribution networks with significant renewable energy integration and/or voltage sags during periods of peak electricity demand (X. Li et al., 2013). BESS plays a crucial role in preserving the grid's nominal voltage level, thereby ensuring grid stability and functionality. These systems achieve this by dynamically injecting and absorbing reactive power to and from the grid. (Kang et al., 2022).

The operation of BESS for various power consumption loads aims to reduce peak demand, a strategy commonly implemented in conjunction with RES to improve the feasibility of this approach (Barchi et al., 2019).

The operation of battery energy storage systems encompasses the strategy of energy arbitrage, which involves purchasing electricity when costs are lower and selling it when prices are higher. Additionally, the system encompasses energy trading, bill reduction, backup solutions, energy shifting and other energy grid support capabilities (Feng et al., 2022).

The BESS model incorporates parameters that encompass the limits on charging and discharging power, the energy storage capacity, as well as the charging and discharging efficiencies (Rezaeimozafar et al., 2024). The BESS model is inherently nonlinear due to the variability in its charging and discharging efficiency parameters. To simplify the model, if these efficiency values are not equal, the linearized form of the BESS energy balance equation can be written like Eq. (24).

$$SoC_{(t+1)}^{BESS} = SoC_{(t)}^{BESS} + \eta_{BC}.P_{(t)}^{BC}.\Delta t - \frac{P_{(t)}^{BD}}{\eta_{BD}}.\Delta t \qquad \forall t \quad (24)$$

Where; the battery state of charge ($SoC_{(t)}^{BESS}$) represents the current level of charge within the BESS. The charging and discharging efficiency of the battery energy storage system are represented as η_{BC} and η_{BD}, respectively. Active power associated

with charging and discharging the BESS are represented as $P_{(t)}^{BC}$ and $P_{(t)}^{BD}$, respectively. Additionally, Δt refers to the time interval.

The battery's state of charge (SoC) indicates the proportion of its nominal energy capacity that remains available. The SoC of a battery refers to the ratio of the remaining energy to the rated energy capacity. Regulating the state of charge within a designated range is essential for the protection of the battery system (Lu et al., 2017).

$$SoC_{min} \leq SoC_{(t)} \leq SoC_{max} \qquad \forall t \qquad (25)$$

Where the SOC_{min} and SOC_{max}values correspond to the lower and upper thresholds of the SoC, respectively.

One of the applications of BESS in this study is employing BESS for load balancing to minimize power losses in the distribution network. The goal of load balancing is to reduce fluctuations in electrical demand throughout the day. This can be accomplished by increasing generation during off-peak hours and storing energy to meet peak demand. Another purpose is to maintain bus voltage levels within regulatory limits by adjusting the active and reactive power of the buses via the connected inverters.

BESS can be integrated with the AC power grid through inverter connections. These inverter interfaces enable BESSs to offer reactive power support to the grid. A comparable configuration can also be applied to PV systems. The technical details of the inverters employed for both BESS and PV applications will be discussed in the following section.

3. CHAPTER: THE OPERATION OF INVERTER

3.1. Introduction

This section examines the reactive power capabilities and control strategies of inverters that function as DC/AC or AC/DC converters during the integration or storage of energy generated or stored as DC within the distribution system.

Researchers and practitioners have extensively investigated the reactive power performance of inverter-based devices. This methodology has enabled both the reduction of reactive power drawn from the grid and the regulation of voltage levels by exploiting the relationship between reactive power and voltage magnitudes.

This chapter examines the capabilities of inverters utilized in PV and BESS. Additionally, it investigates the commonly employed reactive power control strategies implemented by inverter.

3.2. Inverter Capability

The IEEE 1547 Standard requires all new fuel cells, photovoltaics, distributed generation, and energy storage inverters to support various grid-support modes, including Volt-VAR (VV) mode (IEEE, 2018). In VV mode, the inverter can inject reactive power to raise low voltages and absorb reactive power to lower high voltages. If necessary, it may also limit real power output, prioritizing reactive power control.

It is assumed that the inverters interfacing RES such as PV systems and BESSs to the distribution grid have the capability to control reactive power. Nonetheless, the fundamental difference between the inverters associated with BESS and PV systems is the directionality of active power flow.

In a PV system, the active power transmission is unidirectional, conveying solely from the inverter to the electrical load. In contrast, a BESS has a bidirectional active power flow, allowing it to transfer energy from the inverter to the load or from the load to the

inverter. However, both PV and BESS systems have the capability for bidirectional reactive power operation.

The power conversion system of a BESS can operate in four quadrants, as shown in Figure 11 (X. Li et al., 2022), allowing it to exhibit a range of active and reactive power characteristics (Alsaleh et al., 2018; Dantas et al., 2022; Saboori et al., 2015).

- Absorbs active power and inductive reactive power,
- Absorbs active power and capacitive reactive power,
- Supplies active power and inductive reactive power,
- Supplies active power and capacitive reactive power.

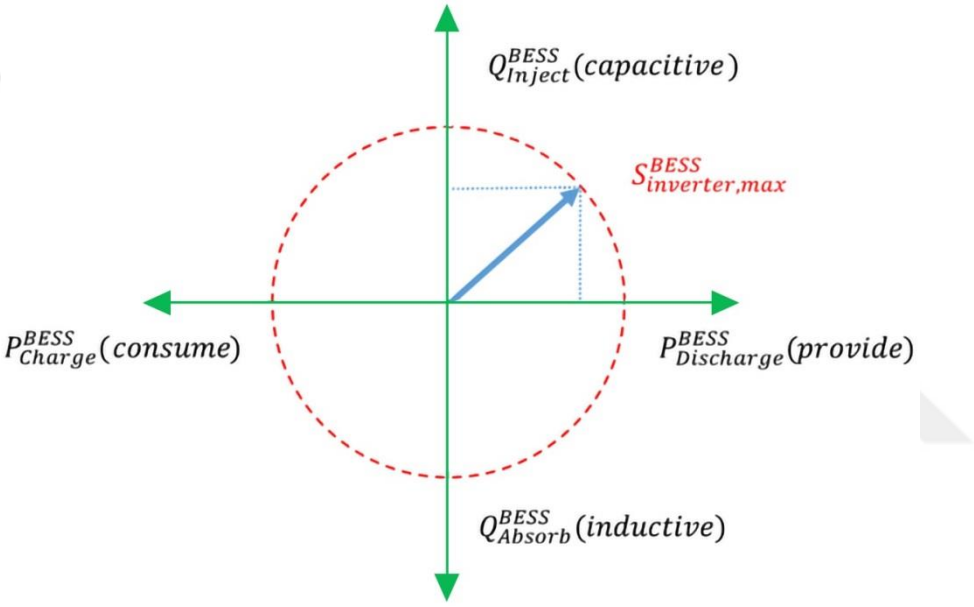

Figure 11. Four-quadrant Operation of BESS Power Convertor System

The apparent power flow of the BESS is described by a nonlinear function that predicated on the active and reactive power exchanged, as formulated in Eq. (26) and Eq. (27) (Gandhi et al., 2016).

$$\sqrt{P^2 + Q^2} \leq S \tag{26}$$

$$\sqrt{(P^{BC}_{(t)} - P^{BD}_{(t)})^2 + (Q^{BC}_{(t)} - Q^{BD}_{(t)})^2} \leq S^{Rated}_{BESS} \quad \forall t \tag{27}$$

$P^{BC}_{(t)}$, BESS charging active power during time *t* period,

$P^{BD}_{(t)}$, BESS discharging active power during time *t* period,

$Q_{(t)}^{BC}$, BESS absorbing reactive power during time *t* period,

$Q_{(t)}^{BD}$, BESS injecting reactive power during time *t* period,

S_{BESS}^{Rated}, Power rating of BESS (kVA).

The PV power conversion system can operate in two distinct quadrants, as depicted in Figure 12, suggesting that its active power and reactive power characteristics can vary accordingly (Venkatasamy et al., 2021).

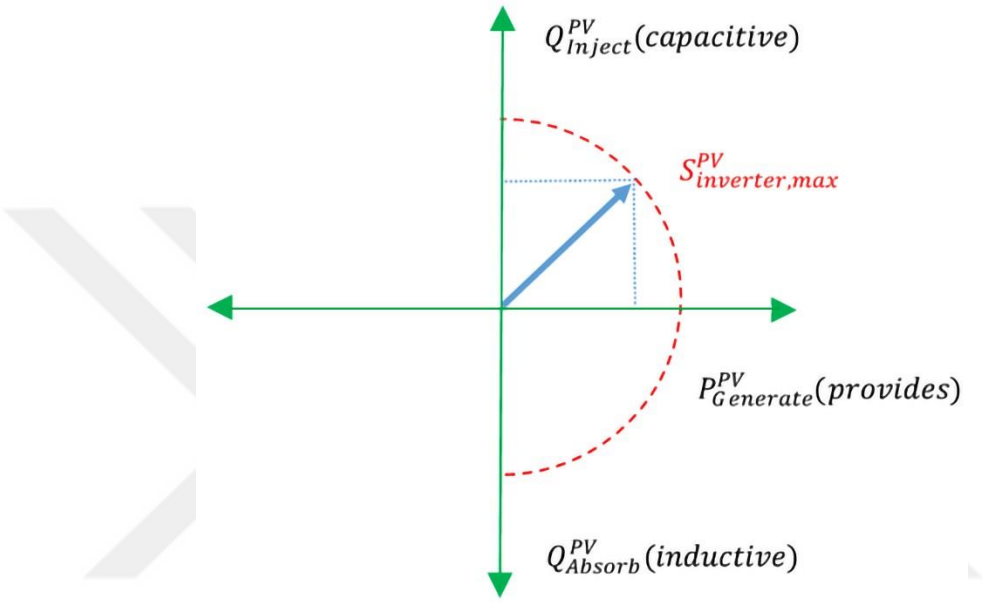

Figure 12. Two-quadrant Operation of PV Power Converter System

- Supplies active power and inductive reactive power,
- Supplies active power and capacitive reactive power.

3.3. The Reactive Power Control Strategy of Inverter

Ensuring adequate reactive power availability is essential for preserving voltage conditions within acceptable thresholds. Reactive power is essential for maintaining overall grid voltage stability in conventional power system practices.

The effectiveness of reactive power support is contingent on the R/X ratio within the power grid. Compared to low-voltage networks with a higher R/X ratio, reactive power compensation is less effective in high-voltage networks. Nevertheless, the purpose of implementing reactive power compensation in low voltage networks is to generate supplementary reactive power flows, thereby mitigating voltage increases caused by

distributed energy sources. Inverters typically employ four distinct control strategies for reactive power support (Almeida et al., 2021; Stanelytė et al., 2022).

(i) Constant Q,
(ii) Constant cos φ,
(iii) Cos φ (P),
(iv) Q (V).

3.3.1. Constant Q

The constant Q method (depicted in Figure 13) results in the PV inverter consistently supplying a set quantity of reactive power, regardless of other system parameters. This approach requires knowledge of load power and PV power profiles to determine an appropriate Q point. However, by disregarding other system variables like voltage, This approach leads to photovoltaic inverters providing reactive power compensation during times when it is not needed.

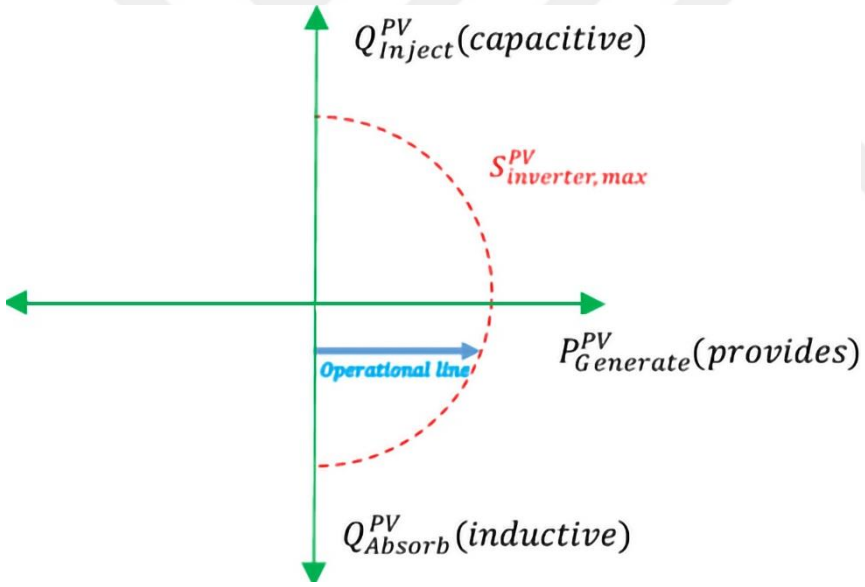

Figure 13. Operational Boundaries for Fixed Q Control

3.3.2. Constant Cos φ

Figure 14 shows that in a constant power factor approach, there is a direct relationship between reactive power generation and active power. The inverter operates at a predefined power factor angle, irrespective of the system variables. As a result, the inverter may provide reactive power compensation even when it is unnecessary, akin to the constant Q approach.

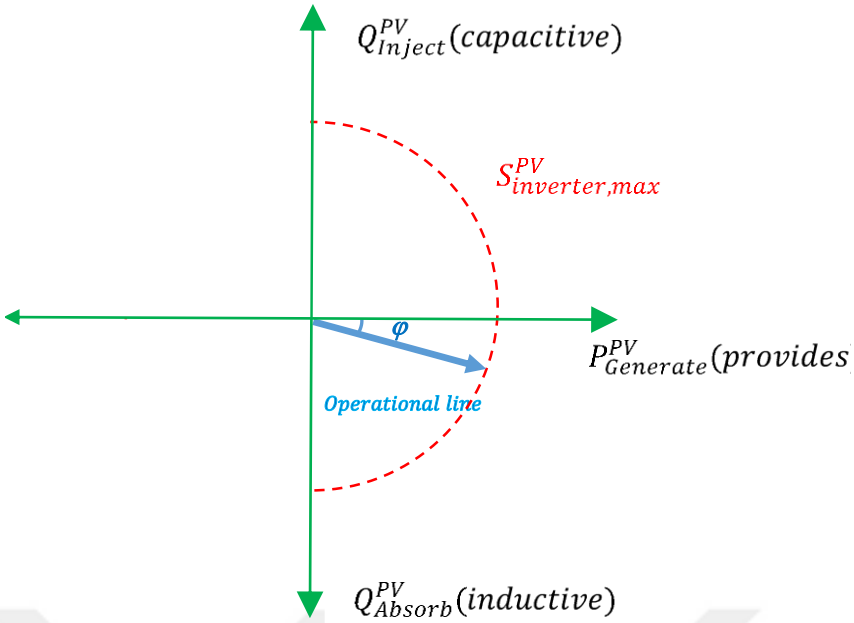

Figure 14. Fixed cos φ Control

By employing leading power factors, which involve absorbing reactive power, the voltage elevation resulting from active power output can be counteracted.

3.3.3. Cos φ (P)

The Cos φ control strategy operates by continuously monitoring the active power output of the inverter and adjusting the power factor accordingly to maintain the desired system performance. The concept entails modulating the power factor in order to provide reactive power compensation when the system's power output reaches a specified threshold, such as 50% of the rated capacity. Figure 15 illustrates operational region and Figure 16 shows a characteristic curve this control approach.

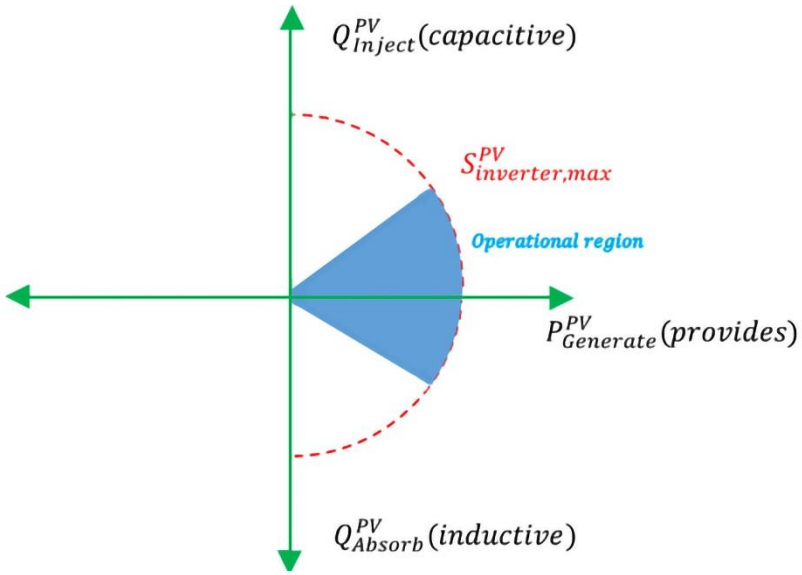

Figure 15. Operational Region of cos φ (P) Control

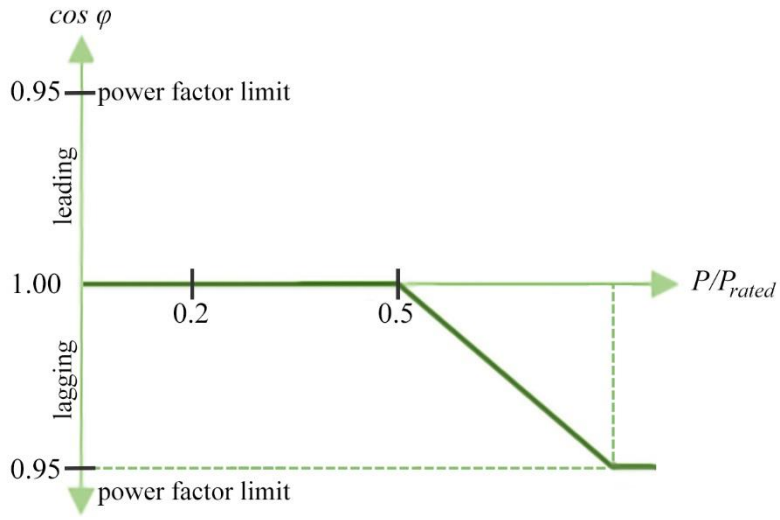

Figure 16. Characteristic Curve of cos φ (P) Control

3.3.4. Volt-Var Control - Q (V)

Within this operational framework, the PV inverter dynamically adjusts its reactive power production or absorption based on the voltage at the bus (Stanelytė et al., 2022). The precise level of reactive power compensation is determined by the Volt-Var setpoint parameters defined by the user or the DSO. As illustrated by the typical Volt-Var curve shown in Figure 17, if the terminal voltage falls below a predetermined lower limit, the inverter injects reactive power to raise the voltage at the connection point. Conversely, if the terminal voltage rises above a predetermined upper limit (V4), the inverter absorbs reactive power to stabilize the voltage at the connection point.

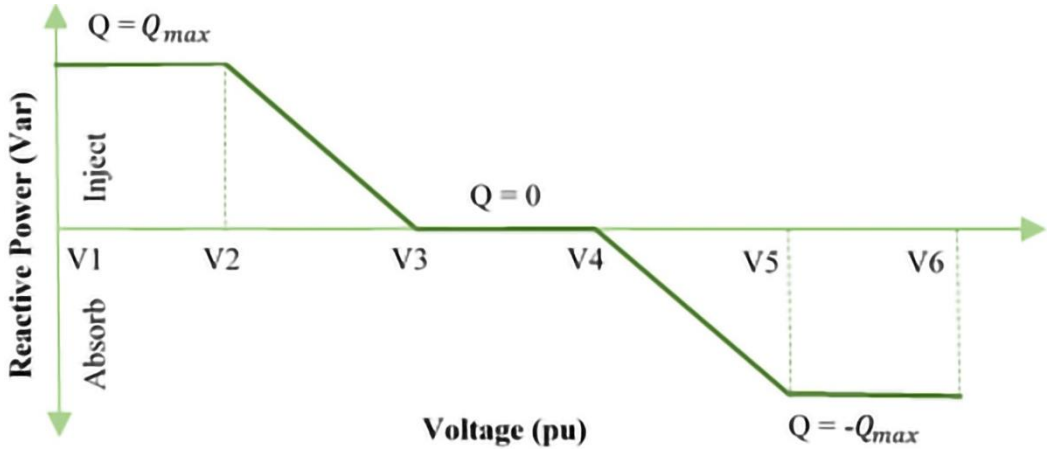

Figure 17. A Generic Volt-Var Curve (Q(V) Control)

The mathematical formulation describing the reactive power injection or absorption by Volt-Var control is presented in Eq. (28).

$$Q_{(t)} = \begin{cases} Q_{\max(t)} & ; if\ V_{(t)} \le V2 \\ \dfrac{V3 - V_{(t)}}{V3 - V2} Q_{\max(t)} & ; if\ V2 < V_{(t)} \le V3 \\ 0 & ; if\ V3 < V_{(t)} \le V4 \\ -\dfrac{V4 - V_{(t)}}{V4 - V5} Q_{\max(t)} & ; if\ V4 < V_{(t)} \le V5 \\ -Q_{\max(t)} & ; if\ V_{(t)} < V5 \end{cases} \quad (28)$$

Where, the terminal voltage is represented as V_t, and the computed reactive power injection enabled by the Volt-Var control is denoted as Q_t.

The Q method, also known as the volt-var function, allows PV inverters to regulate their reactive power injection or absorption in accordance with the voltage at their point of connection, as per the predetermined settings configured within the inverter (Malekpour et al., 2017).

3.3.5. Section Evaluation

All methods are local control functions, influenced by local variables of the inverter or the grid. However, when communication infrastructures are employed, these strategies can be implemented in a centralized control manner, optimizing the overall assets of the network and delivering improved voltage regulation. This centralized

control approach allows for the coordination of multiple local control functions, enabling the optimization of the entire distribution system rather than just individual components. By considering the interconnected nature of the grid, this centralized control can provide enhanced voltage regulation and performance across the entire network. The use of a centralized control system can bring about several benefits, such as improved coordination of distributed resources, better management of voltage levels throughout the distribution system, and increased overall efficiency of the grid. Adopting a comprehensive perspective of the network enables the centralized controller to make more well-informed decisions and implement strategies that optimize the overall system performance, rather than focusing solely on individual components or localized areas.

3.4. The Reactive Power Cost and Loss of Inverter

In (Gandhi, Rodríguez-Gallegos, Reindl, et al., 2018), the authors demonstrated that inverters experience power losses influenced by the apparent power flowing through them. Specifically, when inverter inject reactive power, the increased apparent power flowing through them leads to additional power losses.

The economic impact of reactive power includes the cost of the additional power loss multiplied by the electricity price required to compensate for this extra loss. The cost of reactive power also has two components, as emphasized in Eq. (29): converter losses and converter degradation/lifetime reduction (Gandhi, Rodríguez-Gallegos, Reindl, et al., 2018).

$$C_{(t)}^{Q} = C_{(t)}^{Q,Invloss} + C_{(t)}^{Q,LR} \qquad \forall t \qquad (29)$$

Where the unit costs of reactive power are $C_{(t)}^{Q,invloss}$ due to inverter loss and $C_{(t)}^{Q,LR}$ due to inverter lifetime reduction (LR).

The first challenge arises from the additional power losses that occur in the inverter due to the increased current flowing through it. These extra power losses need to be accounted for and mitigated through appropriate compensation techniques in order to maintain the overall system efficiency and performance (Gandhi et al., 2019a).

$$C_{(t)}^{Q,Invloss} . Q_{(t)}^{Inverter} = C_{(t)}^{Pgrid} . \Delta P_{(t)}^{Invloss} \qquad \forall t \qquad (30)$$

where $\Delta P_{(t)}^{Invloss}$ is the additional losses. The additional losses in the inverter occur because of the reactive power that is injected into the system. This reactive power flow leads to increased current through the inverter components, which in turn results in higher power dissipation and energy losses within the inverter.

The blue data points in Figure 18 (Braun, 2009) represent the measured loss values, while the green points indicate the interpolated values derived from the apparent power output. These interpolated data points are within the same range as the measured values. By employing a second-order polynomial function to approximate the measured data, a black curve is generated, which also aligns with the scattered data points. This consistent alignment serves as evidence supporting the effectiveness of the approximation technique (Braun, 2008).

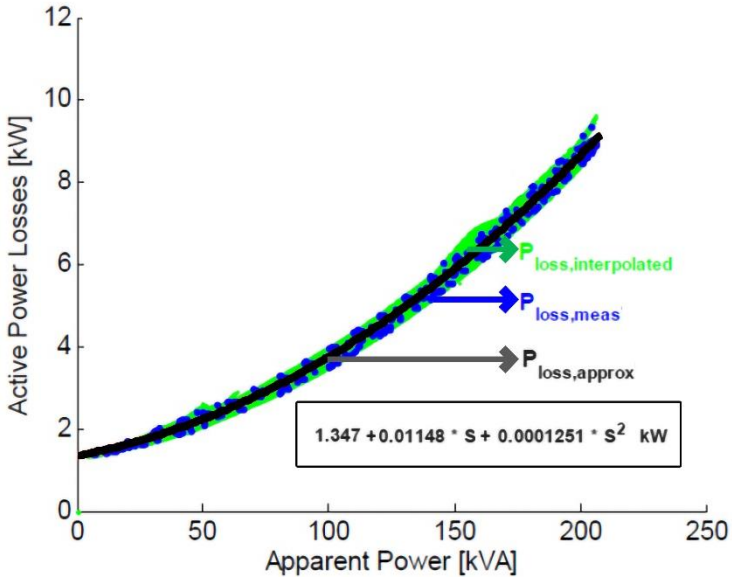

Figure 18. Losses of a 208 kVA PV Inverter Over the Apparent Power Output (Measured: Blue, Interpolated: Green, Approximated: Black)

By means of Eq. (31), the power loss in the inverter is calculated approximately (Gandhi et al., 2016).

$$P_{(t)}^{Invloss} = c_{self} + c_v S_{(t)} + c_R S_{(t)}^2 \qquad \forall t \qquad (31)$$

The power loss of inverter is denoted as $P_{(t)}^{Invloss}$ and the apparent power flowing through the PV/BESS inverter is represented as $S_{(t)}$. The c_{self}, c_v and c_R constants determined experimentally to fit the inverter's power loss curve are given in Table 6 (Braun, 2008).

Table 6. The Coefficients of the Fitting of Power Loss in The Inverter

Coefficients	Value
c_{self}	1.347
c_v	0.01148
c_R	0.0001251

c_{self}: Internal consumption, independent of the load,

c_v: Voltage losses in power semi conductor,

c_R: Ohmic losses (in coils, cables and connectors).

The increased current flowing through the inverter results in additional losses, leading to a rise in temperature within its components. Among these components, the DC-link capacitors, especially the electrolytic ones, are highly sensitive to temperature variations and susceptible to premature failure. Consequently, it is assumed that the inverter's lifespan is directly tied to the longevity of the DC-link capacitors. If an inverter fails prematurely within the system's expected lifespan, replacement becomes necessary.

The shorter lifespan of inverters due to reactive power consumption implies more frequent replacements, which in turn increases the levelized cost of electricity (LCOE) for both the PV and BESS systems. This higher LCOE can be attributed to the reactive power cost component associated with the reduction in inverter lifespan, denoted as $C_t^{Q,LR}$, necessitating appropriate compensation. This leads to a cubic function as described in Eq. (32) (Gandhi, Rodríguez-Gallegos, Reindl, et al., 2018). The coefficients of the inverter used in the study are given in the Table 7 (Gandhi et al., 2019b).

$$C_{(t)}^{Q,LR}.Q_{(t)}^{Inverter} = \eta^{LR,0} + \eta^{LR,1}.Q_{(t)}^{Inverter} + \eta^{LR,2}.(Q_{(t)}^{Inverter})^2 + \eta^{LR,3}.(Q_{(t)}^{Inverter})^3 \quad \forall t \quad (32)$$

Table 7. The Coefficients of the Fitting of Reduction in Inverter Lifespan

Coefficients	Value
$\eta^{LR,0}$	0
$\eta^{LR,1}$	0.74 x 2.133e-4
$\eta^{LR,2}$	0.74 x -1.986e-6
$\eta^{LR,3}$	0.74 x 2.726e-8

3.5. Considerations

Inverter commonly employs control strategies to provide reactive power capabilities. However, these strategies are typically employed in standalone or autonomous PV and BESS systems. In the proposed central energy management system, operated with a central control mechanism, inverters are operated within their reactive power capabilities limits according to optimization results, aligned with the objective function. Accordingly, inverters are operated in alignment with the requirements of the energy management system, injecting reactive power when necessary or absorbing reactive power as needed.

This section underscores several key points, including the capability of inverters to independently inject and absorb reactive power irrespective of active power, as well as the acknowledgment of the costs associated with reactive power production and consumption. Additionally, it is emphasized that the lifetime cost of inverters should be calculated.

4. CHAPTER: THE OVERLOADING OF POWER TRANSFORMERS

The integration of extensive RES introduces a significant challenge to safeguarding the reliable operation of the power grid. By conducting load capacity assessments and dynamically enhancing transformer capabilities, it becomes feasible to fully leverage the load potential and mitigate the risks posed to the grid by composite loads.

For many years, thermal ratings of electrical distribution equipment have been defined and used as Static Thermal Ratings (STR), which are constant values determined based on the equipment's design and ambient conditions (Daminov, 2022).

STR represents a fixed limit, typically expressed in units of current or power, and is commonly calculated for daily-mean ambient temperature (T_{amb}). For instance, Table 8 illustrates the STRs of power transformers used for power system scheduling in Russia, with similar STRs employed in other countries. Despite the widespread use of STR over time, it has been consistently demonstrated that STR serves merely as a rough approximation of true thermal ratings (Daminov, Prokhorov, et al., 2021).

Table 8. STR of Power Transformer as a Function of Daily Mean Temperature

Mean(T_{amb}) °C	-20	-10	0	10	20	30	40
STR, (pu)	1.20	1.20	1.15	1.08	1.0	0.91	0.82

The standard thermal rating approach is limited in its capacity to capture the hourly dynamics of both the ambient temperature (T_{amb}) profile and the load profile.

Consequently, many researchers are exploring Dynamic Thermal Rating (DTR) methods. DTR delineates a daily profile of permissible load levels that can be safely accommodated by the distribution system, typically specified in terms of current or power limits (Biçen et al., 2014; Bracale et al., 2018; Daminov et al., 2019; Gouda et

al., 2012; Kuss et al., 2010; Yigit et al., 2017). This allows for more efficient utilization of the network infrastructure by adjusting the load levels in response to changing environmental conditions and system constraints. Generally, the dynamic thermal rating (DTR) of tranformers exceeds the static thermal rating (STR), but under extreme ambient conditions, such as very high temperatures, the DTR may be set lower than the STR to prevent overheating or mechanical damage to the transformer winding.

The IEC 60076-7 loading guide adopts a simplified thermal diagram, as depicted in Figure 19 (Notingher et al., 2021), to model a significantly more complex distribution system by invoking the assumptions outlined in the guide (IEC 60076-7, 2005).

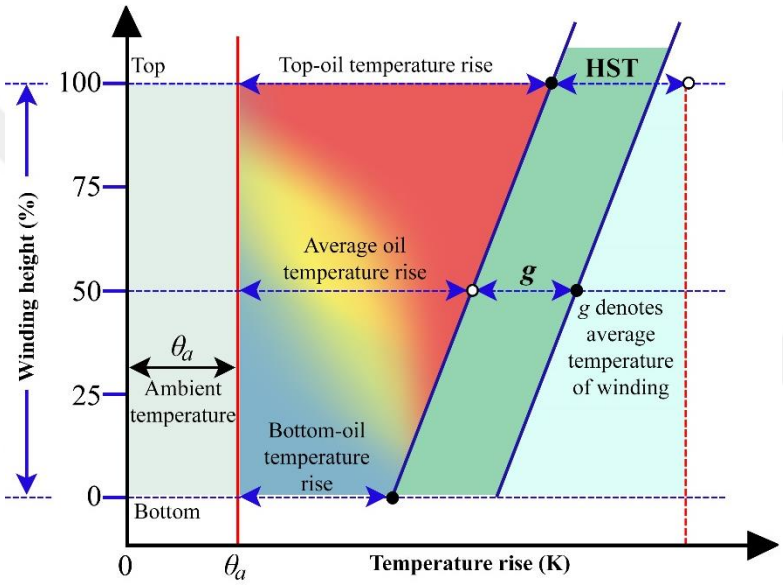

Figure 19. The Thermal Diagram of Power Transformer

Figure 20 illustrates the temperature readings of the distinct sections or components that make up a power transformer (Singh et al., 2015). This visual representation provides valuable information about the thermal profile of the different sections within the transformer. The hot spot temperature (HST) of transformers has been observed and studied in the field, and various models have been developed to represent this phenomenon. The transformer heating model used in this analysis is based on the standard IEC 60076-7:2005, which provides guidance on the loading of oil-immersed power transformers.

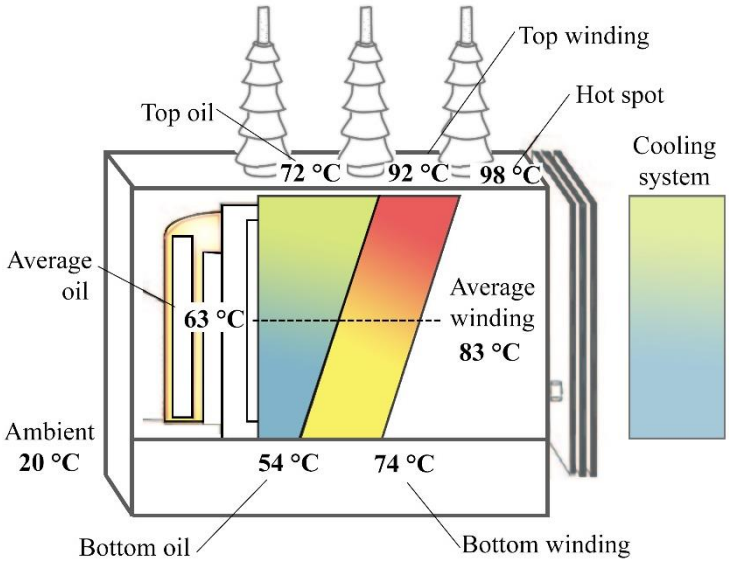

Figure 20. Temperature Variation Inside of Power Transformer

According to the loading guide, the hot-spot temperature, $\theta_{h(t)}$, in a transformer winding is comprised of three distinct components: the ambient temperature $\theta_{a(t)}$, which represents the temperature of the surrounding environment; the top-oil temperature rise, $\Delta\theta_{o(t)}$, which indicates the increase in temperature of the oil at the top of the transformer; and the hot-spot to top-oil gradient, $\Delta\theta_{ho(t)}$, which denotes the temperature difference between the hottest spot in the winding and the top-oil temperature. The combination of these three factors determines the overall hot-spot temperature within the transformer winding.

In this study, the researchers have chosen to focus on the IEC 60076-7:2018 Power Transformers - Part 7: Loading Guide for Mineral-Oil-Immersed Power Transformers standard, which has been adopted for use in Türkiye. This section provides detailed explanations and discussions of the key guidelines and recommendations outlined in this industry standard for the operation and loading of mineral-oil-immersed power transformers.

4.1. The Impact Factor of Transformer Load Capacity

The transformer's load capacity is influenced by multiple factors that are considered during the manufacturing process, including the selection of materials and the implementation of robust process controls. These factors collectively reflect the inherent level of transformer load capacity. The actual loading capacity of an operating

transformer is not exclusively defined by its inherent rating, but is also impacted by various operational factors, including the HST, ambient temperature, and the efficiency of the cooling system employed. The interplay between these inherent and operational factors ultimately dictates the overall load capacity and performance of the transformer in its intended application (Denver Office, 2000).

4.2. Hot Spot Temperature

The transformer's core and windings are the main contributors to heat production, with the highest temperature recorded within the windings, commonly referred to as the HST. Currently, three established methods are employed to determine the HST of transformers, including the direct method, the numerical analysis approach and the thermoelectric analogue model. The permissible HST limits for transformers are specified in the IEC 60076-7 and C57.91-2011-IEEE standards (IEC 60076-7, 2005; IEEE, 2012). Furthermore, the transformer's load conditions can influence the HST.

4.3. Dissipation Mode

The transformer dissipation theory posits that a portion of the heat generated within the transformer's core and windings can be dissipated through the transformer oil and additional dissipative components. This heat dissipation process effectively reduces the internal temperature and enhances the transformer's load-bearing capacity. It is recommended to incorporate the dissipation mode as a factor in assessing the transformer's load capability, which may provide more informed guidance for its optimization (S. Li et al., 2022).

4.4. Ambient Temperature

The ambient temperature is a crucial parameter that impacts the load capacity of transformers. To construct a more precise thermal model, it is essential to account for the daily variations in temperature. Furthermore, under diverse initial load conditions, the permissible overload duration exhibits analogous trends: it diminishes rapidly as the ambient temperature increases. Consequently, the accuracy of the ambient temperature data has a significant influence on the calculation of transformer overload capacity.

4.5. The Dynamic Thermal Modelling of Power Transformer

The IEC 60076-7 standard offers guidance on the loading of oil-immersed power transformers, specifying how these transformers can be operated under diverse ambient conditions and load levels without surpassing the acceptable deterioration threshold of the insulation caused by thermal effects. Additionally, Figure 21 presents a simplified diagram depicting the thermal dynamic model (Sen et al., 2011).

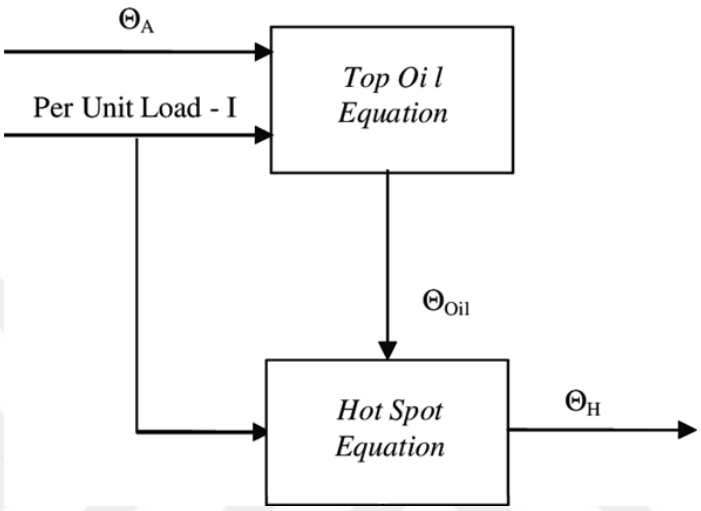

Figure 21. Simplified Transformer Thermal Model

Two different calculation methods for oil-filled power transformer loading recommendations are specified in the IEC 60076-7 standard: the differential equation solution and the exponential equation solution. This study employs the difference equation approach to evaluate the HST.

4.5.1. Differential Equations Solution

The heat transfer differential equations specified in the International Electrotechnical Commission (IEC) standard IEC 60076-7 are illustrated in a block diagram format in Figure 22 (IEC 60076-7, 2005).

The dynamics of the hot-spot temperature illustrated in the second block of the top path in Figure 22 can be described as follows. The first component reflects the inherent rise in hot-spot temperature, which occurs prior to considering the impact of changes in the surrounding oil flow. The subsequent component denotes the fluctuating nature of the oil flow around the hot-spot, a process that unfolds at a much slower rate. The

combined influence of these two factors culminates in a distinct peak in the hot-spot temperature rise shortly after the sudden load change.

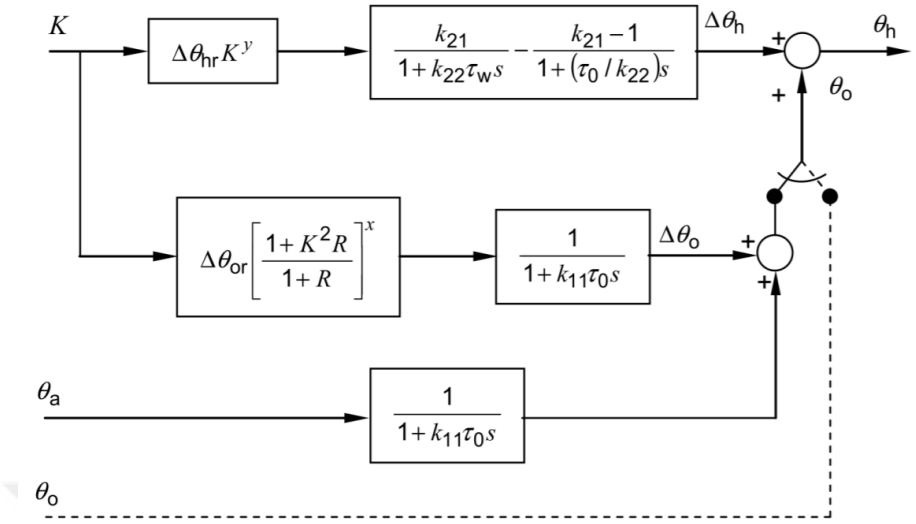

Figure 22. Block Diagram Representation of the Differential Equations

The differential equation that describes the behavior of the top-oil temperature in a transformer is given by:

$$\left[\frac{1+K^2.R}{1+R}\right]^x .\Delta\theta_{or} = k_{11}.\tau_0.\frac{d\theta_0}{dt} + [\theta_0 - \theta_a] \quad (33)$$

Where:

K is the per unit loading factor;

R represents the ratio of load losses at rated current to no-load losses

x is the oil exponent;

$\Delta\theta_{or}$ is the top-oil temperature rise in steady state at rated losses;

k_{11} is a thermal model constant;

τ_0 is the oil time constant;

θ_0 is the top-oil temperature at the load considered;

θ_a is the ambient temperature.

The solution to the differential equation modeling the hot-spot temperature increase can be derived by integrating the solutions of two separate differential equations.

$$\Delta\theta_h = \Delta\theta_{h1} - \Delta\theta_{h2} \tag{34}$$

The two equations are

$$k_{21}.K^y.\Delta\theta_{hr} = k_{22}.\tau_w.\frac{d\Delta\theta_{h1}}{dt} + \Delta\theta_{h1} \tag{35}$$

and

$$(k_{21} - 1).K^y.\Delta\theta_{hr} = \frac{\tau_0}{k_{22}}.\frac{d\Delta\theta_{h2}}{dt} + \Delta\theta_{h2} \tag{36}$$

Where

k_{21} represents a thermal model constant,

y is the winding exponent,

$\Delta\theta_{hr}$ represents the hot-spot-to-top-oil gradient at rated current,

k_{22} is a thermal model constant,

τ_w is the winding time constant,

$\Delta\theta_h$ is the hot-spot-to-top-oil gradient at the load considered.

The final equation for the hot-spot temperature is given by:

$$\theta_h = \theta_0 - \Delta\theta_h \tag{37}$$

4.5.2. Difference Equations Solution

The differential equations have been transformed into difference equations, thereby simplifying the application of the solution (Martins, 2019). The top-oil temperature is expressed as follows:

$$D\theta_0 = \frac{D_t}{k_{11}.\tau_0}\left[\left[\frac{1 + K^2.R}{1 + R}\right]^x.\Delta\theta_{or} - [\theta_0 - \theta_a]\right] \tag{38}$$

The variable difference operator D represents the change in the associated variable across each discrete time step Δt. At each time step, the n^{th} step value of $D\theta_0$ the variable is computed from the previous $(n-1)^{th}$ step value using the specified method.

$$\theta_0(n) = \theta_0(n-1) - D\theta_0(n) \tag{39}$$

Equations (35) and (36) become

$$D\Delta\theta_{h1} = \frac{D_t}{k_{22}.\,\tau_w}[k_{21}.\Delta\theta_{hr}.K^y - \Delta\theta_{h1}] \tag{40}$$

and

$$D\Delta\theta_{h2} = \frac{D_t}{(\frac{1}{k_{22}}).\,\tau_0}[(k_{21}-1).\Delta\theta_{hr}.K^y - \Delta\theta_{h2}] \tag{41}$$

The n^{th} iterations of $\Delta\theta_{h1}$ and $\Delta\theta_{h2}$ are computed using an analogous approach to that described in the referenced Eq. (39).

The total increase in the temperature of the hot-spot location at the n^{th} time step is calculated as follows:

$$\Delta\theta_h(n) = \Delta\theta_{h1}(n) - \Delta\theta_{h2}(n) \tag{42}$$

The hot-spot temperature at the n^{th} time step is given by:

$$\theta_h(n) = \theta_0(n) - \Delta\theta_h(n) \tag{43}$$

To ensure an accurate solution, it is recommended to maintain a time step (Δt) that is as small as feasible, preferably not exceeding half the magnitude of the smallest time constant present in the thermal model.

The recommended thermal parameters for the differential equations, which encompass the top-oil exponent x and the winding exponent y, are presented in Table 9 (IEC 60076-7, 2005).

The transformer-specific constants k_{11}, k_{21}, k_{22} along with the time constants τ_w and τ_0, can be determined through an extended heat-run test conducted during the "no load loss + load loss" period. This test necessitates maintaining the supplied losses and corresponding cooling conditions, such as ON or OF, unaltered from the start until a steady state is reached. It is essential to commence the heat-run test when the transformer is at or near the ambient temperature.

Table 9. Transformer Properties

Characteristic	Small Transformers	Medium and Large Power Transformers						
	ONAN	ONAN restricted	ONAN	ONAF restricted	ONAN	OF restricted	OF	OD
Oil exponent x	0.8	0.8	0.8	0.8	0.8	1.0	1.0	1.0
Winding exponent y	1.6	1.3	1.3	1.3	1.3	1.3	1.3	2.0
Constant k_{11}	1.0	0.5	0.5	0.5	0.5	1.0	1.0	1.0
Constant k_{21}	1.0	3.0	2.0	3.0	2.0	1.45	1.3	1.0
Constant k_{22}	2.0	2.0	2.0	2.0	2.0	1.0	1.0	1.0
Time Constant τ_w min.	180	210	210	150	150	90	90	90
Time Constant τ_0 min.	4	10	10	7	7	7	7	7

It's important to note that transformer-specific parameters k_{21}, k_{22} and τ_w can only be definitively determined if the transformer is equipped with fiber optic sensors. If these parameters are not obtained through a prolonged heat-run test, they can be estimated through calculation. In the absence of transformer-specific values, the recommended values from Table 9 are suggested. However, it is crucial to recognize that these calculated estimates may yield more conservative values to minimize operational risks.

4.6. Examples of The Interrelationship Between Transformer Loading and Temperatures

This section provides an illustrative calculation to demonstrate the relationship between a transformer's loading, ambient temperature, and the resulting HST and Top Oil Temperature (TOT).

The two important constraints of the transformer, namely HST and TOT values, are influenced by two fundamental variables. The first variable is the effect of the ambient or environmental temperature. The loading level of the transformer represents the second influencing variable.

To clearly examine the impact of each factor, calculations are performed by modifying only one factor at a time. The initial analysis focuses on the effect of ambient temperature on TOT and HST.

The load is maintained at 50 %, while the ambient temperature is varied as a step function. It is assumed that the ambient temperature increases from 15 degrees to 25 degrees at 06:00 and remains constant until 12:00. Beginning at 06:00, both HST and TOT start to rise. TOT reaches 47 degrees, and HST reaches 56 degrees. The HST and TOT temperatures of the transformer do not return to their levels prior to the ambient temperature increase until 23:00. In summary, it takes 6 hours to reach the elevated temperature and an additional 11 hours to revert to the previous temperature.

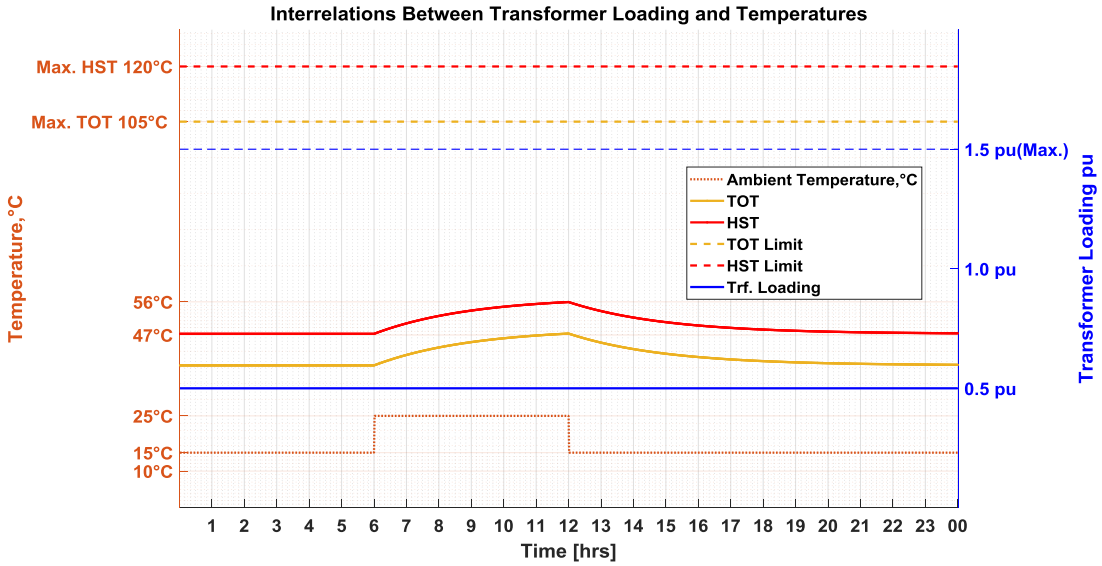

Figure 23. Interrelations Between Transformer Loading and Step Ambient Temperature

Figure 24 shows that the transformer loading remains constant throughout the day, while the ambient temperature fluctuates. As a result, the transformer temperatures HST and TOT also fluctuate accordingly. Two different loading profiles are examined to demonstrate the relationship between transformer temperature and loading.

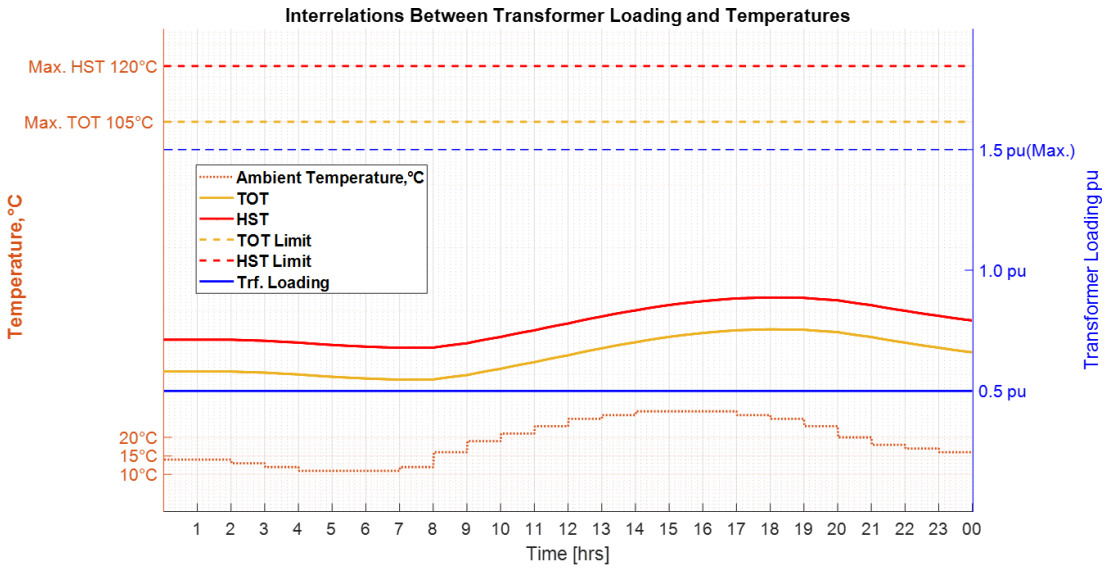

Figure 24. Interrelations Between HST-TOT and Daily Ambient Temperature

The first scenario involves calculations based on the assumption of a short-term overloading occurrence under constant ambient temperature conditions, which results in the temperature variations illustrated in Figure 25, the transformer is loaded at 120 % from 06:00 to 07:00. This 1-hour overload results in a calculated TOT value of 51°C and a calculated HST of 86°C.

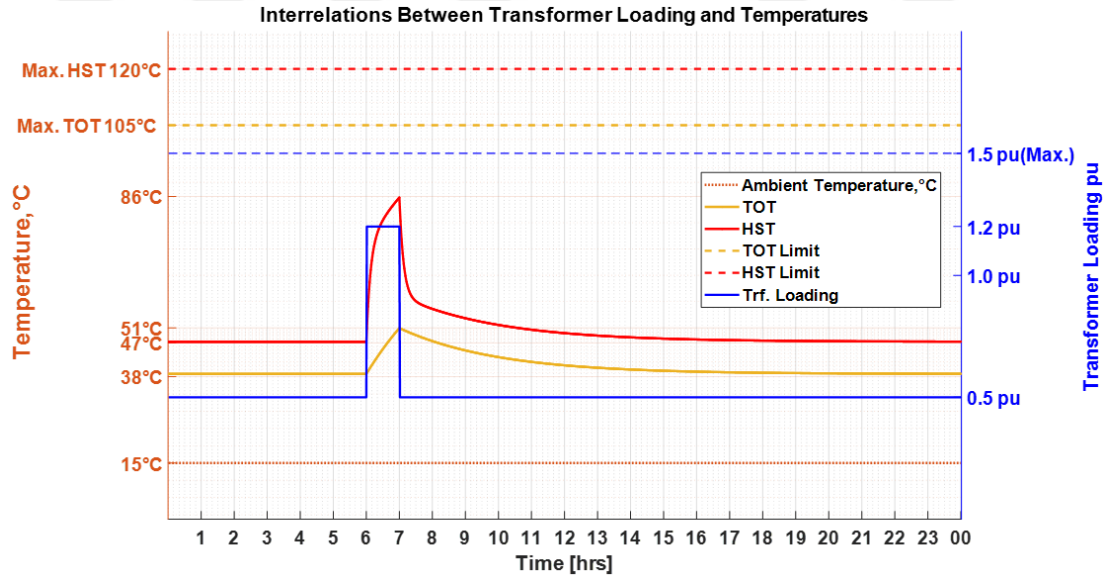

Figure 25. Interrelations Between Short Step Overloading Transformer and Temperatures

In a different overload scenario featuring a 150 % overload, the transformer operated for 3 hours, resulting in the following Figure 26.

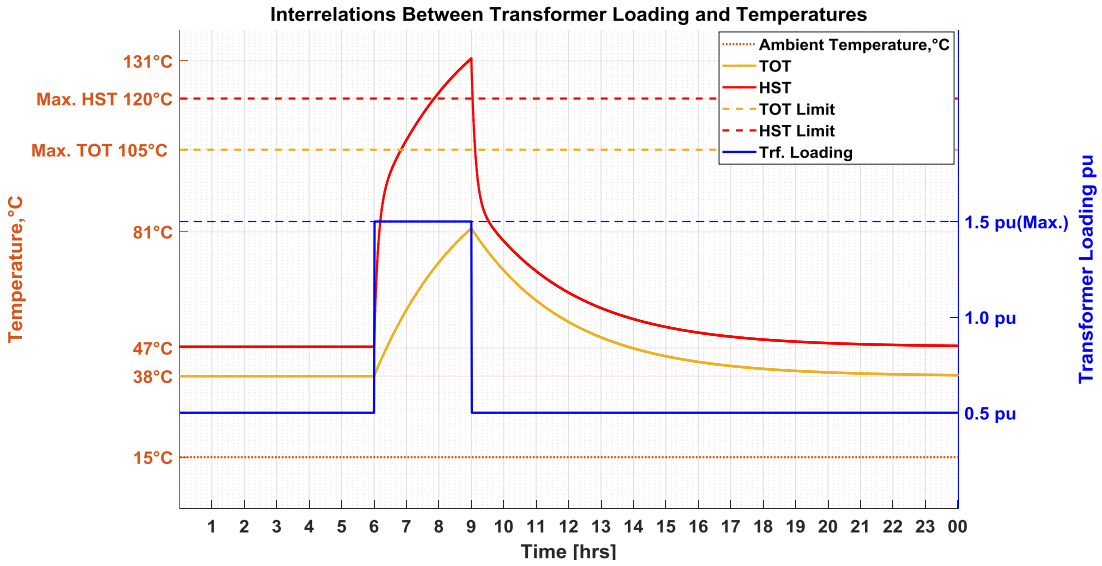

Figure 26. Interrelations Between 1.5 (p.u) and Long-term Step Transformer Overloading and Temperatures

An important point is that when the transformer operates with a 150 % overload for 3 hours, the TOT value reaches 81°C, which is below the upper limit. Thus, it remains within the TOT limit. However, the HST value reaches 131°C, exceeding the upper limit of 120°C, violating the standard's limit.

Although the applied overload profile remains within the TOT limits, it violates the HST limit, rendering this profile unsuitable for the transformer. Another factor affecting transformer temperature is the relationship between the loading ratio in the previous time step and the overloading in the next time step.

In a 24-hour simulation, a transformer initially operates at a loading of 1.0 p.u. for the first hour. After this, an overloading of 1.5 (p.u.) is applied, causing the HST to reach approximately 120°C within about 30 minutes. However, the HST continues to rise until 12:00, after which it stabilizes and shows no significant further increase. This simulation demonstrates that the transformer can handle an overloading of 1.5 (p.u.) for approximately 30 minutes.

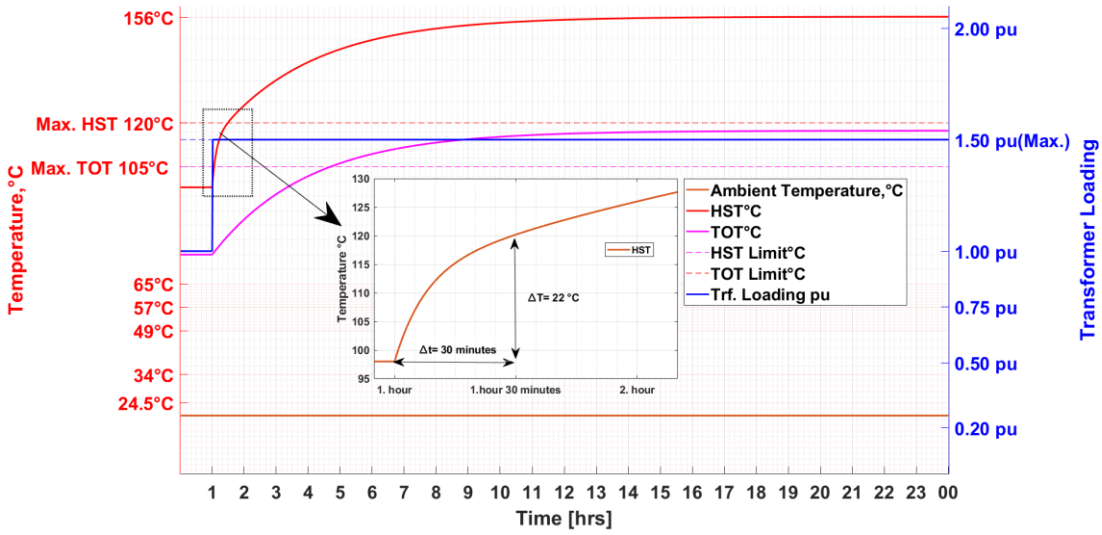

Figure 27. Relationship Between a Loading of 1.0 (p.u.) at the Previous Time Step and a 1.5 (p.u.) Overloading at the Next Time Step

In a 24-hour simulation, after a loading of 0.5 (p.u.) until the end of the first hour, if an overloading of 1.5 (p.u.) is applied from the end of the first hour, the HST value reaches approximately 120°C within about 120 minutes. However, the HST temperature continues to rise until 14:00, after which it stabilizes and shows no significant increase. This simulation demonstrates that a transformer with a loading ratio of 0.5 (p.u.) can withstand an overloading of 1.5 (p.u.) for approximately 120 minutes.

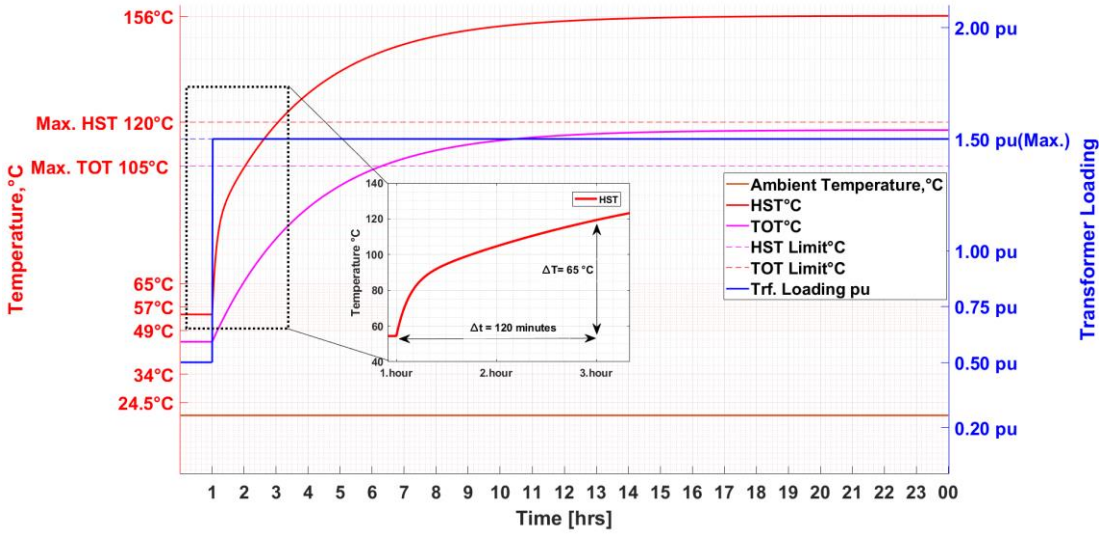

Figure 28. The Relationship Between a Loading of 0.5 (p.u.) at the Previous Time Step and a Subsequent Overloading of 1.5 (p.u.) at the Next Time Step.

The simple examples provided demonstrate the need for careful consideration of the relationship between transformer temperatures and loading. Operating the transformer under overload condition, while remaining within acceptable limits, may be permissible.

5. CHAPTER: MODEL INPUTS

This dissertation requires both hourly PV forecast data to estimate electricity generation from photovoltaics as a renewable energy source, as well as forecasts of the hourly load demands for the IEEE 33 test system . Additionally, information is needed about grid energy purchase and selling prices, which is necessary for situations where demand cannot be met by RES and BESS, necessitating energy procurement from or sale to the grid.

5.1. Modified IEEE 33 Bus Test System Description

The load and line data for the IEEE 33-bus test system are sourced from the reference (Baran et al., 1989). The bus and line data for the IEEE 33-bus test system can be found in the Appendices. The topology of the proposed IEEE 33-bus distribution test system is depicted in Figure 29. This test system comprises a 12.66 kV network consisting of one feeder substation, one transformer positioned at the point of common coupling, four PV systems, and four BESS. The test system includes a total of 33 buses and 32 branches. Buses 4, 9, 13, and 29, which contain PV units, and Buses 6, 11, 15, and 31, which contain BESS, can be treated as PV buses when they are voltage-controlled, and the acceptable bus voltages during system operation should be limited to the range of 0.95 to 1.05 (p.u.). The total active and reactive power demands are 3.715 MW and 2.3 MVAr, respectively.

The battery energy storage system can be conceptualized as either a power-generating or power-consuming unit with a fixed stored energy capacity. The maximum and minimum power injection rates define the upper and lower bounds for its charging and discharging power, respectively. Additionally, the constraints on the stored energy determine the overall energy storage capacity of the system.

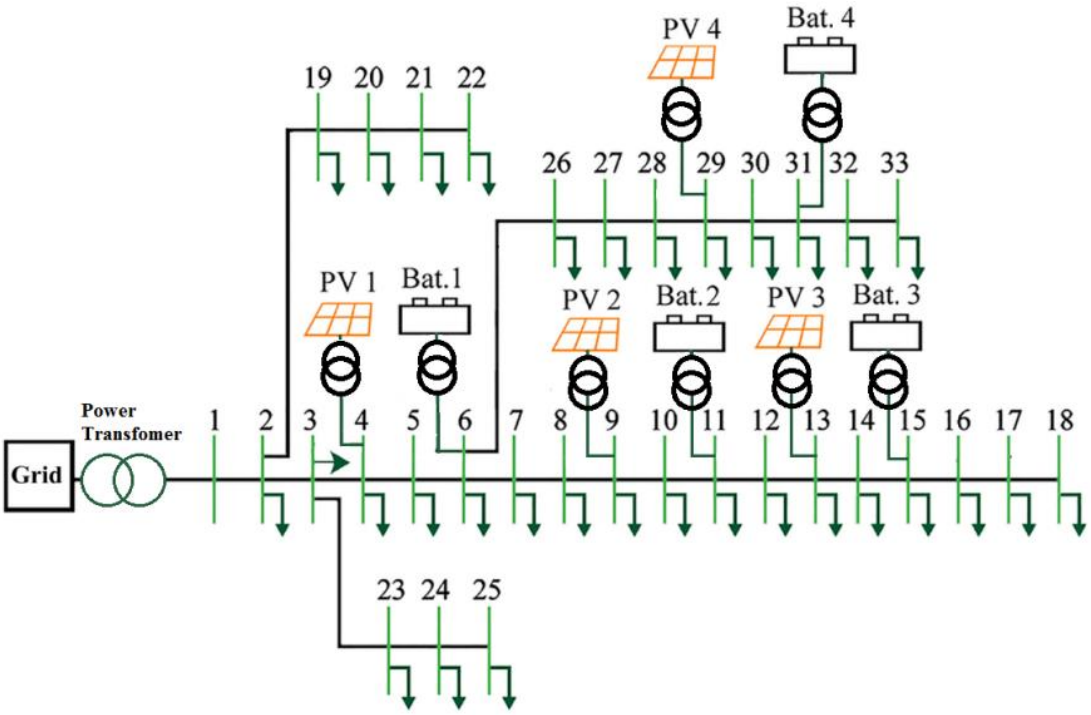

Figure 29. Modified IEEE 33 Bus Test System

5.2. Load Profile

Load forecasting is a critical capability for electric utilities in the effective planning and operation of power systems. The increasing adoption of distribution system has motivated researchers to forecast loads at the micro level, with the aim of enhancing energy control capabilities and facilitating the integration of renewable energy sources into distrabution systems. The process of load forecasting involves capturing customer behavior patterns and predicting load requirements with delivery timescales ranging from minutes to days, depending on the specific application.

Time series modeling is a standard approach utilized in load forecasting. These models typically assume that the predicted load value can be expressed as a linear combination of previously observed load demand data points. A time series is defined as a sequence of data points generated successively over time. The underlying premise of time series models is that future data points exhibit a correlation with historical values within the time series.

The electric load data is provided at 60-minutes intervals. The load profile is assumed to adhere to the IEEE-33 system, as depicted in Figure 30 (Tewari et al., 2021). This

system specifies the hourly peak load as a percentage of the daily peak load for the optimization and operation of the studied distribution system.

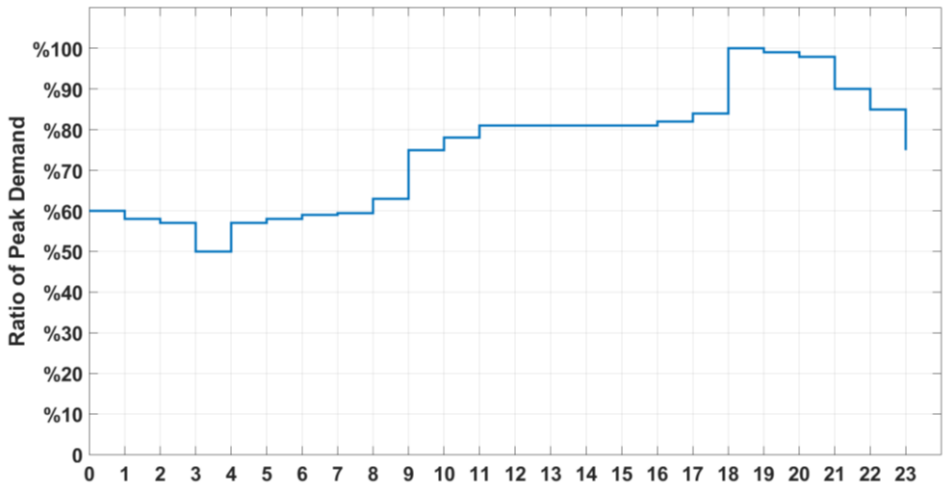

Figure 30. Forecasted Load Profile

5.3. Meteorological Data

In modeling the energy produced by PV panels, hourly irradiation data for the next day is employed as PV forecast data, utilizing historical data from the previous day. The forecast irradiation data is sourced for Izmir from the time series of hourly solar radiation available in the Photovoltaic Geographical Information System provided by the European Commission (JRC 2012). The data presented is specific to the geographical region and time period being examined. The profile of hourly irradiation forecasts for the day ahead, displayed in The Figure 31, is utilized for energy generation by the PV system.

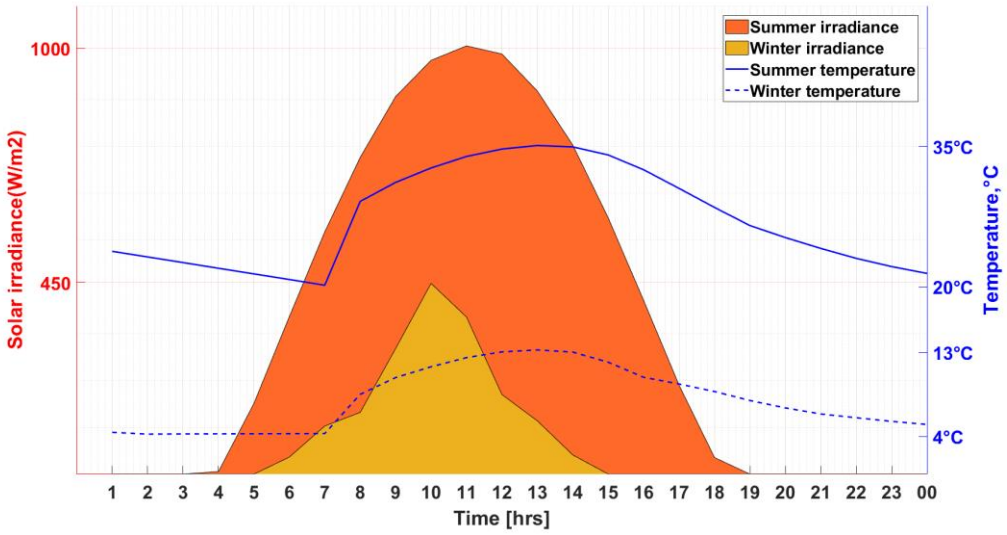

Figure 31. Forecasted Hourly Irradiance and Temperature Profiles

5.4. Grid Tariff

The energy obtained from the electric grid can be subject to various pricing schemes, including fixed-rate and variable-rate tariff structures. Furthermore, there are four distinct categories of price-based electricity tariff models (Zaigham Mahmood, 2012).

- Time-of-Use
- Real-Time Pricing
- Critical Peak Pricing
- Day-Ahead Pricing

Variable pricing tariffs feature fluctuating electricity prices that coincide with peak and off-peak hours. Prices are notably higher during peak periods than off-peak periods. If consumers react to these price variations, their electricity demand exhibits price elasticity. Consequently, customers can lower their utility bills by curtailing usage during peak hours or by shifting consumption to off-peak hours.

The dissertation does not include research on electricity sales pricing, as it is outside the scope of this work. In this study, the hourly change of grid purchases and sales to the grid used by the day-ahead EMS is shown in the Figure 32 (Aghdam et al., 2020).

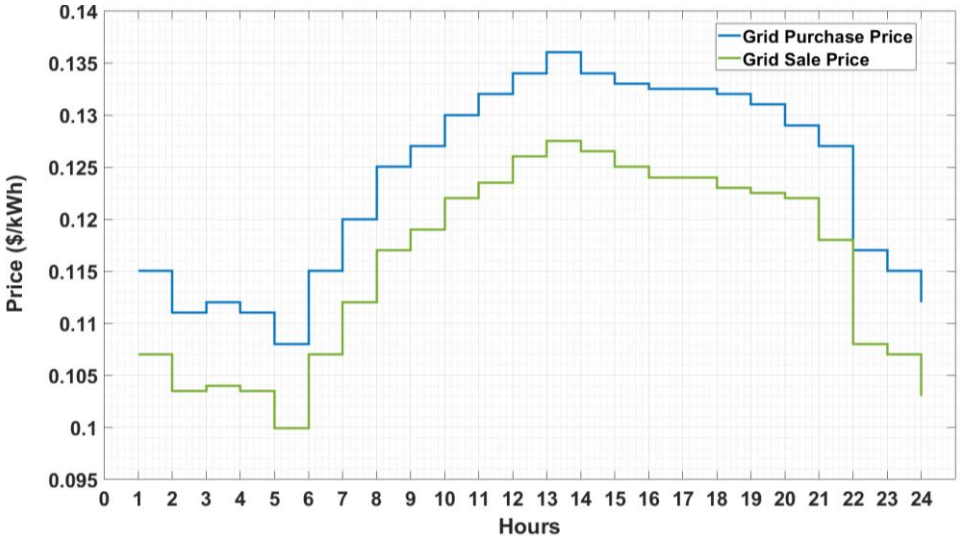

Figure 32. Day-ahead Purchase and Sales Electricity Prices

5.5. Solar Photovoltaic System and Components

The major components for PV system are the solar panels, which convert sunlight into electricity, and the inverters, which convert the generated direct current (DC) into alternating current (AC) that can be used in homes and the electrical grid.

5.5.1. Solar Panel

This research study employed a PV array consisting of multiple PV modules (SPR-435NE-WHT-D of Sun Power) connected in a series-parallel configuration to generate the necessary power output.

The solar panel is composed of 120 monocrystalline silicon cells, where the values of their parameters such as open-circuit voltage, short-circuit current, and maximum power output are determined for the standard test condition (STC) corresponding to a temperature of 25 °C and an irradiation is G = 1000 W/m2 (Sunpower SPR-435NE-WHT-D (435W) Solar Panel - User Manual, 2020).

Table 10. Specification of Solar Panel

Parameter	Value
Brand and Model	Sun Power SPR-435NE-WHT-D
Peak Power	435 Wp
Panel Efficiency	20.1 %
Temperature Coefficient (Power)	– 0.38 %/K
Number of Panel Used	5,748
Classification of Cell	Polycrystalline
Volume of Individual Module	2067 mm x 1046 mm x 54 mm
Module Area	2.162 m^2
Total Module Area for 2.5 MW	12,427.00 m^2

Table 11. PV System Parameters

Equipments	Location	Rated Power (W)	Panel Area(m^2)	Panel Efficiency (η_{pv})
PV-1	Bus-5	2,500,380.00	12,427 m^2	0.20
PV-2	Bus-9	2,500,380.00	12,427 m^2	0.20
PV-3	Bus-13	2,500,380.00	12,427 m^2	0.20
PV-4	Bus-29	2,500,380.00	12,427 m^2	0.20

5.5.2. Inverter Specification

In this study, the Huawei Sun2000-200KTL-H2 specified in Table 12 was used. The technical specifications of the inverter are obtained from the data sheet of Huawei Inverters Company (Technical Data - SUN2000-(196KTL-H0, 200KTL-H2, 215KTL-H0) User Manual - Huawei, 2022).

Table 12. Inverter Specification

Parameter	Value
Nominal AC Active Power	200 kW
Max. AC Apparent Power	215 kVA
Mac AC Active Power (cosφ=1)	215 kW
Output Voltage	800 V
Nominal Output Current	144.4 A
Max. Output Current	155.2 A

It is crucial to distinguish between the nominal power rating and the maximum power capacity of the inverter. The inverter model SUN2000-215KTL-H0 has a nominal power rating of 200 kW, but its maximum apparent power is 215 kVA, and its maximum active power is 215 kW at a unity power factor (cos φ = 1).

Although the inverter manufacturer has restricted the maximum power to 215 kVA, the inverter is capable of delivering 225.80 kVA at a voltage of 1.05 per unit due to voltage variations in the bus. However, at the request of the distribution system

operator, the inverters have been programmed to limit their power output to 215 kVA at a voltage of 1.00 (p.u.). Nevertheless, for the purposes of this study, the inverter is modeled as having a power capacity of 225.80 kVA at 1.05 (p.u.) voltage.

The power-reactive power (PQ) curve showing the power that can be obtained at the inverter's nominal, maximum, and minimum voltage levels is depicted in Figure 33.

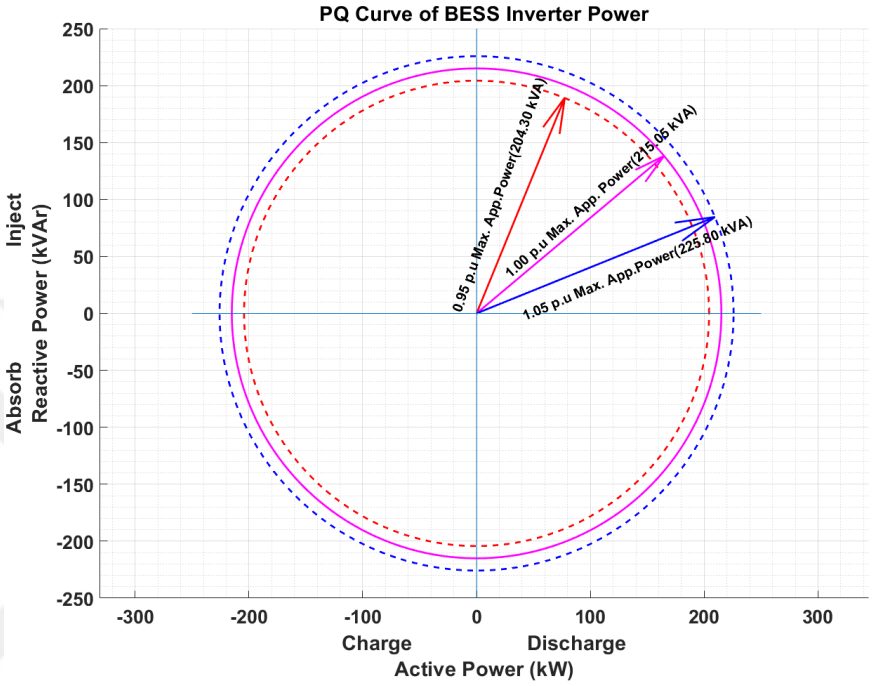

Figure 33. PQ Curve Change of BESS Inverter Power According to Bus Voltage

5.6. BESS and Inverter

The locations, capacities, and efficiencies of the BESS in the proposed system are provided in Table 13. The inverters used in the aforementioned PV system enable DC-to-AC conversion, and the converted AC power is then connected to the bus via an ideal lossless step-up transformer.

Table 13. BESS Parameters

Equipments	**Location**	**Max. Energy Capacity (MWh)**	**Charge Efficiency** (H. A. Taha et al., 2022)	**Discharge Efficiency** (H. A. Taha et al., 2022)	**Degradation Cost ($/kWh)** (H. A. Taha et al., 2022)
BESS-1	Bus-6	1	0.95	0.90	0.042
BESS-2	Bus-11	1	0.95	0.90	0.042
BESS-3	Bus-15	1	0.95	0.90	0.042
BESS-4	Bus-31	1	0.95	0.90	0.042

5.7. Voltage Limits

The voltage levels of the test system bus are generally treated as fixed constraints in the analysis. However, treating them as constraints leads to a system where all voltages are within permissible limits after optimization, suggesting the reduction of excess PV production or utilization of inverter reactive power capability by day-ahead EMS. One effective approach to address this scenario is by incorporating reactive power generation and consumption into the objective function while maintaining specified bus voltages within the desired voltage range.

The voltages at all nodes within the distribution grid networks must be maintained within a defined range. The acceptable voltage profile limits are well-established in international standards. This bus voltage constraint can be formulated as;

$$V^{min} \leq V_{(i)(t)} \leq V^{max} \qquad \forall t, i \quad (44)$$

V^{min} and V^{max} mean lower/upper permissible voltage limits in Eq. (44).

5.8. Penalty-Based Power Factor Limitation Approach

The rising deployment of distributed energy generation technologies, including PV and BESS, within electric distribution networks introduces a variety of new technical complexities.

Reactive power injections and absorptions through grid-connected loads, PV and BESS inverters can significantly reduce the real power demand at the distribution transformer center due to reactive power. This situation can also lead to unnecessary loading on the distribution lines.

This condition reduces the real power to reactive power ratio, exposing customers to low power factor penalties. Increasingly, the reactive power capabilities of inverters utilized in photovoltaic and battery energy storage systems have become crucial in regulating the real and reactive power flows within distribution networks.

The formulation of power factor calculation is given below:

$$\text{Power Factor} = \frac{P}{\sqrt{P^2 + Q^2}} \qquad (45)$$

Where P is total active power and Q is total reactive power. The key point is that the utilization of RES and BESS enables microgrids or distribution systems to sell energy to the grid. This can result in decreased operating costs or increased revenue. Furthermore, the active power P becomes negative in such scenarios, indicating that energy is being supplied to the grid rather than consumed from it.

The feasible region of the power factor, which illustrates the association between active and reactive power, is presented in Figure 34 (Hashmi et al., 2020, 2023).

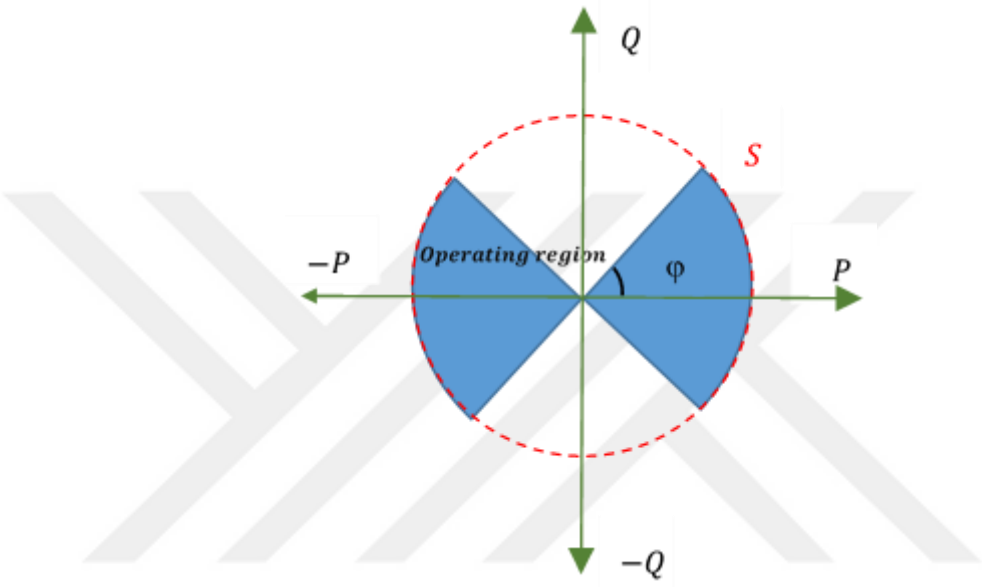

Figure 34. The Feasible Power Factor Range Without Reactive Power Penalty

The active and reactive power generated by the microgrid or distribution system can have a detrimental or beneficial impact on the power factor observed by the utility grid. To maintain the power factor within acceptable bounds, the following criteria must be satisfied.

$$-\tan\varphi \leq \frac{Q}{|P|} \leq \tan\varphi \tag{46}$$

The limits in the referenced Eq. (46) are presumed to be equivalent for both leading and lagging power factors. It is crucial to understand that the limitations outlined in this context are established by the distribution system operator, and these may differ different countries.

As long as customers stay within the limits set by system operators, they do not incur charges for reactive power. However, if they exceed those limits, they will be subject to a penalty fee for the reactive power they consume. The structure and formulation of the penalty function used in this study are illustrated in detail in Figure 35.

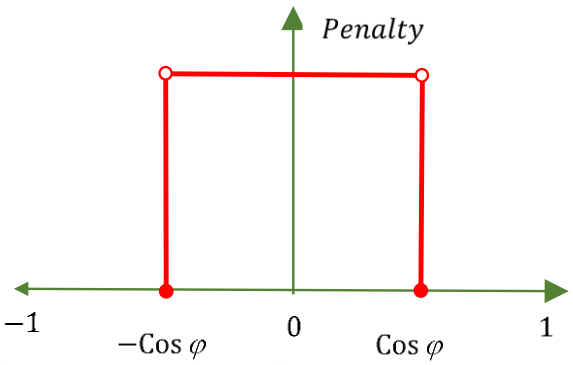

Figure 35. Penalty Function With Power Factor Variation

The penalty function for the power factor ($Cos\ \varphi$) is reformulated. The mathematical expression for this penalty function is provided in Eq. (47).

$$\begin{aligned}\text{Penalty Function} &= 180 - (90 \\ &+ \tan^{-1}(a_1.\left(\left|Cos\ \varphi_{(t)}\right|\right. \\ &\left. - Cos\ \varphi_{limit}\right).a_2)).\left(\frac{\left(\frac{\lambda_{(t)}^{pp}}{2}.Q^{GB}\right)}{180}\right)\end{aligned} \qquad \forall t \quad (47)$$

The relevant fitting parameters are denoted as a_1 and a_2. The active energy tariff obtained from the grid is represented by $\lambda_{(t)}^{pp}$, while the reactive power tariff is set at half of this value. Q^{GB} signifies the reactive power observed by the grid. The Energy Market Regulatory Authority (EPDK) in Türkiye has determined that the penalty rate for reactive power is equivalent to 50 % of the active power cost.

6. CHAPTER: MODELLING OPTIMAL DAY-AHEAD SCHEDULING OF MICROGRID WITH BATTERY ENERGY STORAGE AND PV SYSTEM CONSIDERING DYNAMIC TRANSFORMER MODEL

6.1. Introduction

BESS can serve various purposes in the electrical grid, such as mitigating the risk of renewable generation fluctuations, providing base load arbitrage, distribution system stability, and improving the quality of electric power services.

This dissertation makes key contributions to the existing literature by summarizing its findings as follows:

- The model incorporates the influence of voltage on load characteristics.
- This study underscores the reactive power compensation capabilities of inverters, an aspect that has been infrequently explored in the literature.
- This study proposes a technique that utilizes BESS and PV inverters to minimize the grid power consumption costs. It is recommended that modeling the inverters based on their current capabilities, rather than their power ratings, provides a more accurate approach, as the power capacities are limited by the semiconductor components in their designs.
- The optimization has incorporated the inverters' provision of necessary reactive power during operation to enhance the accuracy of the calculations.
- The life-time reduction cost associated with the reactive power consumption of inverters has been incorporated into the day-ahead energy management system.
- The losses in inverters due to apparent power are modeled as loads.
- The thermal model of the power transformer at the PCC in distribution system has been used to analyze the feasibility of operating the transformer above its rated power capacity while utilizing a lower-rated unit.

- The impact of the operational costs of BESS and PV systems on the overall operational performance of the distribution network has been examined.

This section presents the mathematical formulation of the day-ahead EMS. Rather than the traditional approach of modeling for the BESS and PV system based on their given power, the proposed approach utilizes current and voltage combinations to represent the energy balance, in contrast to the power-based representation of the equipment.

6.2. Objective Function Modeling

In a dynamically priced electricity market, the energy price fluctuates throughout the day. Consequently, with BESS, it is possible to purchase energy from the market when the price is low and store it. When the stored excess energy price is higher compared to other hours, this energy can then be sold back to the electricity market. The reactive power support provided by BESS and PV inverters enables voltage regulation, bar voltage control, and the prevention of voltage violations. Furthermore, line losses can also be reduced. In this study, the objective function is defined by considering the balance between constraints and conflicting objectives for the optimization analysis, requiring the microgrid operator to make the most suitable decisions. Constraints and conflicting objectives must be carefully considered to determine the most appropriate decisions for the optimization analysis.

The schematic diagram depicted in Figure 36 presents the architecture of the day-ahead EMS model implemented for the modified IEEE 33 under investigation, illustrating the interconnections between the input and output parameters.

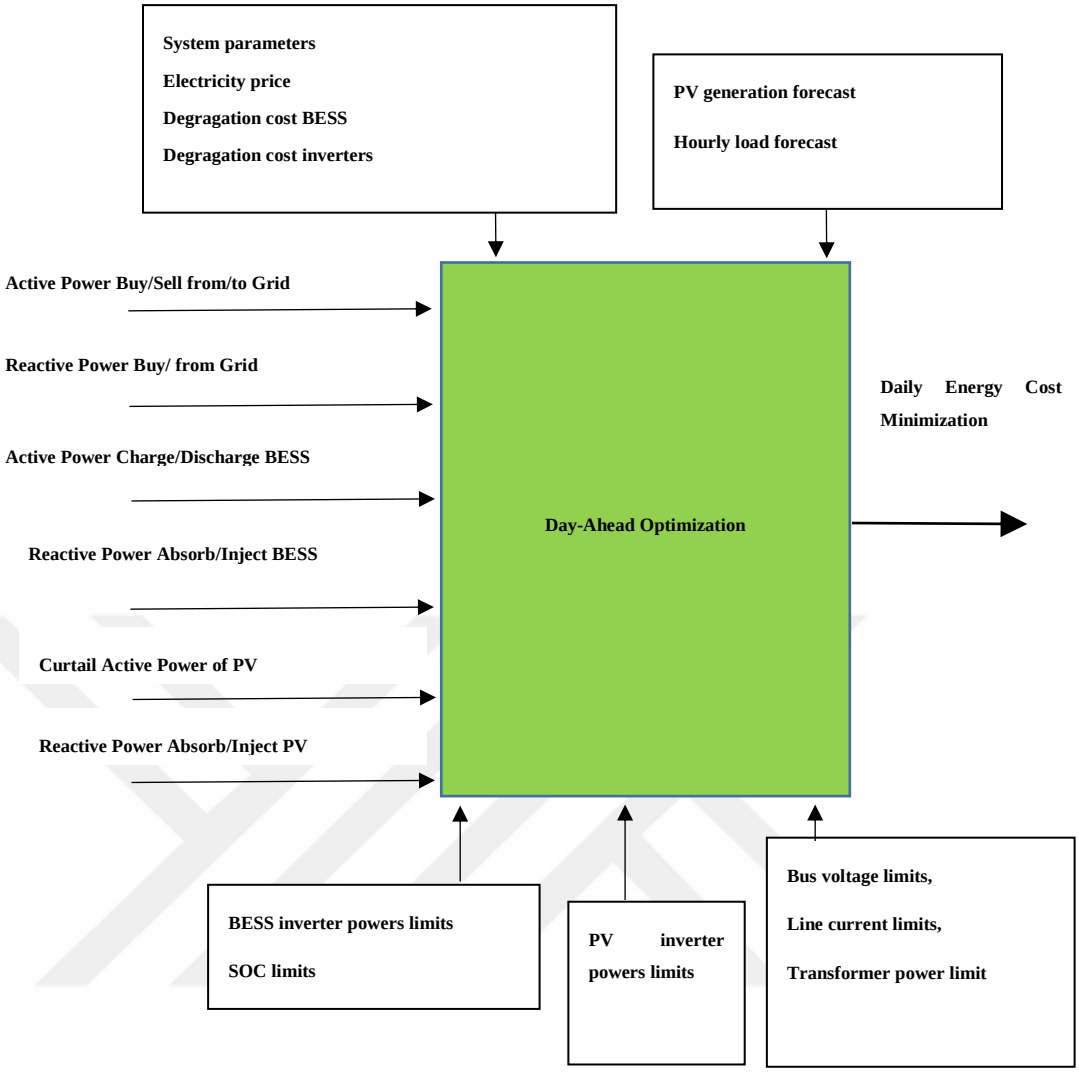

Figure 36. The Input and Output Scheme of Energy Management System

The following sections define the economic objectives, costs of PV and BESS, as well as associated constraints.

6.3. Model Assumptions

6.3.1. Background

Multiplying two complex numbers involves applying the distributive property and combining like terms. Complex numbers are typically expressed in the form $a + jb$, where a represents the real part and b represents the imaginary part. When multiplying two complex numbers:

Given two complex numbers:

$$S_1 = \underbrace{a + jb}_{rectangular\ form} = \underbrace{\mathrm{S1}\angle\theta_1}_{polar\ form} \tag{48}$$

$$\mathrm{a} = \underbrace{|\mathrm{S1}|\cos\theta_1}_{real\ component} \tag{49}$$

$$\mathrm{b} = \underbrace{|\mathrm{S1}|\sin\theta_1}_{imaginary\ component} \tag{50}$$

$$S_1 = \mathrm{S1}\cos\theta_1 + j\mathrm{S1}\sin\theta_1 \tag{51}$$

and

$$S_2 = c + jd = \mathrm{S2}\angle\theta_2 \tag{52}$$

$$c = |\mathrm{S2}|\cos\theta_2 \tag{53}$$

$$d = |\mathrm{S2}|\sin\theta_2 \tag{54}$$

$$S_2 = S2\cos\theta_2 + jS2\sin\theta_2 \tag{55}$$

If we multiply two numbers, the product $S_1.S_2$ is given by;

$$\mathrm{S1}\angle\theta_1.\mathrm{S2}\angle\theta_2 = |\mathrm{S1}|.|\mathrm{S2}|\angle(\theta_1 + \theta_2) \tag{56}$$

or, we can write as;

$$(a + jb).(c + jd) = (ac - bd) + j(ad + bc) \tag{57}$$

If $\theta_1 = 0$

$$S_1 = \underbrace{a + jb}_{rectangular\ form} = \underbrace{\mathrm{S1}\angle\theta_1}_{polar\ form} \tag{58}$$

$$S_1 = a + jb = \mathrm{S1}\angle 0 \tag{59}$$

$$a = |S1|\ \underbrace{cos\ 0}_{1} = S1 \tag{60}$$

$$b = |S1| \underbrace{sin\ 0}_{0} = 0 \tag{61}$$

S_1 is obtained as below;

$$S_1 = a + j0 \tag{62}$$

If we multiply two numbers, the product $S_1.S_2$ is given by:

$$\mathrm{S1}\angle\theta_1.\,\mathrm{S2}\angle\theta_2 = |\mathrm{S1}|.\,|\mathrm{S2}|\angle(\theta_1 + \theta_2) \tag{63}$$

$$(a + j\underbrace{b}_{0})\ x\ (c + jd) = (ac - \underbrace{bd}_{0}) + j\left(ad + \underbrace{bc}_{0}\right) \tag{64}$$

$$\mathrm{S1}\angle\theta_1.\,\mathrm{S2}\angle\theta_2 = \underbrace{a.c}_{real\ part} + j\ \underbrace{(a.d)}_{imaginary\ part} \tag{65}$$

Left side of above Eq. (65) is form as;

$$(\mathrm{S1}.\,\mathrm{S2})\angle(0 + \theta_2) = (\mathrm{S1}.\,\mathrm{S2})\angle\theta_2 \tag{66}$$

Transforming the equation's real and imaginary parts

$$|\mathrm{S1}|.\,|\mathrm{S2}|.\cos\theta_2 = \underbrace{a.c}_{real\ part} \tag{67}$$

$$|\mathrm{S1}|.\,|\mathrm{S2}|.\sin\theta_2 = \underbrace{(a.d)}_{imaginary\ part} \tag{68}$$

When we apply the approach to power calculation;

If $\mathrm{S1}\angle\theta_1$ is voltage magnitude and angle;

If $\mathrm{S2}\angle\theta_2$ is current magnitude and angle;

The powers are calculated as follows

Apparent power is;

$$\mathrm{S=V.I^*} \tag{69}$$

$$S = |S1|.|S2| \quad (70)$$

$$\text{Active power} = P = \text{re}(S) = S\cos(\theta_1 - \theta_2) \quad (71)$$

$$\text{Reactive Power} = Q = \text{Im}(S) = S\sin(\theta_1 - \theta_2) \quad (72)$$

If $\theta_1 = 0$;

$$S = S1\angle 0.\, S2\angle\theta_2 = |S1|.|S2|\angle(0 - \theta_2) = |S1|.|S2|\angle(-\theta_2) \quad (73)$$

$$P = \text{Re}(S) = |S1|.|S2|.\cos\theta_2 = a.c \quad (74)$$

$$Q = \text{Im}(S) = |S1|.|S2|.\sin\theta_2 = a.d \quad (75)$$

Where

a is real part of voltage,

b is imaginary part of voltage (assumed to be zero),

c is real part of current,

d is imaginary part of current.

The fact that the voltage angle is close to zero provides an advantage by providing ease of calculation by allowing us to get rid of trigonometric functions in power calculation. In this way, the calculation load and calculation time are reduced.

6.3.2. Demand Load Calculation

The simulation study assumes the test system loads conform to the exponential load model, specifically with an industrial load type. The relevant parameters α = 0.18 and β = 6 are employed in the calculations.

$$P_i = P_0\left(\frac{V_i}{V_0}\right)^{\alpha} \quad \forall i \quad (76)$$

$$Q_i = Q_0\left(\frac{V_i}{V_0}\right)^{\beta} \quad \forall i \quad (77)$$

$\bar{I}$ is complex vector of fundamental of the current. Re$\{\bar{I}\}$ is the real part of $\bar{I}$ and Im$\{\bar{I}\}$ is the imaginary part of $\bar{I}$. $\bar{I}$ is the magnitude of the vector.

$$\bar{I} = \sqrt{\text{Re}\{\bar{I}\}^{\,2} + \text{Im}\{\bar{I}\}^{\,2}} \tag{78}$$

Given that the real and imaginary parts of the current are mutually perpendicular, Kirchhoff's current law can be applied to each of these components independently.

$$I^{Load}_{Active(i),(t)} = \left(\frac{P_0 \left(\frac{V_{(i),(t)}}{V_0} \right)^{\alpha}}{\left| V_{(i),(t)} \right|} \right)^{*} \qquad \forall i, t \tag{79}$$

$$I^{Load}_{Reactive(i),(t)} = \left(\frac{Q_0 \left(\frac{V_{(i),(t)}}{V_0} \right)^{\beta}}{\left| V_{(i),(t)} \right|} \right)^{*} \qquad \forall i, t \tag{80}$$

The real component refers to the active current, which is the component of the current that is in phase with the voltage and produces real power. The imaginary component refers to the reactive current, which is the component of the current that is produces reactive power.

$$\begin{aligned} I^{Load}_{Apparent(i),(t)} &= (I^{Load}_{Active(i),(t)} + jI^{Load}_{Reactive(i),(t)}) \\ &= (I^{Load}_{Real(i),(t)} + jI^{Load}_{Imaginary(i),(t)}) \end{aligned} \tag{81}$$

6.3.3. BESS Power Calculation

The DC power generated by the battery bank is transformed into AC power through an inverter. The low-voltage power is then stepped up to the base voltage level required by the test system using a step-up transformer. Conversely, for the reverse energy flow, the high-voltage power from the grid is first stepped down to a suitable voltage level for storage, and then stored in battery banks via a rectifier.

In this study, the high-voltage side of the transformer is connected to the grid at a base voltage of 12.66 kV, while the low-voltage side is assumed to have the same voltage as the inverter output, which is 800 V. For the purposes of simplification, the

transformer is considered to be lossless and ideal. Additionally, as depicted in Figure 37, BESS can be connected to the grid through a step-up transformer.

The BESS can only store and provide active power through its battery bank. Nonetheless, the inverter integrated within the BESS allows for the injection or absorption of reactive power. The specific characteristics of the inverter's operational performance are elaborated upon in Section 3.2.

In contrast to the conventional approach of using power decision variables in BESS and inverter optimization, this study utilizes a current decision variable approach for calculations. With the current decision variable approach, four variables are employed in a BESS system, comprising the charging and discharging currents, along with their real and imaginary components. In a BESS, the net real part of the current is the absolute difference between the discharging and charging currents. Similarly, the net imaginary part is the absolute difference between the injection and absorption currents. These net real and imaginary currents represent the real and imaginary components that make up the overall current used by the power semiconductor parts of the inverter, and their vector sum determines the total inverter current.

Inverter has current-limited capacities due to their internal structures, in addition to having power capacity limits. Consequently, inverters have current operating limits based on the current they can supply or draw, necessitating current constraints. The representation for the current decision variable approach mentioned above is shown in Figure 37.

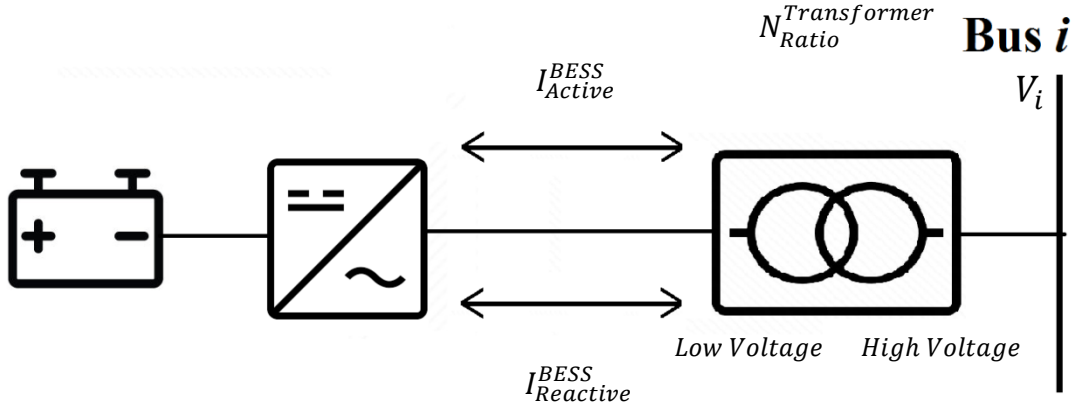

Figure 37. Schematic Drawing of a BESS, Power System Coupling and Currents Directions (Source: Author)

The current flowing through the inverter component of BESS can be represented by the equation shown in Eq. (82).

$$I^{BESS}_{(i),(t)} = \left(I^{BESS}_{Real(i),(t))} + jI^{BESS}_{Imaginary(i),(t)}\right) \qquad \forall t, i \quad (82)$$

The real and imaginary parts of the current can also be referred to as the active and reactive components of the current in Eq. (83).

$$I^{BESS}_{Apparent(i),(t)} = \left(I^{BESS}_{Active(i),(t)} + jI^{BESS}_{Reactive(i),(t)}\right) \qquad \forall t, i \quad (83)$$

The real part or active component of the current can be determined by the absolute difference between the discharging and charging components

$$I^{BESS}_{Real(i),(t)} = I^{BESS}_{Active(i),(t)} = (I^{Discharge}_{p(i),(t)} - I^{Charge}_{p(i),(t)}) \qquad \forall t, i \quad (84)$$

An important point to note is that charging and discharging cannot occur simultaneously. In the discharging mode, the active power of the I^{BESS}_{Real} is a positive value, while in the charging mode, it is a negative value.

Using a similar approach, the imaginary component of the current, which represents the reactive component, can also operate in either the inject or absorb mode of reactive current.

$$I^{BESS}_{Imaginary(i),(t)} = I^{BESS}_{Reactive(i),(t)} = (I^{Inject}_{q(i),(t)} - I^{Absorb}_{q(i),(t)}) \qquad \forall t, i \quad (85)$$

The phasor representation of the current in the inverter of the BESS is provided by Eq.(86).

$$I^{BESS}_{Apparent(i),(t)} = I^{BESS}_{Apparent(i),(t)} \angle \theta^{BESS}_{I} \qquad \forall t, i \quad (86)$$

Where θ^{BESS}_{I} represents the phase angle between the real and imaginary components of the current. The real part of the inverter current is calculated using the relevant Eq. (87).

$$I^{BESS}_{Active(i),(t)} = I^{BESS}_{Apparent(i),(t)}.Cos(\theta^{BESS}_{I}) \qquad \forall t, i \quad (87)$$

The imaginary component of the inverter current can be calculated using the associated Eq. (88).

$$I^{BESS}_{Reactive(i),(t)} = I^{BESS}_{Apparent(i),(t)}.Sin(\theta^{BESS}_{I}) \qquad \forall t,i \quad (88)$$

The active power at the point of connection can be determined using Eq. (89).

$$P_{BESS(i),(t)} = \sqrt{3}.\left|V^{BESS}_{Bus(i),(t)}\right|.\left|I^{BESS}_{Apparent(i),(t)}\right|.Cos(\theta^{BESS}_{V} - \theta^{BESS}_{I}).N^{transformer}_{ratio} \qquad \forall t,i \quad (89)$$

Where $N^{Transformer}_{Ratio}$ is the cuurent conversion ratio of the step-up transformer. The voltage angle of the bus to which BESS is connected is denoted as θ^{BESS}_{V}.

The power of the charging at the bus connected to the BESS can be derived from the aforementioned equations and can be determined using the current and voltage parameters as Eq. (90).

$$P^{Charge}_{BESS(i),(t)} = \sqrt{3}.\left|V^{BESS}_{Bus(i),(t)}\right|.\left|(I^{Charge}_{p(i),(t)} + jI^{BESS}_{Reactive(i),(t)})\right|.Cos(\theta^{BESS}_{V} - \theta^{BESS}_{I}).N^{Transformer}_{Ratio} \quad (90)$$

I^{Charge}_{p} is the real component of the current in the charging mode. $I^{BESS}_{Reactive}$ is the imaginary part of the current, which can either be in the inject or absorb mode.

The discharging power can be calculated using Eq. (91).

$$P^{Discharge}_{BESS(i),(t)} = \sqrt{3}.\left|V^{BESS}_{Bus(i),(t)}\right|.\left|(I^{Discharge}_{p(i),(t)} + jI^{BESS}_{Reactive(i),(t)})\right|.Cos(\theta^{BESS}_{V} - \theta^{BESS}_{I}).N^{Transformer}_{Ratio} \qquad \forall t,i \quad (91)$$

The reactive power at the terminal can be calculated using a similar calculation approach as described Eq. (92).

$$Q_{BESS(i),(t)} = \sqrt{3}\left|V^{BESS}_{Bus(i),(t)}\right|.\left|I^{BESS}_{Apparent(i),(t)}\right|.Sin(\theta^{BESS}_{V} - \theta^{BESS}_{I}).N^{Transformer}_{Ratio} \qquad \forall t,i \quad (92)$$

The reactive power supplied to the grid can be determined using the current components, as detailed in the Eq. (93).

$$Q_{BESS(i),(t)}^{Inject} = \sqrt{3}.\left|V_{Bus(i),(t)}^{BESS}\right|.\left|(I_{Active(i),(t)}^{BESS} + jI_{p(i),(t)}^{Inject})\right|.Sin(\theta_V^{BESS} - \theta_I^{BESS}).N_{Ratio}^{Transformer} \quad \forall t,i \quad (93)$$

Where I_{Active}^{BESS} can operate in charging or discharging modes.

The reactive power consumed from the electrical grid by the BESS inverter can be calculated using Eq. (94).

$$Q_{BESS(i),(t)}^{Absorb} = \sqrt{3}.\left|V_{Bus(i),(t)}^{BESS}\right|.\left|(I_{Active(i),(t)}^{BESS} + jI_{p(i),(t)}^{Absorb})\right|.Sin(\theta_V^{BESS} - \theta_I^{BESS}).N_{Ratio}^{Transforme} \quad \forall t,i \quad (94)$$

In low-voltage grid systems, the voltage angle at the bus can be approximated as zero, as the angle of the voltage is negligible compared to the angle of the current ($\theta_V^{BESS} \ll \theta_i^{BESS}$).

To simplify the computation and facilitate the solution, it may be beneficial to avoid trigonometric calculations involving sine and cosine functions.

Assuming θ_V^{BESS} is approximately zero, the power of the BESS at the terminal in discharge mode can be expressed as:

$$P_{BESS(i),(t)}^{Discharge} = \sqrt{3}.\left|V_{Bus(i),(t)}^{BESS}\right|.\left|(I_{p(i),(t)}^{Discharge} + jI_{Reactive(i),(t)}^{BESS})\right|.Cos(0 - \theta_i^{BESS}).N_{Ratio}^{Transformer} \quad \forall t,i \quad (95)$$

This allows us to obtain $P_{BESS}^{Discharge}$ and $P_{BESS}^{Discharge}$, which can then be reformulated accordingly.

$$P_{BESS(i),(t)}^{Discharge} = \sqrt{3}.\left|V_{Bus(i),(t)}^{BESS}\right|.\left|I_{p(i),(t)}^{Discharge}\right|.N_{Ratio}^{Transformer} \quad \forall t,i \quad (96)$$

Also P_{BESS}^{Charge} can be reformulated as follow:

$$P_{BESS(i),(t)}^{Charge} = \sqrt{3}.\left|V_{Bus(i),(t)}^{BESS}\right|.\left|I_{p(i),(t)}^{Charge}\right|.N_{Ratio}^{Transformer} \quad \forall t,i \quad (97)$$

The active power at the bus connected to the BESS can be calculated as the product of the current and voltage magnitudes in radial distribution networks when using the proposed $P_{BESS}^{Discharge}$ and P_{BESS}^{Charge}.

Similar approach is applied for reactive power.

$$Q_{BESS(i),(t)}^{Inject} = \sqrt{3}.\left|V_{Bus(i),(t)}^{BESS}\right|.\left|I_{Apparent(i),(t)}^{BESS}\right|.Sin\left(\theta_V^{BESS} - \theta_i^{BESS}\right).N_{Ratio}^{Transformer} \quad \forall t,i \quad (98)$$

$$Q_{BESS(i),(t)}^{Inject} = \sqrt{3}.\left|V_{Bus(i),(t)}^{BESS}\right|.\left|(I_{Active(i),(t)}^{BESS} + jI_{q(i),(t)}^{Inject})\right|.Sin\left(\theta_V^{BESS} - \theta_i^{BESS}\right).N_{Ratio}^{Transformer} \quad \forall t,\text{i} \quad (99)$$

$$\theta_V^{BESS} \ll \theta_i^{BESS} \text{ and } \theta_V^{BESS} \approx 0$$

$$Q_{BESS(i),(t)}^{Inject} = \sqrt{3}.\left|V_{Bus(i),(t)}^{BESS}\right|.\left|I_{q(i),(t)}^{Inject}\right|.Sin\left(0 - \theta_i^{BESS}\right).N_{Ratio}^{Transformer} \quad \forall t,i \quad (100)$$

$$Q_{BESS(i),(t)}^{Inject} = \sqrt{3}.\left|V_{Bus(i),(t)}^{BESS}\right|.\left|I_{q(i),(t)}^{Inject}\right|.N_{Ratio}^{Transformer} \quad \forall t,i \quad (101)$$

The reactive power injected into the distribution network by the inverter integrated into the BESS can be calculated using the Eq. (101).

The reactive power absorbed from the distribution network by the inverter integrated in the BESS can be calculated using a similar calculation approach in Eq. (102) and (103).

$$Q_{BESS(i),(t)}^{Absorb} = \sqrt{3}.\left|V_{Bus(i),(t)}^{BESS}\right|.\left|I_{q(i),(t)}^{Absorb}\right|.Sin\left(0 - \theta_i^{BESS}\right).N_{Ratio}^{Transformer} \quad \forall t,i \quad (102)$$

$$Q_{BESS(i),(t)}^{Absorb} = \sqrt{3}.\left|V_{Bus(i),(t)}^{BESS}\right|.\left|I_{q(i),(t)}^{Absorb}\right|.N_{Ratio}^{Transformer} \quad \forall t,i \quad (103)$$

6.3.4. PV Power Calculation

Analogous to the BESS power calculation method discussed earlier, power calculation can also be applied to the PV system. The first distinction between power calculations for PV systems and BESS systems is that PV systems do not have a charging component for active power. Nonetheless, the approach for calculating reactive power capability remains the same

Another key difference is that the PV system must avoid generating excess power that exceeds technical constraints like voltage limits at the bus. In such cases, the PV system adjusts its output to prevent violations by curtailing the generation current.

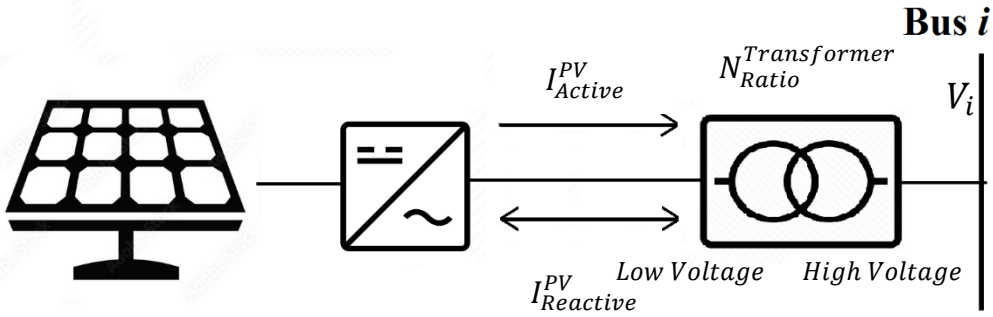

Figure 38. Schematic Illustration of a PV System, Power System Coupling and Currents Directions (Source: Author)

The current in the inverter within the PV can be expressed as in Eq. (104).

$$I^{PV} = \left(I^{PV}_{Real} + jI^{PV}_{Imaginary}\right) \tag{104}$$

The real and reactive components of the current can also be characterized as the active and imaginary parts of the current in Eq. (105).

$$I^{PV}_{Apparent} = (I^{PV}_{Active} + jI^{PV}_{Reactive}) \tag{105}$$

The real part or active component of the current can be expressed as the absolute difference between the available and curtailed components.

$$I^{PV}_{Real(i),(t)} = I^{PV}_{Active(i),(t)} = I^{Available}_{p(i),(t)} - I^{Curtail}_{p(i),(t)} \qquad \forall t, i \tag{106}$$

It is crucial to ensure that the curtailed current does not exceed the available current. Therefore, I^{PV}_{Real} is always zero or greater than zero.

Similar to the reactive approach in BESS, the reactive component of the current can also operate in either inject or absorb mode.

$$I^{PV}_{Imaginary(i),(t)} = I^{PV}_{Reactive(i),(t)} = I^{Inject}_{q(i),(t)} - I^{Absorb}_{q(i),(t)} \qquad \forall t, i \tag{107}$$

The phasor form of the current flowing through the inverter component of the PV system is provided in the Eq. (108).

$$I^{PV}_{Apparent(i),(t)} = I^{PV}_{Apparent(i),(t)} \angle \theta^{PV}_{I} \qquad \forall t, i \quad (108)$$

Where θ^{PV}_{I} represents the angle between the real and imaginary parts of the current. The real part of the inverter current is obtained by applying Eq. (109), which provides a mathematical expression to calculate the real component of the inverter current.

$$I^{PV}_{Active(i),(t)} = I^{PV}_{Apparent(i),(t)}. Cos(\theta^{PV}_{I}) \qquad \forall t, i \quad (109)$$

The imaginary part of the inverter current is obtained by applying Eq. (110), which determines the reactive power component of the current flowing through the inverter.

$$I^{PV}_{Reactive(i),(t)} = I^{PV}_{Apparent(i),(t)}. Sin(\theta^{PV}_{I}) \qquad \forall t, i \quad (110)$$

The active power at the bus can be calculated using the Eq.(111), where the active power is given by the product of the voltage, the current, and the cosine of the phase angle between the voltage and current.

$$P_{PV(i),(t)} = \sqrt{3}. \left|V^{PV}_{Bus(i),(t)}\right|. \left|I^{PV}_{Apparent(i),(t)}\right|. Cos(\theta^{PV}_{V} - \theta^{PV}_{I}). N^{Trar}_{Ratic} \; \forall t, i \quad (111)$$

Where the current conversion ratio $N^{transformer}_{ratio}$ of the step-up transformer is used to increase the voltage from the inverter to the desired level for the power grid.

θ^{PV}_{V} represents the voltage angle of the bus connected to the PV system. Using the equations provided above, the power output of the PV system that is injected into the grid at the bus connected from the PV array can be calculated by utilizing the current and voltage obtained from Eq. (112).

$$P_{PV(i),(t)} = \sqrt{3}. \left|V^{PV}_{Bus(i),(t)}\right|. \left|(I^{PV}_{Active(i),(t)} + jI^{PV}_{Reactive(i),(t)})\right|. Cos(\theta^{PV}_{V} - \theta^{PV}_{I}). N^{Transformer}_{Ratio} \qquad \forall t \quad (112)$$

The real component of the current is represented by I^{PV}_{Active} while the imaginary part is denoted as $I^{PV}_{Reactive}$. The reactive power at the bus can be calculated using a similar calculation approach as described in Eq. (113).

$$Q_{PV(i),(t)} = \sqrt{3}.\left|V^{PV}_{Bus(i),(t)}\right|.\left|I^{PV}_{Apparent(t)}\right|.Sin(\theta^{PV}_{V} - \theta^{PV}_{I}).N^{Transformer}_{Ratio} \quad \forall t,i \quad (113)$$

The reactive power supplied to the grid can be calculated in terms of the current components, as expressed in the corresponding Eq. (114).

$$Q^{Inject}_{PV(i),(t)} = \sqrt{3}.\left|V^{PV}_{Bus(i),(t)}\right|.\left|(I^{PV}_{Active(i),(t)} + jI^{Inject}_{p(i),(t)})\right|.Sin(\theta^{PV}_{V} - \theta^{PV}_{I}).N^{Transformer}_{Ratio} \quad \forall t,i \quad (114)$$

The reactive power consumed from the utility grid by the PV inverter can be computed using the Eq. (115).

$$Q^{Absorb}_{PV(i),(t)} = \sqrt{3}.\left|V^{PV}_{Bus(i),(t)}\right|.\left|(I^{PV}_{Active(i),(t)} + jI^{Absorb}_{p(i),(t)})\right|.Sin(\theta^{PV}_{V} - \theta^{PV}_{I}).N^{Transformer}_{Ratio} \quad \forall t,\text{i} \quad (115)$$

In low-voltage or medium-voltage power systems, the voltage angle at the bus can be considered negligible compared to the current angle ($\theta^{PV}_{V} \ll \theta^{PV}_{i}$), allowing it to be approximated as zero. Reducing the complexity of the computational methods can facilitate the problem-solving process. To this end, it may be beneficial to refrain from employing trigonometric calculations that require the use of sine and cosine functions.

Assuming θ^{PV}_{V} is approximately equal to zero, the power output of the photovoltaic system at the point of coupling can be expressed mathematically as:

$$P^{Net}_{PV(i),(t)} = \sqrt{3}.\left|V^{PV}_{Bus(i),(t)}\right|.\left|((I^{Available}_{p(i),(t)} - I^{Curtail}_{p(i),(t)}) + jI^{PV}_{Reactive(i),(t)})\right|.Cos(0 - \theta^{PV}_{i}).N^{Transformer}_{Ratio} \quad \forall t,i \quad (116)$$

Then, we can achieve P^{Net}_{PV}. The formulation of P^{Net}_{PV} can be revised as follows:

$$P^{Net}_{PV(i),(t)} = \sqrt{3}.\left|V^{PV}_{Bus(i),(t)}\right|.\left|(I^{Available}_{p(i),(t)} - I^{Curtail}_{p(i),(t)})\right|.N^{Transformer}_{Ratio} \quad \forall t,i \quad (117)$$

Also $P^{Available}_{PV}$ can be reformulated as follow:

$$P^{Available}_{PV(i),(t)} = \sqrt{3}.\left|V^{PV}_{Bus(i),(t)}\right|.\left|I^{Available}_{p(i),(t)}\right|.N^{Transformer}_{Ratio} \quad \forall t,i \quad (118)$$

And also, $P_{PV}^{curtail}$ can be reformulated as follow:

$$P_{PV(i),(t)}^{Curtail} = \sqrt{3}.\left|V_{Bus(i),(t)}^{PV}\right|.\left|I_{p(i),(t)}^{Curtail}\right|.N_{Ratio}^{Transformer} \qquad \forall t,i \quad (119)$$

The active power at the point of interconnection for the PV system can be determined by multiplying the magnitudes of the current and voltage within the distribution network, utilizing the proposed P_{PV}^{net} , $P_{PV}^{Available}$ and $P_{PV}^{Curtail}$ approaches.

A similar technique is utilized for reactive power.

$$Q_{PV(i),(t)}^{Inject} = \sqrt{3}.\left|V_{Bus(i),(t)}^{PV}\right|.\left|I_{Apparent(i),(t)}^{PV}\right|.Sin(\theta_V^{PV} - \theta_i^{PV}).N_{Ratio}^{Transformer} \qquad \forall t,i \quad (120)$$

$$Q_{PV(i),(t)}^{Inject} = \sqrt{3}.\left|V_{Bus(i),(t)}^{PV}\right|.\left|(I_{Active(i),(t)}^{PV} + jI_{q(i),(t)}^{Inject})\right|.Sin(\theta_V^{PV} - \theta_i^{PV}).N_{Ratio}^{Transformer} \qquad \forall t,i \quad (121)$$

$$\theta_V^{PV} \ll \theta_i^{PV} \text{and } \theta_V^{PV} \approx 0$$

$$Q_{PV(i),(t)}^{Inject} = \sqrt{3}.\left|V_{Bus(i),(t)}^{PV}\right|.\left|I_{q(i),(t)}^{Inject}\right|.Sin(0 - \theta_i^{PV}).N_{Ratio}^{Transformer} \qquad \forall t,i \quad (122)$$

$$Q_{PV(i),(t)}^{Inject} = \sqrt{3}.\left|V_{Bus(i),(t)}^{PV}\right|.\left|I_{q(i),(t)}^{Inject}\right|.N_{Ratio}^{Transformer} \qquad \forall t,i \quad (123)$$

The reactive power injected into the distribution network can be calculated by using the voltage of the bus to which the inverter, integrated into the PV system, is connected and the reactive component of the inverter current by Eq. (123).

$$Q_{PV(i),(t)}^{Absorb} = \sqrt{3}.\left|V_{Bus(i),(t)}^{PV}\right|.\left|I_{q(i),(t)}^{Absorb}\right|.Sin(0 - \theta_i^{PV}).N_{Ratio}^{Transformer} \qquad \forall t,i \quad (124)$$

$$Q_{PV(i),(t)}^{Absorb} = \sqrt{3}.\left|V_{Bus(i),(t)}^{PV}\right|.\left|I_{q(i),(t)}^{Absorb}\right|.N_{ratio}^{transformer} \qquad \forall t,i \quad (125)$$

The reactive power absorbed from the distribution network can be calculated by using the voltage of the bus to which the inverter, integrated into the PV system, is connected and the reactive component of the inverter current by Eq. (125).

6.3.5. Inverter Loss Calculation

It is discussed in Chapter 3 that inverters require active power due to the reactive power they produce. The required active power is obtained from the connected grid, which is sometimes sourced from PV production and other times purchased from the grid. Consequently, an inverter loss is modeled as an active load, and the current drawn from the grid depends on the voltage of the grid-connected bus.

The total number of PV and BESS inverters considered in the study corresponds to the number of inverters for which losses are calculated in Eq. (126). These losses can be expressed in terms of load currents in Eq. (127).

$$P_{Inverter\ Loss(t)} = \sum_{m=1}^{M=Number\ of\ BESS\ inverter} P^{BESS}_{Inverter\ Loss(t)} + \sum_{k=1}^{K=Number\ of\ PV\ inverter} P^{PV}_{Inverter\ Loss(t)} \quad \forall t, m, k \quad (126)$$

$$I_{invloss(t)} = \left(\frac{(P_{invloss(t)} + i0)}{V_{i(t)}}\right)^{*} \quad \forall t, i \quad (127)$$

6.3.6. Bus Power Calculation

The provided calculations depict a single-line diagram that shows the active and reactive components of loads, PV, BESS, and losses in Figure 39. If there is a PV system and load connected to a bus, the powers affecting that bus are modeled as the active and reactive power of the PV system, the active and reactive components of the load, and the active losses of the inverter. This equivalent model is then incorporated into the power flow calculation and solved through optimization. This approach is applied across all buses, with separate matrices created for each piece of equipment to solve the optimization problem.

These matrices encompass the load, PV, and BESS matrices, as well as the inverter loss matrix. While the former three matrices incorporate both active and reactive components, the inverter loss matrix is exclusively represented as active power loss.

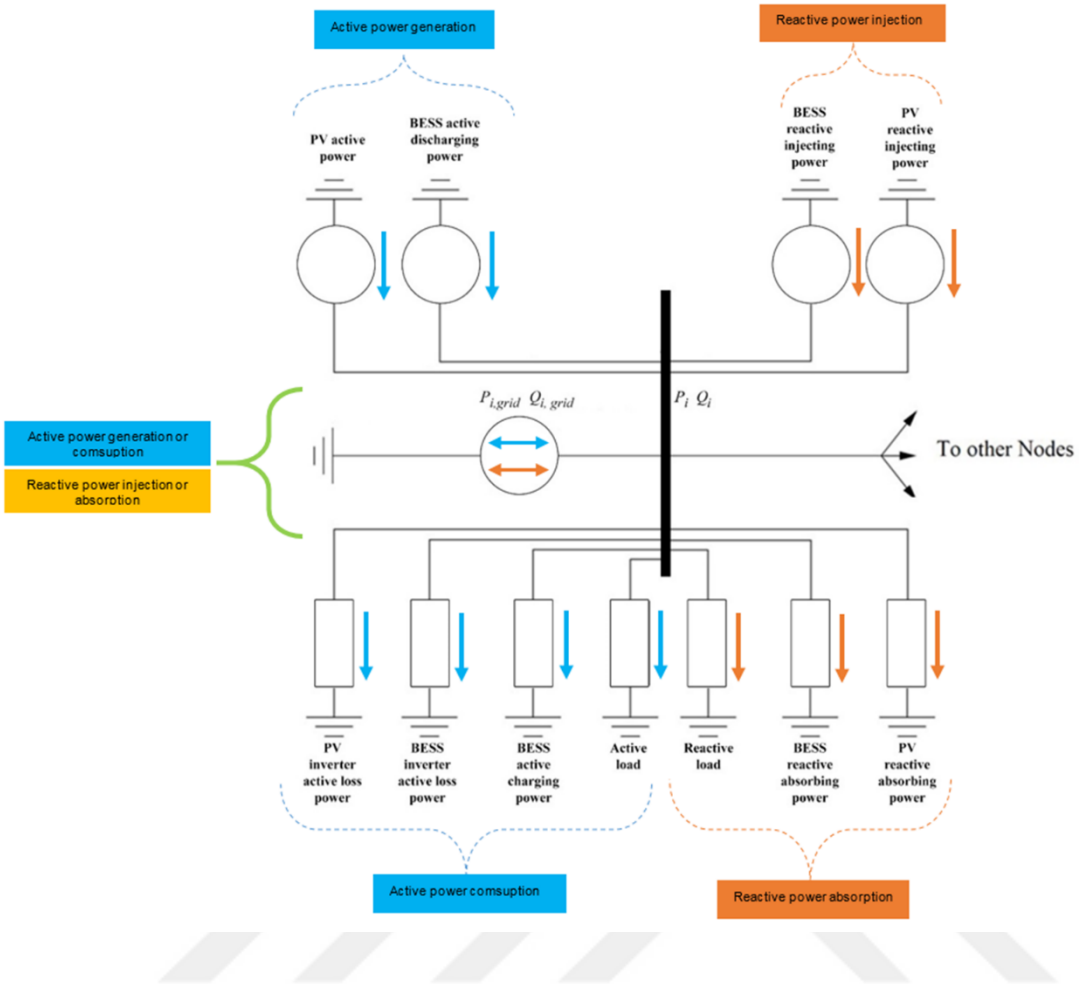

Figure 39. The Equivalent Circuit Diagram of Bus Equipment (Source: Author)

6.4. The Matrix Formulation of Problem

The model presented in the dissertation is more advantageous and efficient for solving an optimization problem by formulating it in matrix form and implementing it through computer algorithms. Consequently, the vector of decision variables necessary for the solution, denoted as vector X, can be constructed by partitioning it into three parts in Eq. (128).

$$X = [X_{grid};\ X^{M\ BESS}_{inverter\&\ battery};\ X^{K\ PV}_{PV}]$$

Where;

$$X_{grid} = \begin{bmatrix} P^{t}_{Grid_{purchase\ active}}(1:N) \\ P^{t}_{Grid_{sell\ active}}(1:N) \\ Q^{t}_{Grid_{purchase\ reactive}}(1:N) \\ Q^{t}_{Grid_{sell\ reactive}}(1:N) \end{bmatrix}$$

$$X^{K\ BESS}_{inverter\&\ battery} = \begin{bmatrix} I^{1,t}_{discharge_{real}}(1:N) \\ I^{1,t}_{charge_{real}}(1:N) \\ E^{1,t}_{Battery\ energy}(1:N) \\ I^{1,t}_{inject_{imaginary}}(1:N) \\ I^{1,t}_{absorb_{imaginary}}(1:N) \\ \vdots \\ I^{K,t}_{discharge_{real}}(1:N) \\ I^{K,t}_{charge_{real}}(1:N) \\ E^{K,t}_{Battery\ energy}(1:N) \\ I^{K,t}_{inject_{imaginary}}(1:N) \\ I^{K,t}_{absorb_{imaginary}}(1:N) \end{bmatrix} \quad (128)$$

$$X^{M\ PV}_{PV} = \begin{bmatrix} I^{1,\mathrm{t}}_{PV\ curtail_{real}}(1:N) \\ I^{1,\mathrm{t}}_{inject\ imaginary}(1:N) \\ I^{1,\mathrm{t}}_{absorb\ imaginary}(1:N) \\ \vdots \\ I^{\mathrm{M,t}}_{PV\ curtail_{real}}(1:N) \\ I^{\mathrm{M,t}}_{inject\ imaginary}(1:N) \\ I^{\mathrm{M,t}}_{absorb\ imaginary}(1:N) \end{bmatrix}$$

Elements presented in braces are one-dimensional arrays; those with indices are N×1 vectors, where the M and K indices denote the BESS system and PV system, respectively.

The components of the vector X_{grid} are real-valued quantities denoting the active and reactive power levels. Likewise, the elements of the vector $X^{K'th\ BESS}$ represent the electric currents in the BESS inverter as well as the stored energy of the BESS.

The elements in vector X_{PV} are real numbers, which represent the currents in the PV systems. Furthermore, X_{grid} is (4N) x 1 vectors, $X_{inverter\&\ battery}$ is (5N x K) x 1

vectors, X_{PV} is (3N x M) x 1 vectors. The solution vector consists of N (4+5K+3M) variables that need to be determined through the optimization process.

In this study, an optimization model is created using 24 time steps over one day, as there are four BESS and four PV systems and a time step of 1 hour is chosen. To solve the optimization problem, 24 x (4 + (5 x 4) + (3 x 4)) = 864 decision variables are needed.

6.5. Optimization Technique

Developing an appropriate solution scheme is a crucial aspect of day-ahead energy management system planning. The objective function under investigation is a nonlinear programing (NLP) problem that is solved using the "fmincon" function in MATLAB.

The fundamental nonlinear programming solver (fmincon) programming structure is as follows:

$$\min_{x} f(x) \tag{129}$$

$$\text{Subject to } \begin{cases} c(x) \leq 0 \\ ceq(x) \leq 0 \\ A.x \leq b \\ A_{eq}.x = b_{eq} \\ lower\_b \leq x \leq upper\_b \end{cases} \tag{130}$$

The constrained optimization problem is defined by the linear inequality constraints characterized by the matrix A and vector b, as well as the linear equality constraints given by the matrix A_{eq} and vector b_{eq}. Additionally, the problem is bounded by the lower and upper limits specified in the vectors $lower\_b$ and $upper\_b$, respectively. The objective function and constraint functions can take on nonlinear forms, represented by $c(x)$ and $ceq(x)$.

6.5.1. Objective Function

The objective function aims to minimize the cost of active energy procured from the grid while maximizing the sale of active energy to the grid in Eq. (132). Additionally, it seeks to minimize the aging costs associated with the charging and discharging cycles of the BESS deployed in the system in Eq. (133). Furthermore, the objective

function aims to reduce the lifetime reduction costs resulting from the reactive power usage of the inverters in the BESS and PV systems in Eq. (134) and Eq. (135). Another cost consideration is the penalty function, which aims to maintain the power factor at the grid connection point within specified limits in Eq. (136). In the event of limit violations, the penalty involves charging or discharging reactive energy from or to the grid at half the price of purchasing active energy. The main subject is to maintain the active and reactive energy balance of the test system by leveraging the inverters in the system to offset it and alternatively, to procure energy from the grid at lower costs and without violating constraints.

$$min\ (F) = C_{Grid}^{Cost} + C_{BESS}^{DegraCost} + C_{BESS}^{Inverter\ Cost} + C_{PV}^{Inverter\ Cost} + C_{reactive\ power}^{Penalty\ Cost} \quad (131)$$

$$C_{Grid}^{Cost} = \Delta t. \sum_{t=1}^{T} (\underbrace{\underbrace{P_{(t)}^{GB}.\lambda_{(t)}^{pp}}_{cost}}_{Active\ Grid\ Purchase} - \underbrace{\underbrace{P_{(t)}^{GS}.\lambda_{(t)}^{SP}}_{revenue}}_{Active\ Grid\ Sell}) \quad \forall t \quad (132)$$

$$C_{BESS}^{DegraCost} = \Delta t. \sum_{t=1}^{T} \sum_{k=1}^{K_{BESS}} \underbrace{(P_{(t)}^{BC}.\beta_{CC} + P_{(t)}^{BD}.\beta_{DC})}_{cost} \quad \forall t, k \quad (133)$$

$$C_{BESS}^{Inveter\ Cost} = \Delta t. \sum_{t=1}^{T} \sum_{k=1}^{K_{BESS}} (\eta^{LR,1}.Q_{(t)}^{BESSInverter} + \eta^{LR,2}.(Q_{(t)}^{BESSInverter})^2 + \eta^{LR,3}.(Q_{(t)}^{BESSInverter})^3) \quad \forall t, k \quad (134)$$

$$C_{PVs}^{Inverter\ Cost} = \Delta t. \sum_{t=1}^{T} \sum_{m=1}^{M_{PV}} (\eta^{LR,1}.Q_{(t)}^{PVInverter} + \eta^{LR,2}.(Q_{(t)}^{PVInverter})^2 + \eta^{LR,3}.(Q_{(t)}^{PVInverter})^3) \quad \forall t, m \quad (135)$$

$$C_{Reactive\ Power}^{Penatly\ Cost} = 180 - (90 + \tan^{-1}(a_1.(\left|Cos\varphi_{(t)}\right| - Cos\varphi_{limit}).a_2)).\left(\frac{\left(\frac{\lambda_{(t)}^{pp}}{2}.Q^{GB}\right)}{180}\right) \quad \forall t \quad (136)$$

6.5.2. Constraints

Ensuring the stability and balance of the system necessitates meeting certain constraints while minimizing the objective function mentioned above. These constraints involve maintaining the balance of active and reactive energy, keeping the voltages at the selected buses within limits, preserving the energy balance of the BESS, and operating the PV and BESS inverters within the specified limits provided by their specifications.

6.5.2.1 Active Power Balance

The active power balance ensures that, for each time step '*t'* in the optimization model, the energy obtained from or sold to the grid equals the self-production and consumption powers of the test system. This constraint must be satisfied for all time instances in the optimization.

The key point is to emphasize the modeling of losses in the lines, BESS charging power, and inverter losses as loads, while BESS discharging and PV generation are modeled as negative loads. Additionally, the loads at buses are modeled as voltage-dependent. The active power balance of the distribution network is given in Eq. (137).

$$\underbrace{\underbrace{P_{(t)}^{GB}}_{Grid\ Purchase}}_{Desicion\ Variable} - \underbrace{\underbrace{P_{(t)}^{GS}}_{Grid\ Sell}}_{Decision\ Variable}$$

$$= \underbrace{\sum_{Load} P_i^{BusLoad} \left(\frac{V_i}{V_0}\right)^{\alpha}}_{nonlinear\ term}$$

$$+ \underbrace{\sum_{t=1}^{T} \sum_{Branch=1}^{Number\ of\ Branch} \underbrace{r^{ij}.(I_{(t)}^{ij})^2}_{Active\ Power\ Line\ Loss}}_{nonlinear\ term} \qquad \forall t, i, j \quad (137)$$

$$+ \underbrace{\sum_{Loss} P_{(t)}^{PVinverterloss}}_{nonlinear\ term} + \underbrace{\sum_{Loss} P_{(t)}^{BESSinverterloss}}_{nonlinear\ term}$$

$$+ \underbrace{\sum_{BESS} P_{BESS}^{Charge}}_{nonlinear\ term} - \underbrace{\sum_{BESS} P_{BESS}^{Discharge}}_{nonlinear\ term} - \underbrace{\sum_{PV} P_{PV}^{Net}}_{nonlinear\ term}$$

The right-hand side of the Eq. (137) contains numerous nonlinear terms derived from current and voltage variables.

The active load is represented on bus i at time t as $P_{(i),(t)}$ and the total load of the system is given in Eq. (138).

$$\underbrace{\sum_{Load} P_{(i),(t)}^{BusLoad}}_{nonlinear\ term}\ is\ obtained\ from\ P_{(i),(t)} = P_{(i),(t)}^{BusLoad} \left(\frac{V_{(i),(t)}}{V_0}\right)^{\alpha} \qquad \forall t, i \quad (138)$$

Active losses in the lines in the distribution system can be calculated by Eq. (139).

$$\underbrace{\sum_{Loss} P_{(ij),(t)}^{LineLoss}}_{nonlinear\ term}\ is\ obtained\ from =$$

$$\sum_{t=1}^{T} \sum_{Branch=1}^{Number\ of\ Branch} \underbrace{r^{ij}.(I_{(t)}^{ij})^2}_{Active\ Power\ Line\ Loss} \qquad \forall t, i, j \quad (139)$$

The active power loss due to apparent power in each inverter used in the PV system is calculated by Eq. (140).

$$\underbrace{\sum_{Loss} P_{(t)}^{PV\ InverterLoss}}_{nonlinear\ term} \quad is\ obtained\ from = \qquad \forall t, i \quad (140)$$

$$P_{(i),(t)}^{PV\ InverterLoss} = c_{self} + c_v S_{(i),(t)}^{PV} + c_R (S_{(i),(t)}^{PV})^2$$

Where $S_{(i),(t)}^{PV}$ is calculated by Eq. (141).

$$S_{(i),(t)}^{PV} = V_{Bus_{(i),(t)}}^{PV} . (I_{Apparent_{(i),(t)}}^{Net})^* . N_{Ratio}^{Transformer} \qquad \forall t, i \quad (141)$$

Similarly, the total losses of the inverters used in BESS can be calculated with Eq. (142).

$$\underbrace{\sum_{Loss} P_{(t)}^{BESS\ inverterloss}}_{nonlinear\ term} \quad \text{is obtained from} \qquad \forall t, i \quad (142)$$

$$P_{(t)}^{BESS\ inverterloss} = c_{self} + c_v S_{(i),(t)}^{BESS} + c_R (S_{(i),(t)}^{BESS})^2$$

Where $S_{(i),(t)}^{BESS}$ is calculated by Eq. (143).

$$S_{(i),(t)}^{BESS} = V_{Bus_{(i),(t)}}^{BESS} . (I_{Apparent_{(i),(t)}}^{Net})^* . N_{Ratio}^{Transformer} \qquad \forall t, i \quad (143)$$

Where $S_{(i),(t)}^{BESS}$ is the apparent power of the inverter on *i* bus, at *t* time and is calculated by multiplying the voltage of the bus to which it is connected and the inverter current.

6.5.2.2 Reactive Power Balance

Similarly, the reactive power balance in Eq. (144) must also be maintained in addition to the active power balance, as both are crucial for the proper operation of the distribution system.

$$\underbrace{\underbrace{Q_{(t)}^{GB}}_{Grid\ Purchase}}_{Decision\ Variable} - \underbrace{\underbrace{Q_{(t)}^{GS}}_{Grid\ Sell}}_{Decision\ Variable} = \underbrace{\sum_{Load} Q_{(i),(t)}^{BusLoad} \left(\frac{V_{(i),(t)}}{V_0}\right)^{\beta}}_{nonlinear\ term} + \underbrace{\sum_{t=1}^{T} \sum_{Branch=1}^{Number\ of\ Branch} \underbrace{x^{ij}.(I_{(t)}^{ij})^2}_{Reactive\ Power\ Line\ Loss}}_{nonlinear\ term} + \underbrace{\sum_{BESS} Q_{(t)}^{Absorb}}_{nonlinear\ term} - \underbrace{\sum_{BESS} Q_{(i),(t)}^{Inject}}_{nonlinear\ term} + \underbrace{\sum_{PV} Q_{(i),(t)}^{Absorb}}_{nonlinear\ term} - \underbrace{\sum_{PV} Q_{(i),(t)}^{Inject}}_{nonlinear\ term} \quad \forall t, i, j \quad (144)$$

The sum of the reactive powers in the bus and the reactive powers absorbed by the BESS and PV systems and also the reactive line losses in the lines are calculated as the total reactive load. The reactive powers injected by the BESS and PV systems are as the reactive power source. In short, the difference between the reactive power received from the grid and the reactive power supplied is equal to the difference between the total reactive load and the total reactive power injected by the inverters.

6.5.2.3 Grid Constraints

The optimization model contains a substantial number of nonlinear terms, which results in computationally intensive calculations. To improve computational simplicity and efficiency, voltage constraints are only applied to the buses connected to BESS-PV systems and end of the brach buses ensuring their voltage levels remain within the specified limits in Eq. (145).

$$V^{min} \leq V_{(i),(t)} \leq V^{max} \qquad For\ all\ BESS, PV\ and\ end\ of\ the\ brach\ buses \qquad \forall t, i \quad (145)$$

The active and reactive power exchanges with the grid are modeled as distinct variables. To prohibit the test system from simultaneously purchasing and selling active power at any given time, Eq. (146) is employed to force the system to either buy or sell power, but not both, at any given time *t*.

$$P_{(t)}^{GB}.P_{(t)}^{GS}=0 \qquad \textit{Active Power Grid buy/sell avoid simultaneously} \qquad \forall t \quad (146)$$

$$Q_{(t)}^{GB}.Q_{(t)}^{GS}=0 \qquad \textit{Reactive Power Grid buy/sell avoid simultaneously} \qquad \forall t \quad (147)$$

A similar restriction must be applied to reactive power and can be provided by Eq. (147).

6.5.2.4 Dynamic Thermal Rating Constraints

In the test system, the power transformer is operated in a safe manner by ensuring that values obtained from dynamic thermal rating (DTR) modeling, such as total oil temperature (TOT), hot-spot temperature (HST) and per-unit loading (PUL), remain within the limits specified in IEC 60076-7.

$$TOT_{(t)} \leq TOT^{max} \qquad \forall t \quad (148)$$

$$HST_{(t)} \leq HST^{max} \qquad \forall t \quad (149)$$

$$PUL_{(t)} \leq PUL^{max} \qquad \forall t \quad (150)$$

The calculation method for TOT and HST is detailed in Chapter 4. The IEC recommends using a time interval at the minute level for accurate calculation because the fixed coefficients provided for the transformer in the IEC are intended for minute resolution calculations. Therefore, each time step should be used as a minute in the calculation of TOT and HST. However, in the optimization problem, each time interval in the day-ahead EMS is selected as one hour. Consequently, while the time step for the transformer DTR is one minute, the optimization time step is 60 minutes. To address this discrepancy in time scales, it is necessary to overcome the problem arising from the difference in time slots.

To address the issue of differing time slots, certain transformations are suggested. The day-ahead EMS optimization model represents transformer loading as one time step equivalent to 60 minutes. For the DTR model, assuming transformer loading ratio is constant for the entire 60 minutes within a single time step, the 24 time steps are converted to 24 × 60 = 1440 time steps.

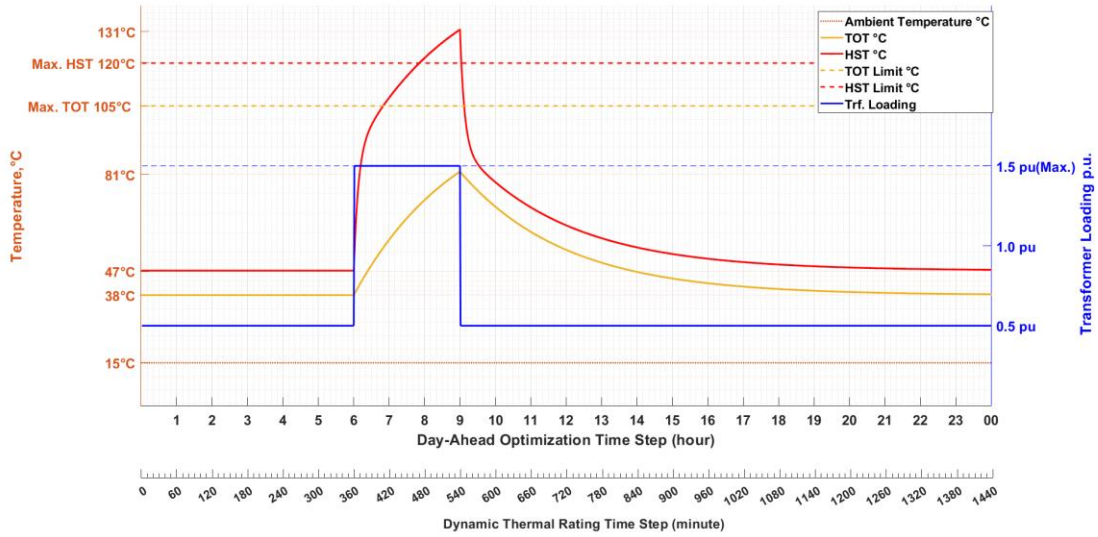

Figure 40. Interrelations Between 150 % Overloading Transformer and Step Ambient Temperature with Dual Time Slot

6.5.2.5 BESS Constraints

The inverter within the BESS must not exceed the current limit specified in the product catalog, and the energy balance of the battery group, as represented by SoC, should be maintained within safe limits.

The BESS inverter is designed to avoid simultaneous charging and discharging Eq. (151). This condition also applies to reactive power operation in Eq. (152).

$$I_{p(i),(t)}^{Discharge(BESS)} . I_{p(i),(t)}^{Charge(BESS)} = 0 \qquad \forall t, i \quad (151)$$

$$I_{q(i),(t)}^{Inject(BESS)} . I_{q(i),(t)}^{Absorb(BESS)} = 0 \qquad \forall t, i \quad (152)$$

It is critical that the maximum current limit specified in the BESS inverter catalog not be exceeded.

$$I_{Apparent(t)}^{BESS} \leq I_{Apparent\_max}^{BESS} \qquad \forall t \quad (153)$$

The current values specified in the product catalog are represented as the vector sum of real and imaginary components within the optimization model, as shown in Eq. (154).

$$\left|(I_{Real(t)}^{BESS} + jI_{Imaginary(t)}^{BESS})\right| \leq I_{Apparent\_max}^{BESS} \qquad \forall t \quad (154)$$

$$\sqrt{(I_{p(i),(t)}^{Discharge} - I_{p(i),(t)}^{Charge})^2 + (I_{q(i),(t)}^{Inject} - I_{q(i),(t)}^{Absorb})^2} \leq I_{Apparent\_max}^{BESS} \quad \forall t, i \qquad (155)$$

In the equation formed in Eq. (155), either the discharge current or the charge current of the BESS is greater than zero, which constitutes the real part of the inverter current. Only one of the reactive components of the current, $I_{q(i),(t)}^{Inject}$ and $I_{q(i),(t)}^{Absorb}$, is greater than zero. The sum of these two components represents the reactive part of the current. By Eq. (155), it is ensured that the magnitude of the net active current component and the net reactive current component is equal or smaller than the maximum allowable limit of the inverter.

The energy balance of the battery group in the BESS is represented by Eq. (156), in which is the product of current and voltage components instead of power in Eq. (24).

$$\begin{aligned} & SoC_{(i),(t+1)}^{BESS} \\ & = SoC_{(i),(t)}^{BESS} \\ & + \left(\eta_{BC} . \sqrt{3} . V_{Bus(i),(t)}^{BESS} . I_{p(i),(t)}^{Charge(BESS)} . N_{Ratio}^{Transformer} . \Delta t\right) \qquad \forall t, i \quad (156) \\ & - \left(\frac{\sqrt{3} . V_{Bus(i),(t)}^{BESS} . I_{p(i),(t)}^{Discharge(BESS)} . N_{Ratio}^{Transformer}}{\eta_{BD}} . \Delta t\right) \end{aligned}$$

The lifespan of the batteries in the BESS is extended by ensuring that the lower and upper energy level limits are not exceeded.

$$SoC^{min} \leq SoC_{(i),(t)}^{BESS} \leq SoC^{max} \qquad \forall t \quad (157)$$

6.5.2.6 PV System Constraints

The PV inverter is designed to avoid simultaneously absorbing and injecting reactive current in Eq.(158).

$$I_{q(i),(t)}^{Inject(PV)} . I_{q(i),(t)}^{Absorb(PV)} = 0 \qquad \forall t \quad (158)$$

To prevent the current generated by the PV system from exceeding the voltage limits of the bus, it must be curtailed. The curtailed current should always be lower than the available current at any given time in Eq. (159).

$$I_{p(i),(t)}^{Curtail} \leq I_{p(i),(t)}^{Available} \qquad \forall t, i \quad (159)$$

The maximum current limit specified in the PV inverter catalog should not be exceeded in Eq. (160).

$$I_{Apparent(i),(t)}^{PV} \leq I_{Apparent\_max}^{PV} \qquad \forall t, i \quad (160)$$

The current specified in the catalog is represented in the optimization model as real and imaginary components in Eq. (161).

$$\left|(I_{Real(i),(t)}^{PV} + jI_{Imaginary(i),(t)}^{PV})\right| \leq I_{Apparent\_max}^{PV} \qquad \forall t, i \quad (161)$$

The magnitude of the real and imaginary parts in the Eq. (161) where must not exceed the maximum allowable current of the inverter.

The real component of the current ($I_{Real(i),(t)}^{PV}$) is obtained by the difference between the available current and the curtail current in Eq. (162).

$$I_{Real(i),(t)}^{PV} = I_{Active(i),(t)}^{PV} = I_{p(i),(t)}^{Available} - I_{p(i),(t)}^{Curtail} \qquad \forall t, i \quad (162)$$

If the inverter current limitation is expressed in terms of the variables used in the optimization model, the Eq. (163) constraint is obtained.

$$\sqrt{(I_{p(i),(t)}^{Available} - I_{p(i),(t)}^{Curtail})^2 + (I_{q(i),(t)}^{Inject} - I_{q(i),(t)}^{Absorb})^2} \leq I_{Apparent\_max}^{PV} \qquad \forall t, i \quad (163)$$

By Eq. (163), it is ensured that the magnitude of the net active current component and the net reactive current component is equal or smaller than the maximum permissible limit of the inverter.

7. CHAPTER: SIMULATION RESULTS AND ANALYSIS

In this section, the proposed calculation method and modeling are applied to the modified IEEE 33-bus test system, considering different transformer power ratings at the grid connection point, varying BESS capacities and diverse seasonal days for day-ahead energy scheduling.

The DTR of the transformer enabled the application of various case studies presented in The required transformer power is 5000 kVA, but it is gradually reduced to demonstrate that the system can operate even with lower transformer power. The modified test system is simulated by connecting transformers of different capacities.

The required transformer power is 5000 kVA, but it is gradually reduced to demonstrate that the system can operate even with lower transformer power. The modified test system is simulated by connecting transformers of different capacities.

These case studies demonstrate the energy changes in BESS, PV, and inverters within the system due to transformer system constraints, as well as their effects on daily energy costs.

Table 14. The Case Studies and Features

Case Name	Transformer Power at PCC	Solar Radiation Profile	BESS Capacity
Case 1	3000 kVA	Summer Day	1000 kWh
Case-2	4000 kVA	Summer Day	1000 kWh
Case-3	5000 kVA	Summer Day	1000 kWh
Case-4	6000 kVA	Summer Day	1000 kWh
Case-5	3000 kVA	Summer Day	2000 kWh
Case-6	6000 kVA	Winter Day	1000 kWh

In the peak load case of the base test system, the demand power of the system is calculated as 4552.53 kVA, including losses, as shown in Table 3. To meet the total

demand power, the transformer power to be installed at the PCC should be selected as 5000 kVA by rounding up the demand power. However, with the addition of equipment such as PV and BESS to the system, and thanks to the dynamic modeling of the transformer, case studies are conducted with different transformer powers to demonstrate that the system can operate without exceeding technical limits by installing a lower power transformer.

The required transformer power is 5000 kVA, but it is gradually reduced to demonstrate that the system can operate even with lower transformer power. The modified test system is simulated by connecting transformers of different capacities.

Case-1: In the first case study, the modified test system shown in Figure 29 is assumed to have a 3000 kVA transformer at the PCC. A day-ahead EMS is used to perform daily energy cost optimization.

Using the same test system and model, daily energy cost optimization is performed through the day-ahead energy management system by altering only the transformer power capacity at the PCC for Case-2, Case-3, and Case-4.

The Case-5 study involves a 3000 kVA transformer power at the PCC, and the BESS capacities are increased to 2000 kWh. Additionally, the daily energy cost is optimized using a day-ahead EMS.

In the last case study, the power in the PCC is selected as 6000 kVA and the irradiance profile and ambient temperature are on a winter day, daily energy cost is optimized with the day-ahead EMS.

In the previous case study, the transformer power at PCC is set to 6000 kVA, and the irradiance profile and ambient temperature is representative of a winter day. The daily energy cost is optimized using a day-ahead EMS.

The Figure 41 presents the daily energy costs resulting from the optimization of six different case studies.

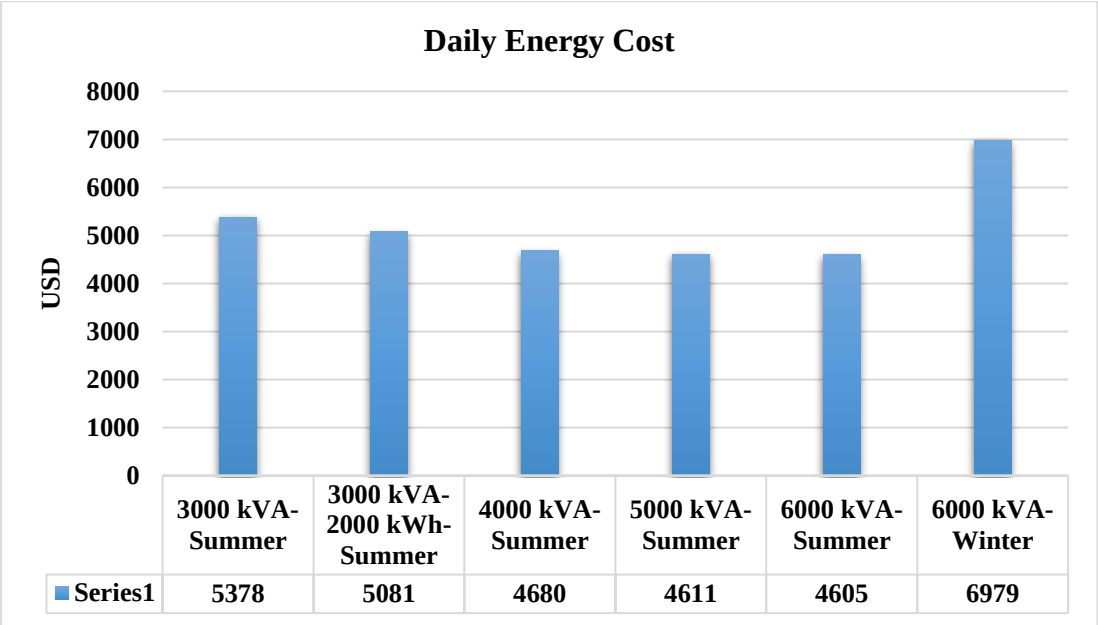

Figure 41. Daily Energy Cost Comparison for Cases

As predicted, the case with the lowest irradiance is Case-6, which also has the highest energy cost. Rather than using BESS to reduce daily energy costs, the aim is to use it to reduce transformer loading in order to meet the constraints. As the transformer power decreases from 6000 kVA to 3000 kVA, the transformer loading increases. Therefore, BESS uses its energy to reduce transformer loading instead of reducing costs.

As a result, in the use of a 3000 kVA transformer, the transformer loading is the highest, leading to the highest daily energy cost. This is because the BESS is used to provide thermal constraints rather than reducing the cost when compared to Case-1, Case-2, Case-3, and Case-4.

Due to the elevated BESS capacity, which is twice that of Case-1, a portion of the stored energy in Case-5 is allocated towards addressing thermal constraints, while the remainder is utilized to minimize energy costs. Therefore, the daily energy cost of Case-5 is lower than Case-1.

Figure 42 provides a comparison of the daily total active and reactive energy losses in the lines.

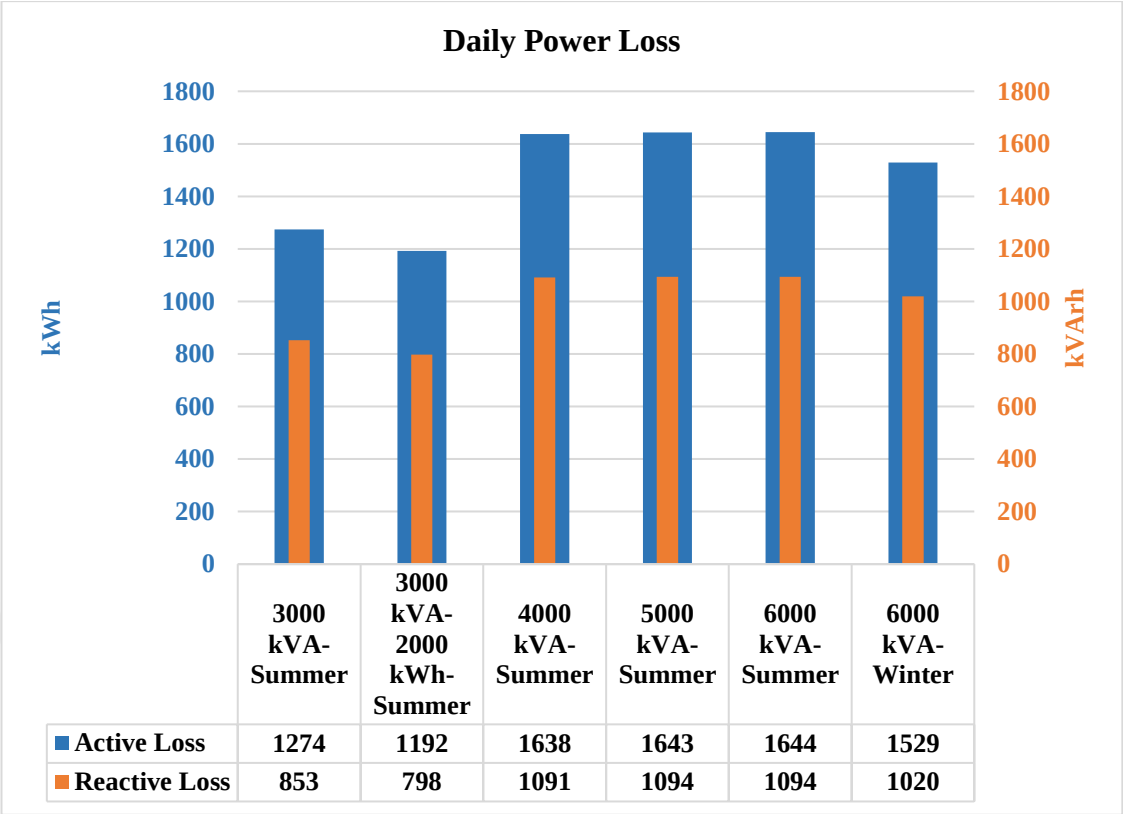

Figure 42. Daily Line Loss Comparison for Cases

When the simulation results are examined, line losses are lower in Case-1 than in Case-2, Case-3, and Case-4, since the energy purchase from the grid is reduced in order to reduce the loading of the transformer. When Case-1 and Case-5 are compared, in Case-5, since the energy stored in BESS is more and the energy purchase from the grid is reduced, the loss in the lines is less compared to Case-1. When Case-5 and Case-6 are compared, since Case-6 has less energy sold to the grid, line losses are less compared to Case-5. The comparison of the energy purchased or sold by the modified test system from the grid is given in the Figure 43.

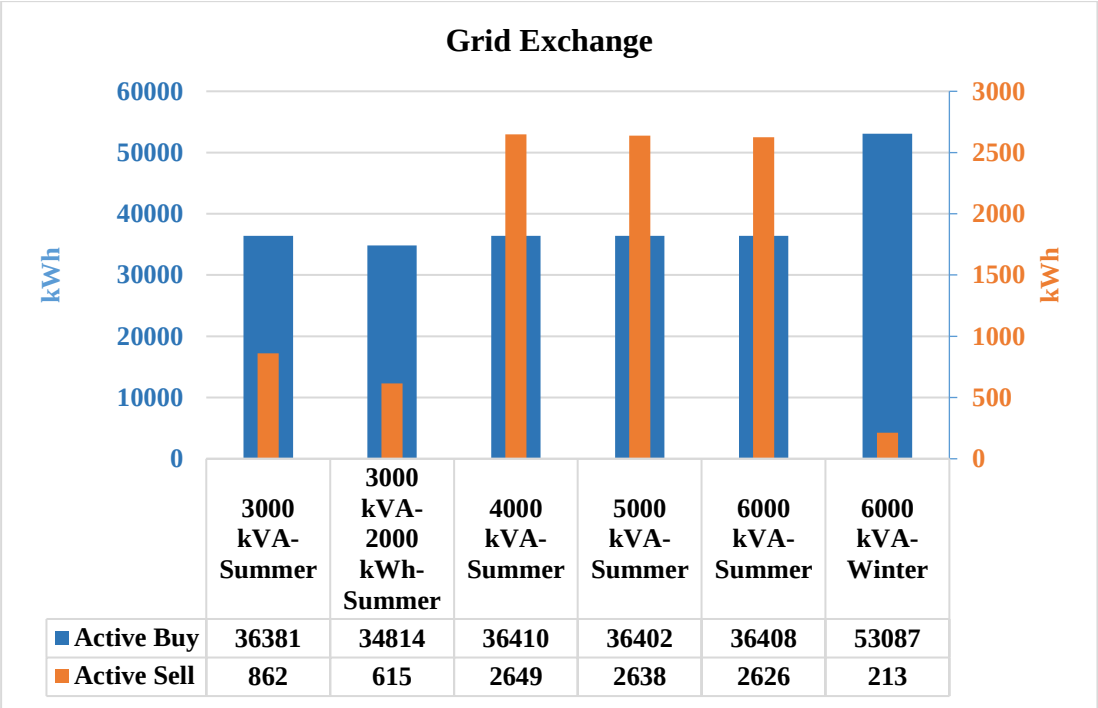

Figure 43. Daily Grid Exchange Comparison for Cases

Since the BESS capacity increases in Case-5 and the stored energy capacity is twice that of Case-1, some of the energy in BESS is used for thermal constraints while the other part of the energy in BESS is used to reduce energy costs so that it exchanges less energy from the grid. For this reason, the daily energy exchange of Case-5 is lower than Case-1.

The analysis of Case-2, Case-3, and Case-4 in comparison to Case-1 indicates that the reduced transformer loading enables greater energy sales.

In Case-6, the lower PV generation results in higher grid energy purchases to meet demand, and reduced excess generation leads to lower energy sales. The comparison of hourly changes of HST in the transformer as a result of 6 case studies is shown in the Figure 44.

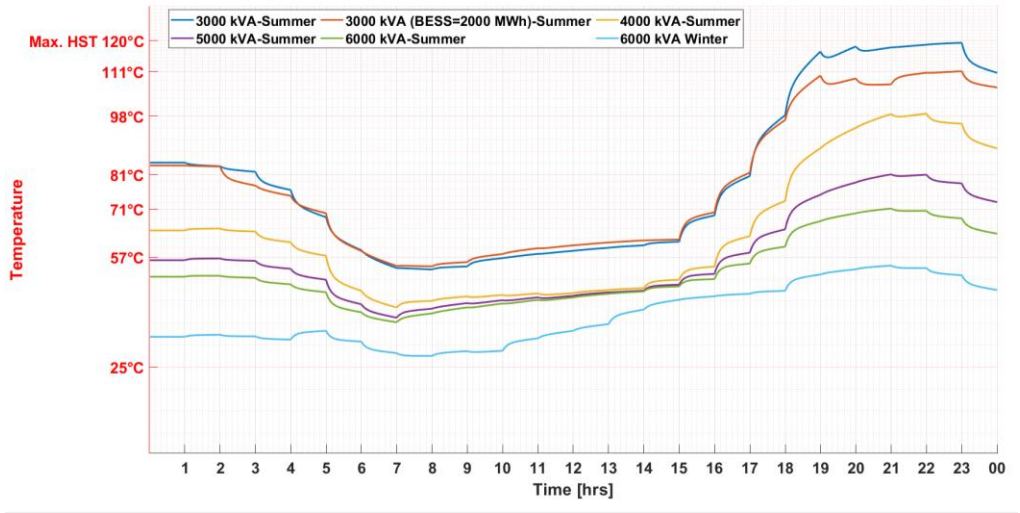

Figure 44. Daily HST Comparison for Cases

As expected, the main effect of the increase in HST is the loading of the transformer. The transformer in Case-1, which has the lowest power, has the highest transformer loading.

At the end of 18:00, when the demand load is at its highest, the HST value reached the HTS limit. As the thermal effect and loading continue, the HST value remains around 120°C. Since the HST constraint is set at 120°C in the optimization, the constraints are met and the HST limit is not violated. With Case-5, the increased use of BESS results in less loading compared to Case-1, leading to a lower HST in Case-5 than in Case-1.

Comparing Case-1 to Case-5, the loading is reduced since the sales to the grid are lower due to both the low ambient temperature and the low PV production. Consequently, the HST value is lower in Case-6 compared to Case-5.

When a similar comparison is made for TOT, a pattern comparable to that observed for HST can be seen, as illustrated in Figure 45.

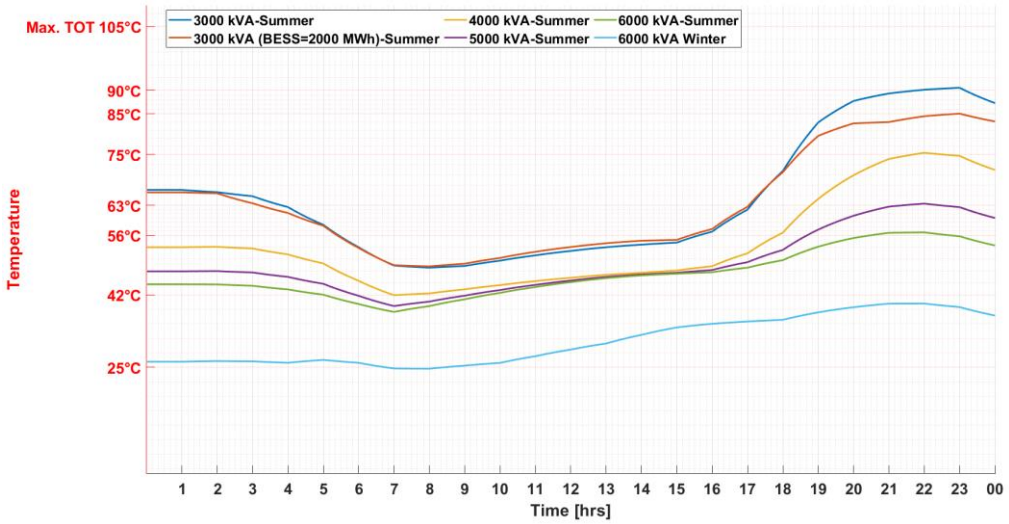

Figure 45. Daily TOT Comparison for Cases

Figure 46 illustrates the active power exchange between the test system and the grid, where positive values indicate power drawn from the grid, and negative values indicate power sold to the grid.

In Case-6, where the PV generation is at its lowest level, the energy purchases from the grid are consequently at their highest, while the energy sales to the grid are correspondingly the lowest. In Case-1 and Case-5, since there is a transformer load limitation, less energy is purchased, while energy sales to the grid are less compared to the other Case-2, Case-3 and Case-4.

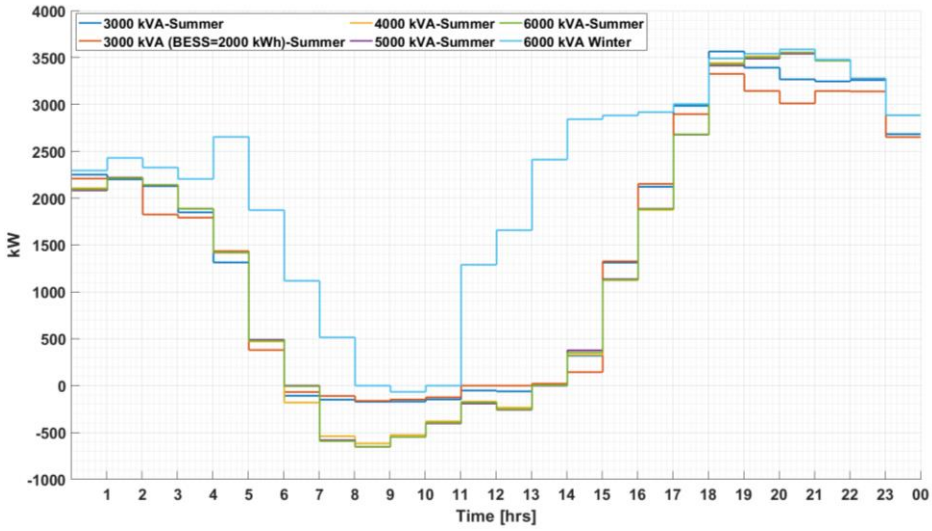

Figure 46. Daily Grid Exchange Active Power Comparison for Cases

The Figure 47 shows the hourly transformer loading rates obtained from different case studies. At 18:00, when the demand load is at its highest, the transformer loading rate is highest in Case-1. Since Case-5 uses more BESS, the transformer loading rate is lower compared to Case-1. In Case-2, as the transformer power increases, the loading rate is slightly lower, while in Case-3 and Case-4, the loading rate gradually decreases.

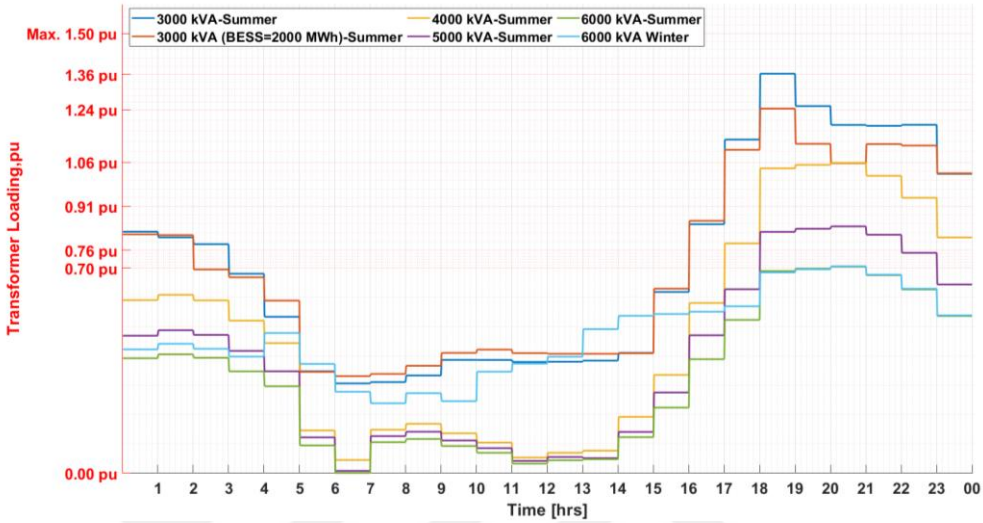

Figure 47. Daily Transformer Loading Comparison for Cases

7.1. Case-1 Analysis

The active power, reactive power, and state of charge fluctuations of the four-battery energy storage systems integrated into the test system throughout the day are illustrated in Figure 48. The initial energy level of all BESSs in the system, as expressed by the SoC, is set at 30%. During the first hours of the day, the BESSs discharge their energy into the system, reducing their SoC to the lower limit of 20%. Then, thanks to PV generation, the BESSs store energy by charging up to the upper level of 80% at noon. By discharging their energy in the evening hours, when the demand load is high, the BESSs reduce the energy cost and ensure optimum operation of the system by minimizing the transformer loading. Finally, the BESSs discharge the stored energy until the last hour of the day, reaching the lowest SoC level of 20%.

In contrast, BESS-3 and BESS-4, particularly those near the line ends, absorb reactive power during the evening hours when active energy is being discharged, in order to maintain the bus voltage within acceptable limits.

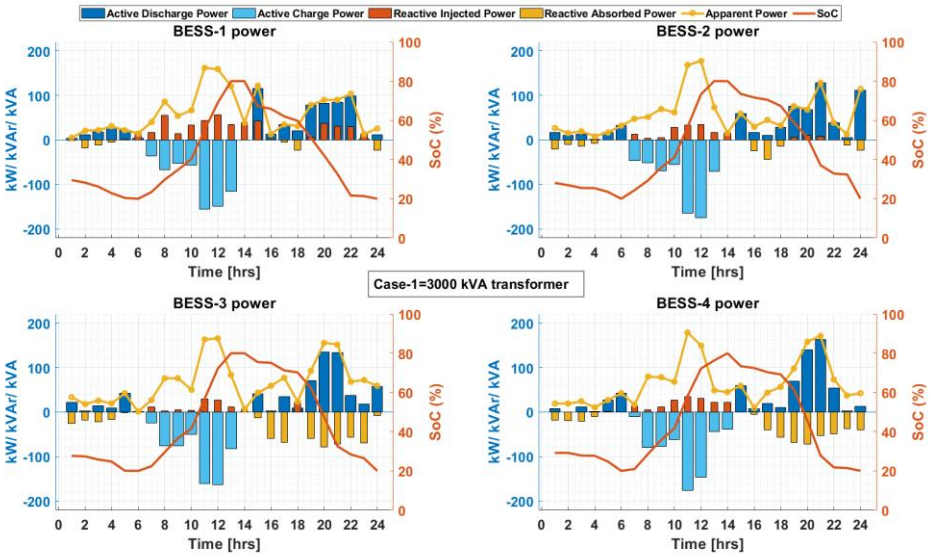

Figure 48. Daily BESS Power and SoC Comparison for Case-1

The Figure 49 displays the PQ operating curve of all BESSs. Each point on the PQ curve indicates the region in which the BESS operates within the four-quadrant PQ curve during that time period. It is seen that the powers in all BESs meet the constraints by remaining within the power circle.

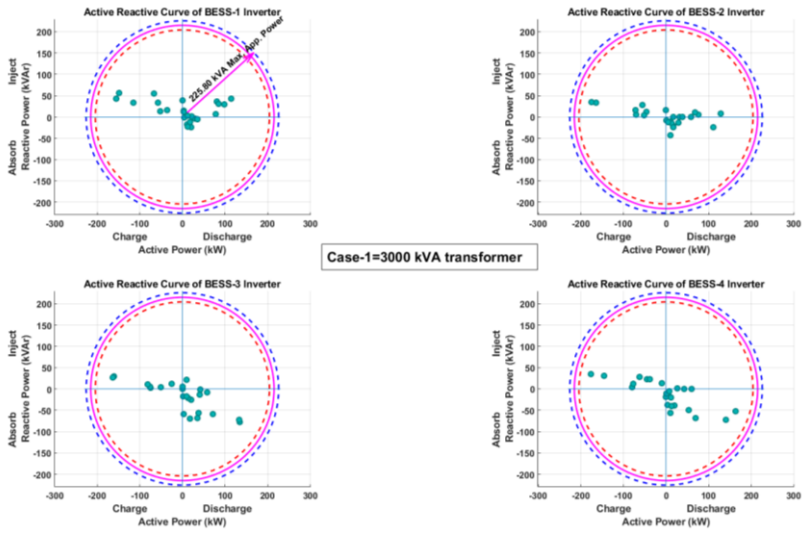

Figure 49. Daily BESS Power PQ Curve Comparison for Case-1

The Figure 50 depicts the hourly current fluctuations of the BESSs, whose power profiles are shown in Figure 49. During the charging mode, all BESSs behave like electrical loads, storing energy. In this mode, they inject reactive power to help prevent

voltage drops on buses. All battery energy storage systems fully discharge their energy by the end of day, helping to reduce costs.

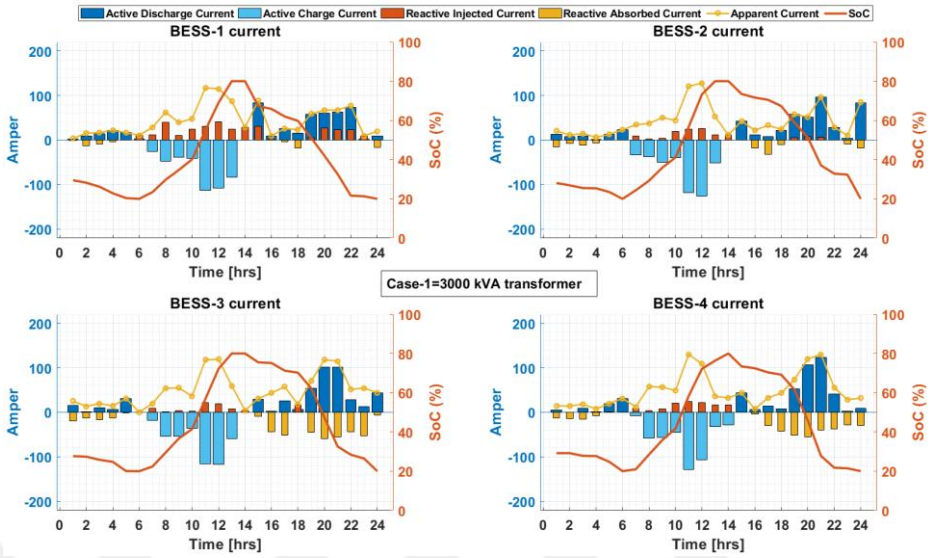

Figure 50. Daily BESS Current and SoC Comparison for Case-1

The Figure 51 shows the PQ operating zone within which the hourly current variations of BESSs remain and are limited by the upper operating limit of 155.2 A. The inverter operates within this maximum current limit at all times.

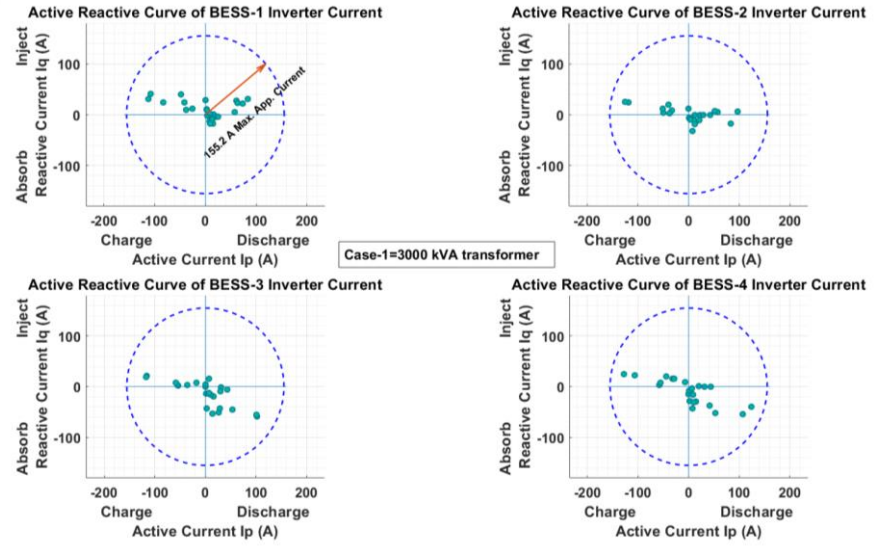

Figure 51. Daily BESS Current Curve Comparison for Case-1

The Figure 52 shows the hourly current and apparent power profile of BESSs. When the apparent power and current changes are examined, the current and power increased during the noon hours when the energy generated by the PV system is stored.

Similarly, in the evening hours when the energy price is higher, the BESS switched to discharge mode, and its usage increased.

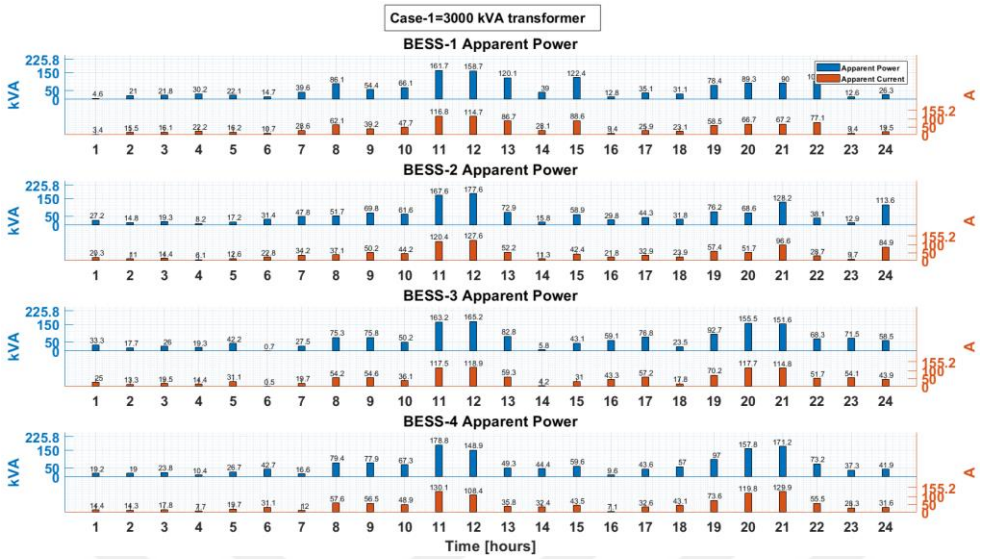

Figure 52. Daily BESS Power and Current Comparison for Case-1

For the PV system integrated into the system, calculations are made by connecting inverters in parallel to meet the capacity requirements. However, since the optimization model uses the actual inverter values and current limits, calculations must be performed separately for each inverter. Consequently, the current and power in the PV system are modeled on a per-inverter basis.

The Figure 53 depicts the current profile of each inverter in the PV system. The optimization model includes a variable that curtails PV energy to maintain the bus voltage within acceptable limits. The green bar in the figure represents this curtailment of PV generation, which prevents the voltage from rising excessively. During periods of low load demand and high PV production, excess PV output is curtailed to ensure voltage limits on the bus and reduce transformer loading.

Regarding reactive power, PV-3 and PV-4, particularly those located near the line ends, absorb reactive power in the evening hours when active energy is discharged by BESSs. This reactive power absorption helps to keep the bus voltage within the desired range limits.

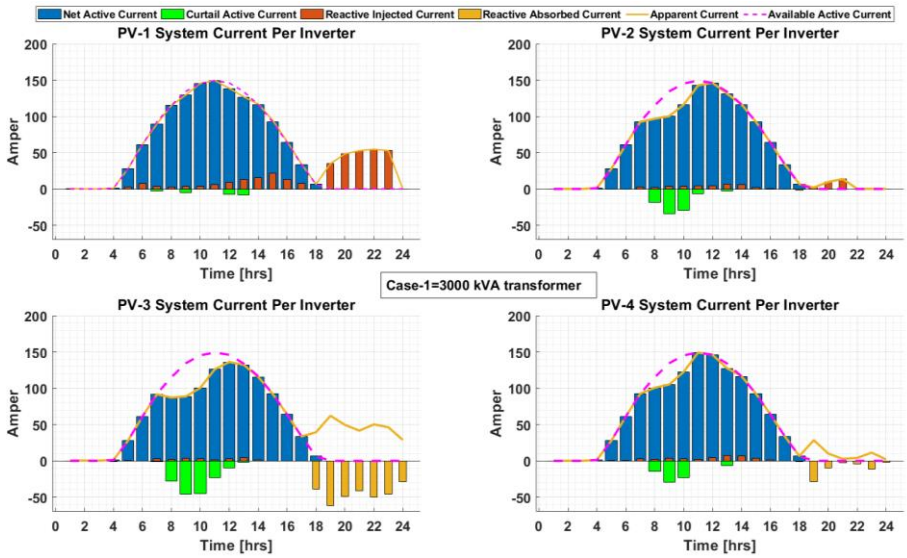

Figure 53. Daily PV Current Per Inverter Comparison for Case-1

The power change profile exhibited by the current graphs presented in Figure 53 is illustrated in Figure 54. At locations distant from the point of common coupling, PV generation was curtailed at PV-2, PV-3, and PV-4 to prevent excessive increases in bus voltages due to high PV production during noon hours.

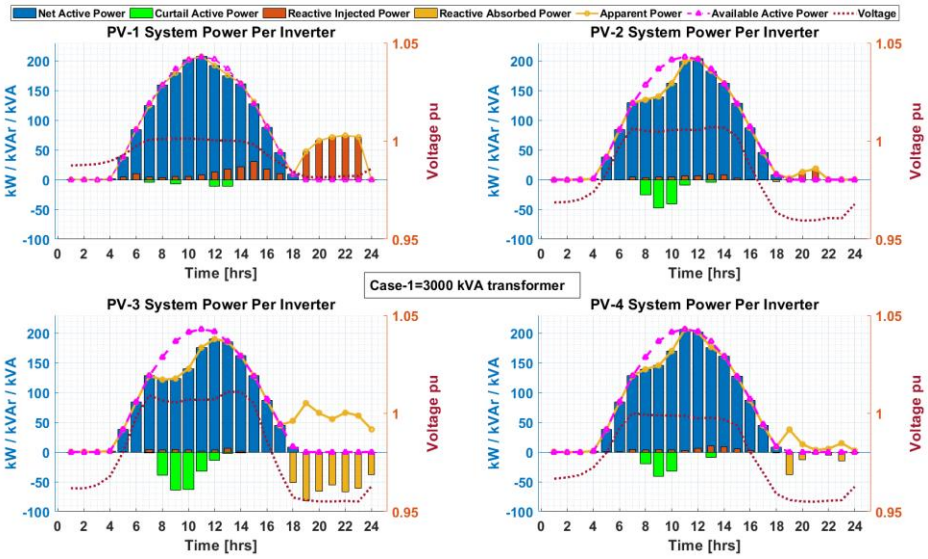

Figure 54. Daily PV Power Per Inverter Comparison for Case-1

The Figure 55 provides an illustration of the total power produced by the inverters within PV systems. During periods of high PV generation, the bus voltage increases, while in the evening hours, the voltage decreases due to increased load and the absence of PV generation.

The voltage profile is highest at PV-1, which is closest to the grid connection point, compared to PV3 and PV4, which are located further away.

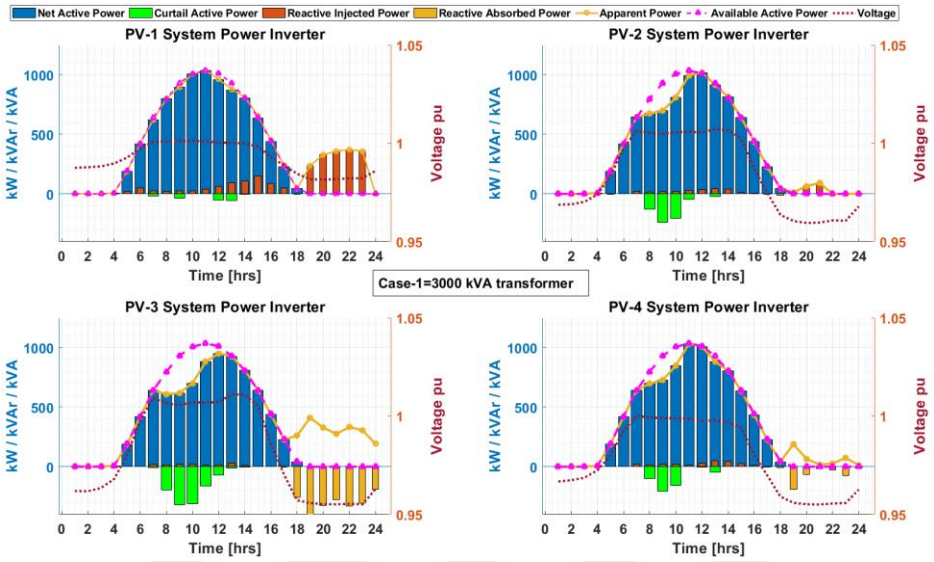

Figure 55. Daily PV Total Power Comparison for Case-1

The hourly current and apparent power profile of the PV systems per inverter is shown in Figure 56. Despite having the same irradiance, the PV systems in the test system provide different power outputs due to their varying connection points. This is necessary to maintain voltage restrictions on the busbars. To achieve this, the systems curtail different power levels and provide distinct reactive power support. Additionally, the load flow calculation shows that the PV systems exhibit different voltages because of their varying distances from the grid. For instance, although PV-2, PV-3, and PV-4 all injected 64 amperes of current at 16:00, they gave different power levels to the bus: PV-2: 87.5 kVA, PV-3: 87.4 kVA and PV-4: 86.9 kVA.

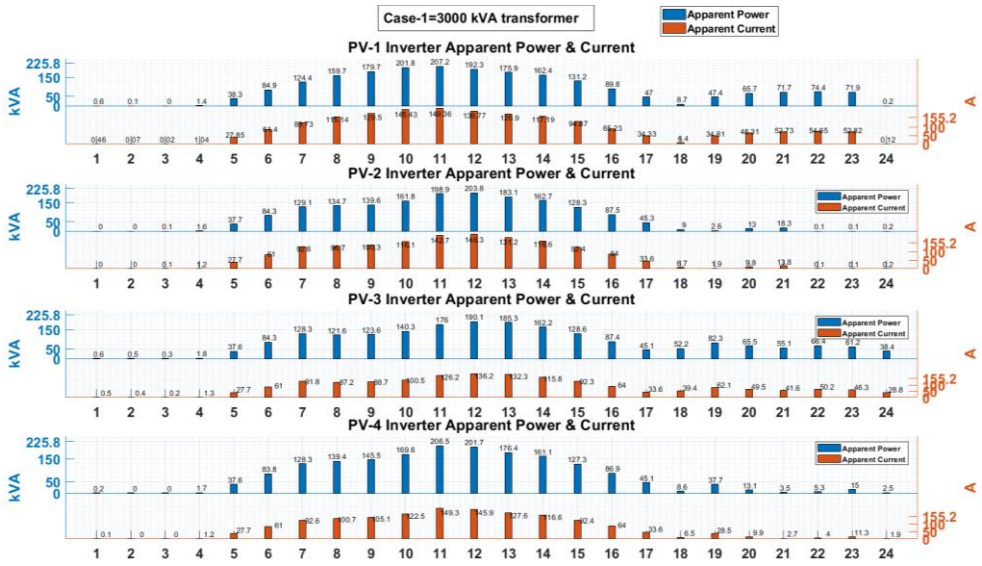

Figure 56. Daily PV Power and Current Per Inverter Comparison for Case-1

The profile of hourly bus voltage changes obtained from the simulation is shown in Figure 57. PV generation at noon causes the bus voltages to rise. During evening hours, the bus voltages decrease due to the lack of PV generation and increased demand load. However, the voltages do not drop below the lower limit of 0.95 per unit at any time.

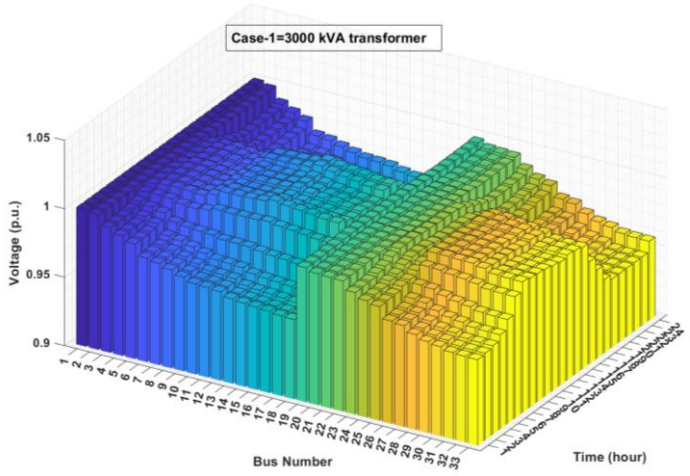

Figure 57. Daily Voltage Profile for Case-1

7.2. Comparison of BESS Profile According to Transformer Powers

As the transformer loading rate changes with variations in transformer power, the BESS power profile also adjusts accordingly. In Case-1, where the transformer power is reduced, the BESS uses its energy to ensure the transformer operates within its designed capacity, enabling it to operate at thermal limits. However, as transformer

power increases, the transformer loading decreases, creating an operating range far from the transformer's thermal limits. In this scenario, the BESS uses its energy to reduce energy costs rather than focusing on reducing transformer loading. Consequently, the BESS discharges energy when the energy cost is high, instead of when the load is high.

A comparison of Case-1 and Case-4 shows that the use of BESS is intended to reduce the cost rather than decrease the transformer loading in Case-4.

The Figure 58 shows the profile of the hourly change of the load and grid purchase price. The important point here is that while the grid purchase price is high at afternoon, the demand load is higher in the evening. This means that transformer loading rises to high levels in the evening hours. However, since the network purchasing price is high in the afternoon hours, BESS usage is expected to be high in order to reduce energy costs.

The Figure 58 shows the profile of the hourly changes in load and grid purchase price. The key point is that while grid purchase price is high in the afternoon, demand load is higher in the evening. This results in transformer loading reaching high levels during the evening hours. However, since the grid purchase price is high in the afternoon, BESS usage is expected to be elevated in order to reduce energy costs.

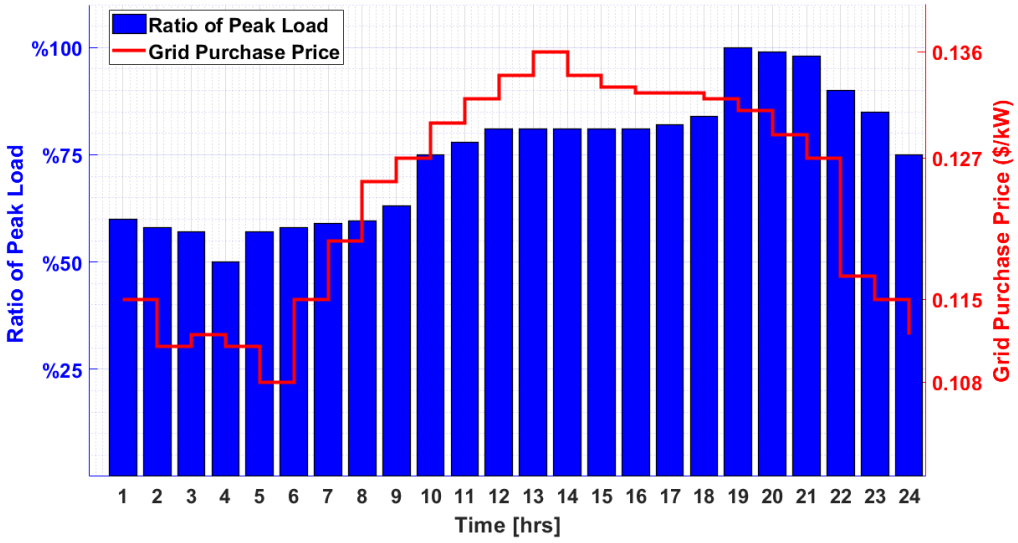

Figure 58. The Hourly Load Demand and Energy Purchase Price Profile

The following BESS power profiles are obtained from two simulations: Case-4 with a transformer power of 6000 kVA and Case-4 with a transformer power of 3000 kVA.

As shown in Figure 59, the BESS discharge powers for Case-1 become more frequent during the evening hours when demand and load are high, while for Case-4, they become more frequent when the grid purchase price is high. The priority of the optimization is to satisfy the constraints and then calculate the lowest cost at which the constraints are met.

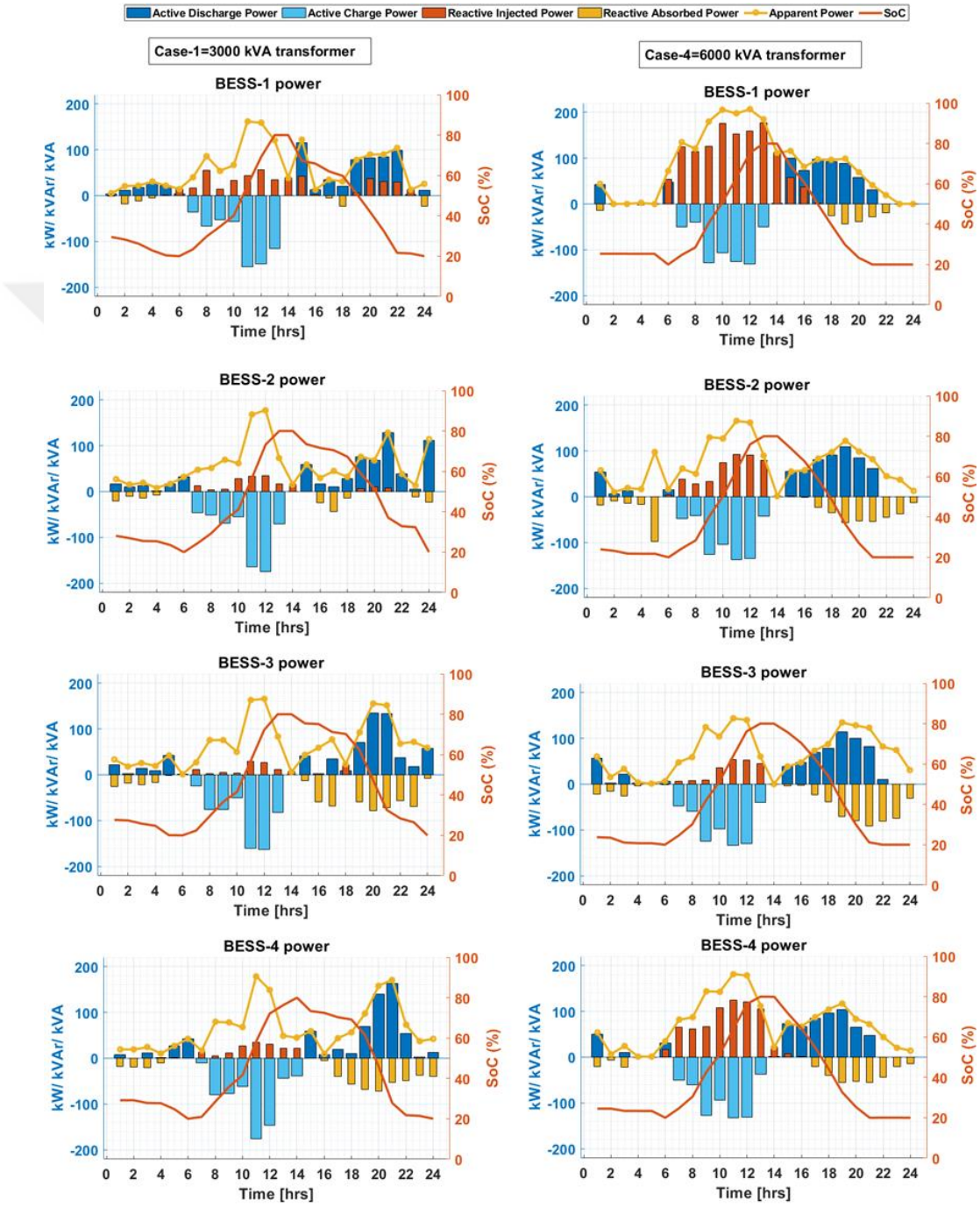

Figure 59. Daily BESS Power and SoC Comparison for Case-1 and Case-4

The PV inverter power profile obtained from the simulation for Case-4 is presented in Figure 60. While the PV generation is curtailed to reduce transformer loading in Case-1, the PV profile in Case-4 shows no such curtailment when compared to the profiles in Case-1.

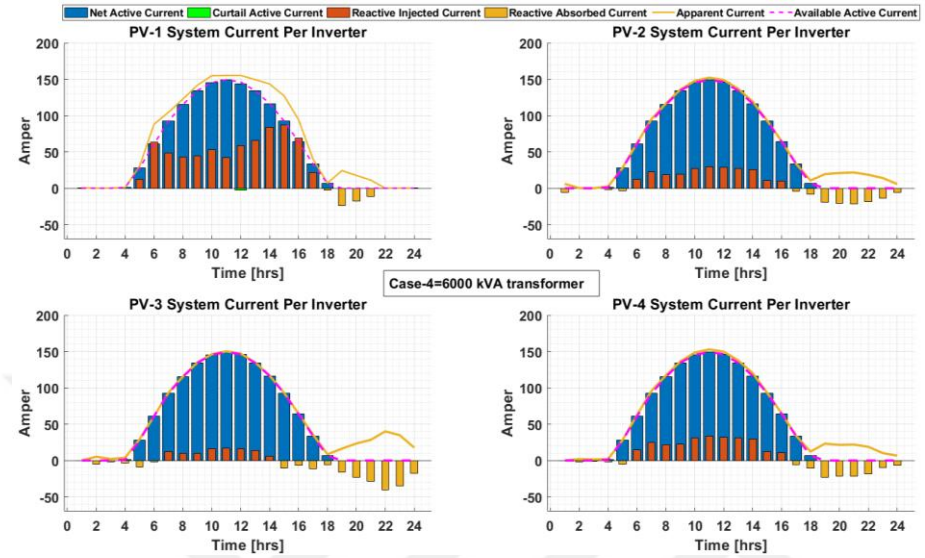

Figure 60. Daily PV Current Per Inverter Comparison for Case-4

The graphs presented illustrate the power profiles for individual inverters and the overall power output within the photovoltaic system, which are showcased in Figure 61 and and Figure 62 for the Case-4 scenario, respectively.

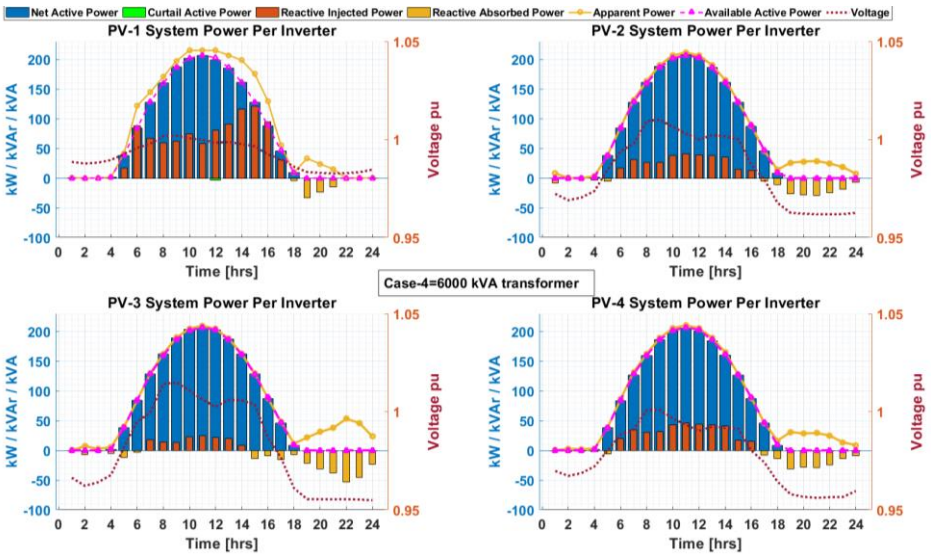

Figure 61. Daily PV Power Per Inverter Comparison for Case-4

In Figure 62, the total power produced by all inverters in a PV system is shown, where it is seen that the bus voltage increases during production hours and decreases during non-production hours. Additionally, to provide voltage support, inverters injected reactive power.

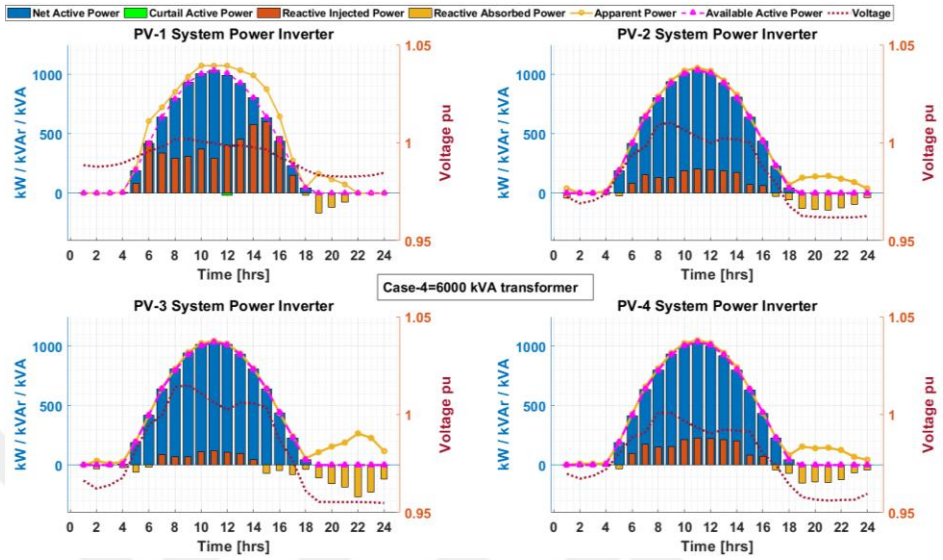

Figure 62. Daily PV Total Power Comparison for Case-4

The profile of the hourly change of bus voltages obtained as a result of the simulation is shown in the Figure 63. Thanks to PV generation at noon, voltage levels in the buses rise. During evening hours, the voltages at the base decrease due to both the no PV generation and the increase in demand load. However, it is not below the bus voltage lower limit of 0.95 (p.u.) at all hours.

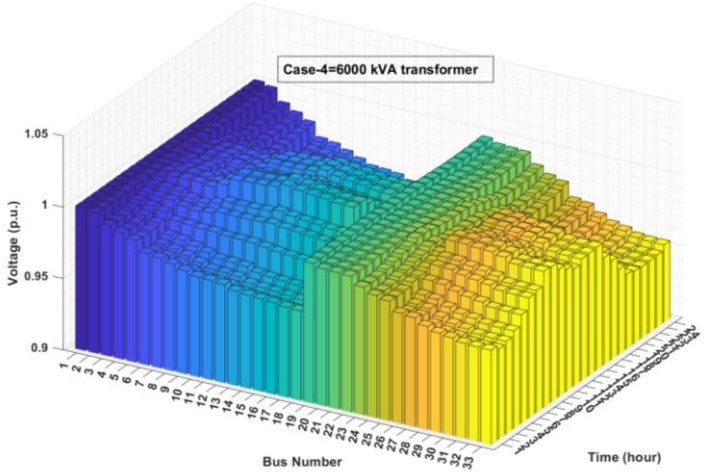

Figure 63. Daily PV Total Power Comparison for Case-4

7.3. Comparison of BESS Capacities in The Case-1 and Case-5

This section analyzes the effects of increasing the BESS capacity when using a 3000 kVA transformer. The simulation results obtained from increasing the BESS energy capacities are presented in Table 15. Increasing the BESS capacity reduces the transformer loading, as more energy is stored in the BESS. Consequently, the transformer's thermal values remain at a lower level compared to a system with lower BESS capacity. Additionally, the increased energy storage enables more of the PV-generated energy to be stored. This allows the BESS to discharge energy when prices are high, rather than purchasing from the grid, thereby reducing the daily energy cost.

Increasing the BESS capacity reduces the transformer loading, as more energy is stored in the BESS. Consequently, the transformer's thermal values remain at a lower level compared to a system with lower BESS capacity. Additionally, the increased energy storage enables more of the PV-generated energy to be stored. This allows the BESS to discharge energy when prices are high, rather than purchasing from the grid, thereby reducing the daily energy cost.

Table 15. Results According to BESS Capacity Change

Transformer Power	Cases	Daily Cost($)	Active Line Loss (kWh)	Reactive Line Loss (kVArh)	BESS Life Time Cost ($)	Max HST (°C)	Max TOT (°C)	Max Loading (pu)
3000 kVA	BESSs 1000 kWh (Case-1)	5378	1274	853	211	119.41	90.63	1.3624
	BESSs 2000 kWh (Case-5)	5081	1192	798	371	111.12	84.55	1.2435

Figure 64 and Figure 65 show the temperature and loading profile of the transformer obtained as a result of Case-1 and Case-5 simulation, respectively. During the high-noon hours when PV production peaks and the grid is not being drawn upon, the transformer loading is low, resulting in correspondingly low HTS and TOT values.

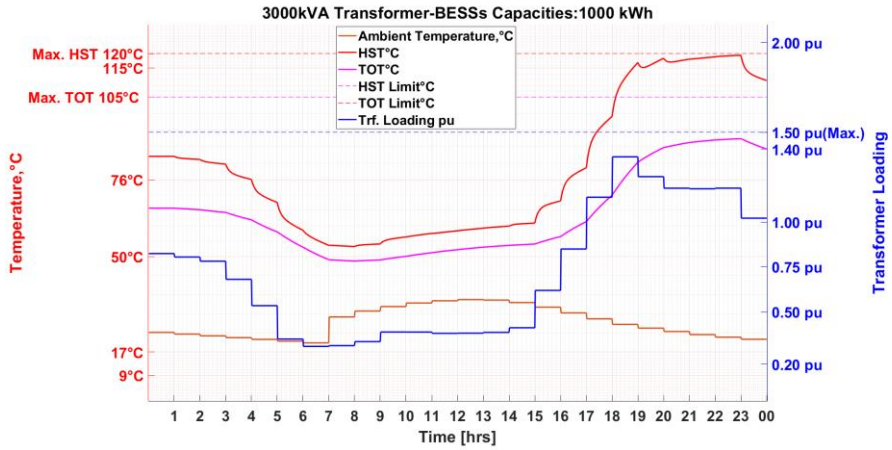

Figure 64. HST, TOT and Loading Variation According to Case-1

The high amount of energy stored in the BESS helps reduce the transformer loading during the evening hours when the demand is high, keeping the HTS and TOT values at lower levels than in Figure 64.

Doubling the BESS capacity not only reduced energy costs but also ensured that the transformer remained below thermal limits. The maximum value of HST decreased from 119°C to 111°C, and the maximum value of TOT decreased from 90°C to 84°C at 23:00.

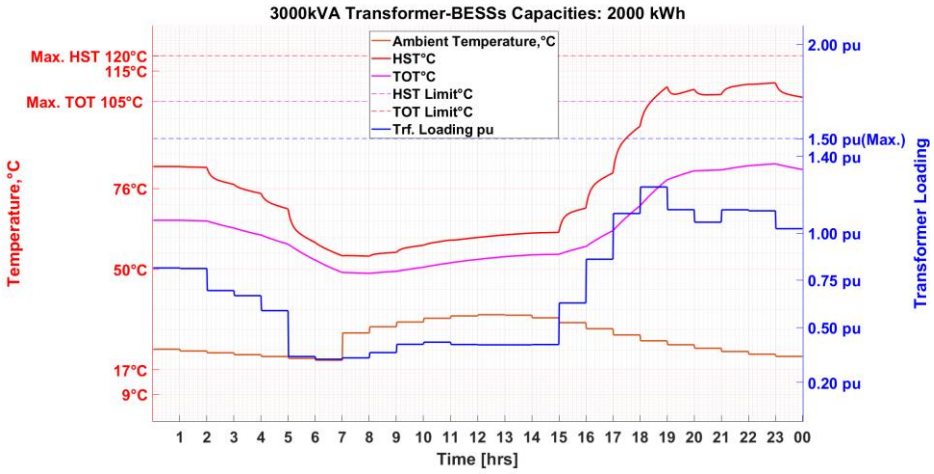

Figure 65. HST, TOT and Loading Variation for Case-5

7.4. Demonstrating The Effect of Inverter Losses On Optimization

In this section, it is emphasized to consider the losses of inverters in PV and BSS integrated into the modified test system. In many studies in the literature, inverter losses are not included in system losses. However, it should be known that in a real

operation, there are inverter losses and there is an energy cost due to these losses. With this study, inverter losses are integrated into optimization and both cost and inverter losses are minimized.

In the first simulation study, by including inverter losses, the total energy of inverter losses for 24 hours is obtained as 2783 kWh.

Table 16. Results With and Without Inverter Losses

Transformer Power	Cases	Daily Cost($)	Inverter Loss (BESS+PV) (kWh)	Inverter Lifetime Cost ($)	PV Inverter Reactive Power (absorb+inject) kVArh	BESS Inverter Reactive Power (absorb+inject) kVArh
3000 kVA	With inverter loss (for Case-1)	5378	347+2436=2783	4.67	13970	4355
	Without inverter loss (for Case-1)	4948	377+5099=5576 (calculated after simulation)	6.84 (calculated after simulation)	18288	5857

For the model where inverter losses are not included, the daily energy cost is $4948, while in the model where they are included, the cost is calculated as $5378. In the model where inverter losses are not included in the optimization model, the energy lost in the inverters at the end of the day is calculated as 5576 kWh as a post-process.

On the other hand, in the model where inverter losses are included, the losses are 2783 kWh, which is seen to provide a 50% reduction compared to the model where they are not included. In the model where losses are not included, 5576 kWh of lost energy is not billed. This will be collected additionally by the DSO at the end of the day as an energy fee. The important point here is that although the inverter losses are calculated as 5576 kWh in the model where they are not included, it is minimized by 50 % and 2783 kWh thanks to its inclusion in the optimization model. Similar situation is valid for inverter life time cost, for without inverter losses model, life time cost is calculated as 6.84 $ as a post-process, for with inverter losses model, cost is 4.67 $ which is reduced by 31%.

Figure 66 and Figure 67 show transformer temperature and loading changes with and without inverter losses included, respectively. By including the inverter circuits in the losses, the total demand load increases and as a result, the transformer loading also increases. On the other hand, if the losses are neglected, the transformer will be loaded more since the power drawn from the network is less due to the absence of losses. As a result, transformer temperatures remain at lower levels than when losses are

included. This difference can be clearly seen, especially from 18:00 when the HST reaches its upper level.

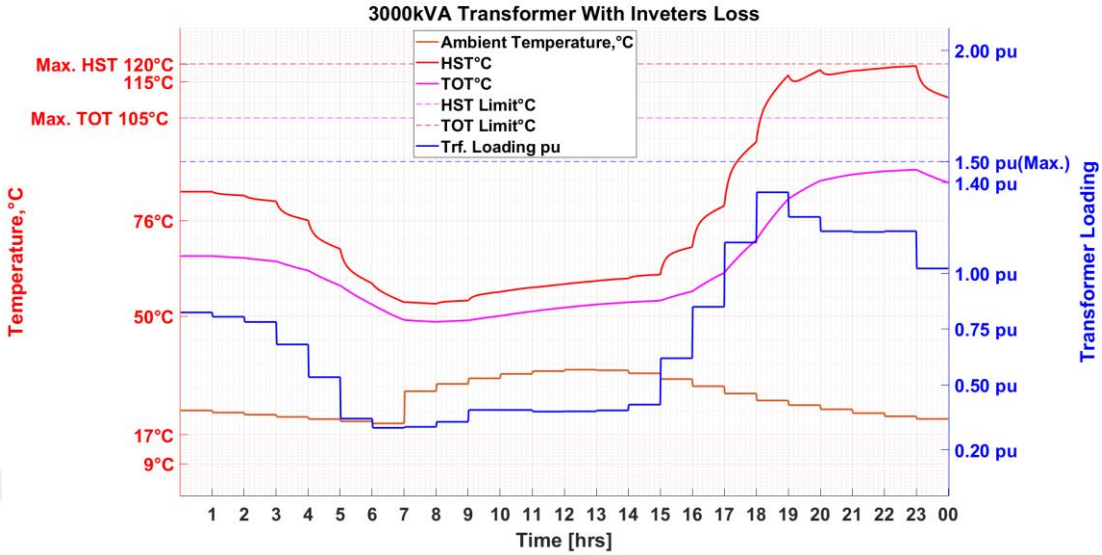

Figure 66. HST, TOT and Loading Variation for Case-1 With Inverter Loss

Although transformer constraints could be provided by adding inverter losses, the loading generally increased with the increase in total load. For this reason, HST and TOT generally remained at higher values.

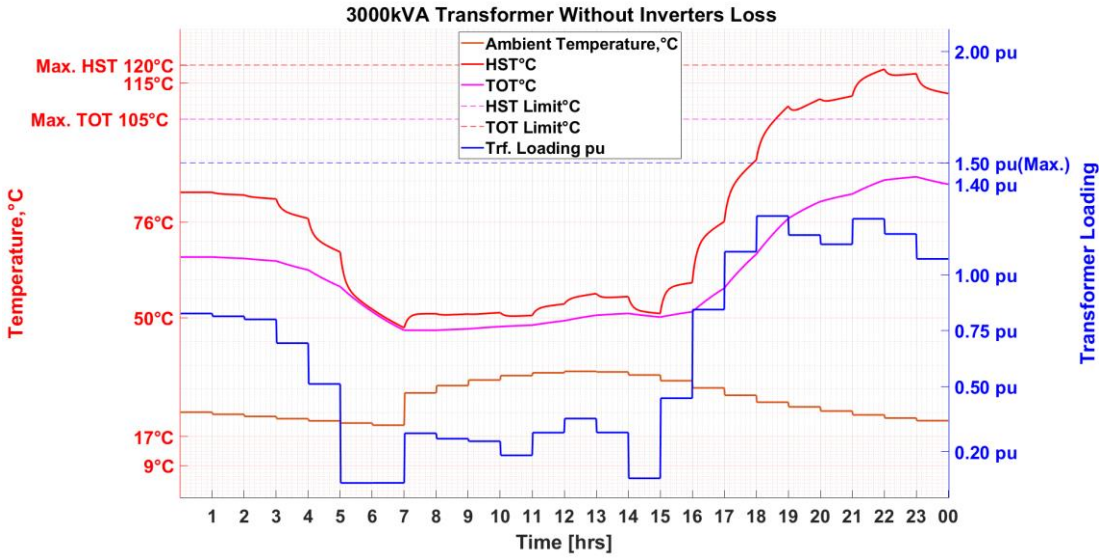

Figure 67. HST, TOT and Loading Variation for Case-1 Without Inverter Loss

Due t o the reactive power support of the inverter, it continuously creates active power loss, which causes the HST to be obtained smoother at each hour transition. The temperature of the transformer declined more slowly due to energy losses.

7.5. Demonstration of Different Powers Obtained Even Though The Inverter Gives The Same Current

The proposed calculation approach controls the current given or drawn by the inverter by modeling its currents as decision variables rather than its powers. The power then varies according to the voltage levels on the bus to which the equipment is connected.

When the same magnitude of current is applied to two buses with different voltages, the calculated powers in the buses will differ due to the voltage difference. As demonstrated in the Case-5 simulation, different powers are calculated at different times and in different buses where the same current magnitude is applied.

The Figure 68 shows the power and current profile of the BESS in Case-5 for one day. The values obtained from the graph are presented in Table 17, which indicates that the maximum current of the inverter is 155.2 A. This maximum current is applied to the bus at different times by the various inverters connected to it.

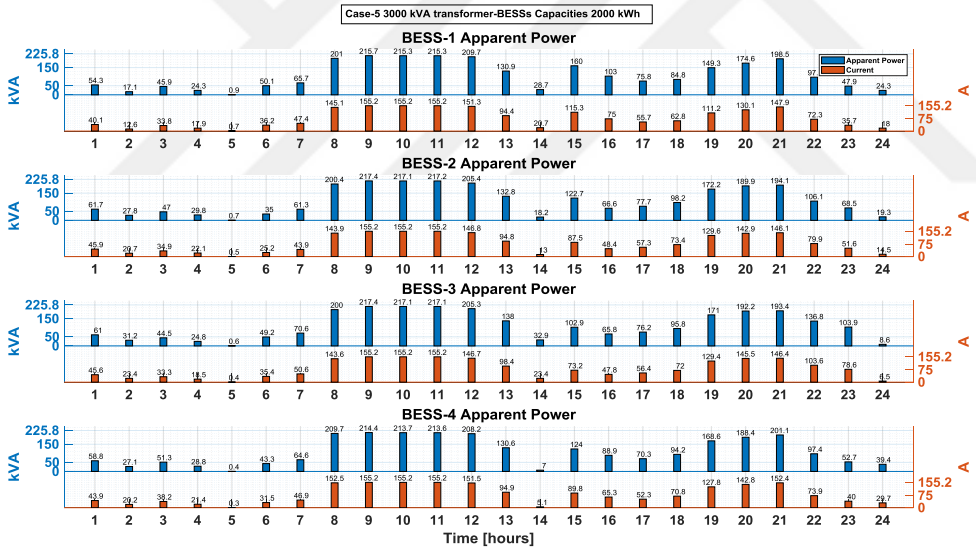

Figure 68. Daily BESS Power and Current Comparison for Case-5

The different voltages are due to factors such as the location of the buses, their distance from the grid, the connected load, and their closeness to the PV system. Consequently, even with the same current magnitude, different powers are obtained.

As can be seen in Table 17, as a result of changing the voltage values in the buses, the current constraint, which is the main restrictive criterion for inverters, and although the maximum current is used, their effects on the network have different powers. This

difference affects the voltages in other buses in the load flow calculation and also causes changes in line losses. For this reason, for a more precise and accurate calculation, it is a more accurate approach to use current instead of using the upper limit constraint power of inverters. For example, in the specifications given by the inverter manufacturer, maximum current is 155.2 A and maximum power is 215 kVA. However, although the current in BESS-4 at 11:00 is 155.2 A, it is calculated as 213.6 kVA because the voltage is less than 1.0 (p.u.). However, in the power-based calculation method, which is the general approach, optimization is made assuming that it can provide 215 kVA power. In the calculation method suggested in this thesis, it is stated that the inverter can provide 213.6 kVA power due to the current limit restriction, and a more accurate and realistic calculation is presented.

Table 17. Current Applied to The Buses and Calculated Powers

Hour	BESS Name	Current	Bus Voltage	Power
09:00	BESS-1	155.2 A	1.0029	215.7 kVA
	BESS-2	155.2 A	1.0111	217.4 kVA
	BESS-3	155.2 A	1.0111	217.4 kVA
	BESS-4	155.2 A	0.9968	214.4 kVA
10:00	BESS-1	155.2 A	1.0012	215.3 kVA
	BESS-2	155.2 A	1.0096	217.7 kVA
	BESS-3	155.2 A	1.0093	217.7 kVA
	BESS-4	155.2 A	0.9936	213.7 kVA
11:00	BESS-1	155.2 A	1.0011	215.3 kVA
	BESS-2	155.2 A	1.0098	217.2 kVA
	BESS-3	155.2 A	1.0095	217.1 kVA
	BESS-4	155.2 A	0.9931	213.6 kVA

8. CHAPTER: CONCLUSIONS

To meet the increasing energy demand, not only the use of low-cost energy resources, but also the correct and intelligent utilization of energy resources can help reduce energy costs. For this reason, energy costs can be minimized with a suitable and sensitive energy management system. However, when creating an effective energy management system, it is crucial to prevent ignored or overlooked energy costs from appearing as energy costs at the end of the day. This can be achieved by modeling the system close to the real physical system and including these costs in the calculation. To that purpose, a day-ahead energy management system model has been created with the basic features listed below.

- The EMS of the distribution system is constructed by formulating a load flow problem using an NLP optimization solver, which incorporates active and reactive power balance.
- The load is modeled using a voltage-dependent power model, which provides a more realistic representation compared to a constant power model.
- The distribution system equipment, including the load, BESS, inverters of the PV system, distribution transformer, and distribution lines, are all managed by a central management system.
- The PV and BESS systems are modeled using the current variable, a limitation of power semiconductor equipment, rather than the general power variable approach.
- When developing the power balance, both the active and reactive power balances are modeled.
- The reactive power capabilities of the inverters used in BESS and PV systems are also modeled, and the reactive power support provided by the BESS and PV inverters is utilized.
- The losses of BESS and PV integrated inverters are modeled as loads.

- The battery degradation and inverter lifetime costs are modeled and optimized.
- The use of a DTR model for the distribution transformer connected to the grid ensures that the transformer can be safely operated above its rated power value.

Chapter-2 explores modeling methods for equipment in the distribution system. Various load modeling types are investigated, and load flow calculation examples are analyzed based on load models. The example distribution system representation, which is the IEEE 33 bus, discusses different load modeling methods. The power calculation generated from the panel in the PV system is examined, and the effect of ambient temperature is shown. Furthermore, the calculation method of the energy balance in the BESS is discussed.

In Chapter-3, the active and reactive power operating limits of inverters integrated into BESS and PV systems are investigated. It is shown that PV inverters can operate in two-quadrants, while BESS inverters can operate in four-quadrants. This indicates that the inverter can provide reactive power support. Reactive power control methods of inverters are then discussed. The losses caused by the apparent power that the inverters can inject or absorb due to their reactive power support, as well as their own operating self-consumption, have been examined. Another cost is that the equipment, such as capacitors, used to produce the necessary reactive power has a limited lifespan due to the reactive support of inverters. As a result, it has been shown that the reactive power support of the inverter causes a decrease in equipment life. It is emphasized that inverter losses and lifespan should be taken into consideration in the optimization model for realistic and precise modeling.

In Chapter-4, the distribution transformer is a fundamental component of the distribution system, serving as the connection point to the grid. The transformer's power capacity is a limiting factor, in terms of both the power drawn from and supplied to the grid. However, within the recommended calculations and limits, distribution transformers can be operated above their rated power value. This section examines the loading limits of the transformer and the calculation method. A sample simulation demonstrates the effect of ambient temperature and loading on the transformer's HST and TOT. Thanks to dynamic thermal modeling, it is concluded that the transformer can be safely operated with overload, even for short periods, within the specified limits.

In Chapter-5, a modified test system is constructed by integrating four PV units, four BESS, and inverters into the IEEE 33 test system, which represents a sample distribution network. The required irradiance data for PV generation, technical specifications of the PV panels, BESS, and the featured limits of the employed inverters are provided. Additionally, the optimization problem utilizes data on hourly demand load changes and ambient temperatures. The key factor in minimizing energy costs, the primary objective of the optimization problem, is the energy purchase price from the grid and the sale price to the grid. The variations in the hourly energy purchasing and selling prices used in the model are presented. Furthermore, the purchased active energy is not the sole fee paid to the distribution network. If the limits are exceeded, a reactive power penalty may need to be paid. Consequently, a penalty function is created with the mathematical formula for the reactive power penalty cost that may occur if the limits are exceeded.

In Chapter-6, to enable more realistic and precise calculations, the created models must be combined and transformed into an optimization problem for the day-ahead EMS. The decision variables, limits, and objective function are then determined to solve this optimization problem. Unlike the existing literature, a different power and current calculation method is recommended, and the assumptions and methods for its solution are discussed in this section. The key assumption here is that the voltage angle in the buses is considered to be close to zero, which eliminates the need for trigonometric calculations. This results in a shorter calculation time. Since the mathematical equations, such as load flow, power calculations, and constraints, are non-linear, the optimization problem can be transformed into a non-linear programming (NLP) problem and solved using the fmincon solver available in MATLAB. This section describes the creation of the matrices and equation sets required for the NLP solution.

In Chapter-7, different case studies are conducted for the day-ahead energy management system, which is transformed into an optimization problem. The results show that the connection transformer to the grid must have a power rating of 5000 kVA due to a maximum demand power of approximately 4500 kVA in the basic case. However, by utilizing dynamic thermal modeling of the transformer and reducing transformer loading through BESS, it is demonstrated that lower power transformer installations can function effectively. Simulation results revealed that 5000 kVA, 4000 kVA, and 3000 kVA transformer power ratings could be viable. Further analysis

indicates that increasing BESS capacity can improve both energy costs and thermal limits. Another case study simulates a winter day, showing that low PV generation and ambient temperatures cause reduced transformer loading and temperatures well within limits. In an additional scenario, incorporating inverter losses into the model has demonstrated a 50 % decrease in active energy losses compared to the model that excluded inverter losses. Furthermore, the optimization model that accounted for inverter losses has been found to yield a 31% reduction in the inverter's lifetime reduction cost. Finally, it has been shown that even if the current drawn or given to a bus is of the same magnitude, different powers are obtained in cases where it has different voltages.

REFERENCES

Aghdam, F. H., Kalantari, N. T., & Mohammadi-Ivatloo, B. (2020). *A chance-constrained energy management in multi-microgrid systems considering degradation cost of energy storage elements*. Journal of Energy Storage; Elsevier. doi: 10.1016/j.est.2020.101416

Ahmed, H. M. A., Ahmed, M. H., & Salama, M. M. A. (2022). A Linearized Multiobjective Energy Management Framework for Reconfigurable Smart Distribution Systems Considering BESSs. *IEEE Systems Journal*, *16*(1), 1258–1269. doi: 10.1109/JSYST.2021.3062491

Akarne, Y., Essadki, A., Nasser, T., & Bhiri, B. El. (2024). Experimental Analysis of Efficient Dual-Layer Energy Management and Power Control in an AC Microgrid System. *IEEE Access*, *12*, 30577–30592. doi: 10.1109/ACCESS.2024.3370681

Alavi, S. A., Ahmadian, A., & Aliakbar-Golkar, M. (2015). Optimal probabilistic energy management in a typical micro-grid based-on robust optimization and point estimate method. *Energy Conversion and Management*, *95*, 314–325. doi: 10.1016/j.enconman.2015.02.042

Almeida, D., Pasupuleti, J., & Ekanayake, J. (2021). Comparison of reactive power control techniques for solar pv inverters to mitigate voltage rise in low-voltage grids. *Electronics (Switzerland)*, *10*(13), 1–16. doi: 10.3390/electronics10131569

Alramlawi, M. (2020). *Model-based optimization of PV-based microgrids considering grid blackout and battery lifetime*.

Alsaleh, I., & Fan, L. (2018). *Volt / Var Optimization with Minimum Equipment Operation under High PV Penetration*. *September*.

Appelbaum, J., & Maor, T. (2020). Dependence of pv module temperature on incident time-dependent solar spectrum. *Applied Sciences (Switzerland)*, *10*(3). doi: 10.3390/app10030914

Arguence, O., & Cadoux, F. (2020). Sizing power transformers in power systems planning using thermal rating. *International Journal of Electrical Power & Energy Systems*, *118*, 105781. doi: 10.1016/j.ijepes.2019.105781

Bagheri, A. (2024). Optimal transformer loss of life management in day-ahead scheduling of wind-rich power systems at the presence of dynamic ratings. *Electric Power Systems Research*, *231*(November 2023), 110259. doi: 10.1016/j.epsr.2024.110259

Bahloul, M., Daoud, M., & Khadem, S. K. (2024). Optimal dispatch of battery energy storage for multi-service provision in a collocated PV power plant considering battery ageing. *Energy*, *293*(January), 130744. doi: 10.1016/j.energy.2024.130744

Baran, M. E., & Wu, F. F. (1989). Network reconfiguration in distribution systems for loss reduction and load balancing. *IEEE Transactions on Power Delivery*, *4*(2), 1401–1407. doi: 10.1109/61.25627

Barchi, G., Pierro, M., & Moser, D. (2019). Predictive energy control strategy for peak switch and shifting using BESS and PV generation applied to the retail sector. *Electronics (Switzerland)*, *8*(5). doi: 10.3390/electronics8050526

Basir Khan, M. R., Jidin, R., & Pasupuleti, J. (2016). Multi-agent based distributed control architecture for microgrid energy management and optimization. *Energy Conversion and Management*, *112*, 288–307. doi: 10.1016/j.enconman.2016.01.011

Biçen, Y., & Aras, F. (2014). Loadability of power transformer under regional climate conditions: The case of Turkey. *Electrical Engineering*, *96*(4), 347–358. doi: 10.1007/s00202-014-0301-6

Boztepe, M. (2017). Fotovoltaik güç sistemlerinde verimliliği etkileyen parametreler. *Elektrik Mühendisleri Odası Dergisi*, 13–17.

Bracale, A., Carpinelli, G., Pagano, M., & De Falco, P. (2018). A probabilistic approach for forecasting the allowable current of oil-immersed transformers. *IEEE Transactions on Power Delivery*, *33*(4), 1825–1834. doi: 10.1109/TPWRD.2018.2791181

Braun, M. (2008). Provision of Ancillary Services by Distributed Generators [PhD, University of Kassel as]. In Transformation (Vol. 14). Retrieved from http://www.upress.uni-kassel.de/katalog/abstract.php?978-3-89958-339-7

Braun, M. (2009). *Provision of ancillary services by distributed generators: Technological and economic perspective* (Vol. 10). kassel university press GmbH.

Brito, E. M. da S., Cupertino, A. F., Pereira, H. A., & Mendes, V. F. (2022). Reliability-based trade-off analysis of reactive power capability in PV inverters under different sizing ratio. *International Journal of Electrical Power and Energy Systems*, *136*(May 2021). doi: 10.1016/j.ijepes.2021.107677

Chen, C., Wang, F., Zhou, B., Chan, K. W., Cao, Y., & Tan, Y. (2015). An interval optimization based day-ahead scheduling scheme for renewable energy management in smart distribution systems. *Energy Conversion and Management*, *106*, 584–596. doi: 10.1016/j.enconman.2015.10.014

Chenier, R., & Aubin, J. (2024). Economic benefit and risk evaluation of power transformer overloading. *2001 IEEE Power Engineering Society Winter Meeting. Conference Proceedings (Cat. No.01CH37194)*, *2*(2), 459–462. doi: 10.1109/PESW.2001.916887

Cortés-Caicedo, B., Molina-Martin, F., Grisales-Noreña, L. F., Montoya, O. D., & Hernández, J. C. (2022). Optimal Design of PV Systems in Electrical Distribution Networks by Minimizing the Annual Equivalent Operative Costs through the Discrete-Continuous Vortex Search Algorithm. *Sensors*, *22*(3). doi: 10.3390/s22030851

Daminov, I. (2022). *Dynamic Thermal Ratings of Power Transformers : Modelling, Concepts, and Application case* [Université polytechnique de Tomsk (Russie)]. Retrieved from https://theses.hal.science/tel-03772184

Daminov, I., Prokhorov, A., Caire, R., & Alvarez-Herault, M. C. (2019). Receding

horizon algorithm for dynamic transformer rating and its application for real-time economic dispatch. *2019 IEEE Milan PowerTech, PowerTech 2019*, 1–6. doi: 10.1109/PTC.2019.8810511

Daminov, I., Prokhorov, A., Caire, R., & Alvarez-Herault, M. C. (2021). Assessment of dynamic transformer rating, considering current and temperature limitations. *International Journal of Electrical Power and Energy Systems*, *129*(January). doi: 10.1016/j.ijepes.2021.106886

Daminov, I., Rigo-Mariani, R., Caire, R., Prokhorov, A., & Alvarez-Hérault, M.-C. (2021). Demand Response Coupled with Dynamic Thermal Rating for Increased Transformer Reserve and Lifetime. *Energies*, *14*(5), 1378. doi: 10.3390/en14051378

Dantas, N. K. L., Souza, A. C. M., Vasconcelos, A. S. M., Junior, W. de A. S., Rissi, G., Dall'orto, C., Maciel, A. M. A., Castro, J. F. C., Liu, Y., & Rosas, P. (2022). Impact Analysis of a Battery Energy Storage System Connected in Parallel to a Wind Farm. *Energies*, *15*(13), 1–16. doi: 10.3390/en15134586

Denver Office. (2000). Permissible Loading of Oil-Immersed Transformers and Regulators. *Facilities Instruction,Standards and Techniques*, *1*(APRIL 1991), 1–25. Retrieved from https://www.usbr.gov/power/data/fist/fist1_5/vol1-5.pdf

Diaz-Aguilo, M., Sandraz, J., Macwan, R., De Leon, F., Czarkowski, D., Comack, C., & Wang, D. (2013). Field-validated load model for the analysis of CVR in distribution secondary networks: Energy conservation. *IEEE Transactions on Power Delivery*, *28*(4), 2428–2436. doi: 10.1109/TPWRD.2013.2271095

Diaz, G., Gomez-Aleixandre, J., & Coto, J. (2016). Direct Backward/Forward Sweep Algorithm for Solving Load Power Flows in AC Droop-Regulated Microgrids. *IEEE Transactions on Smart Grid*, *7*(5), 2208–2217. doi: 10.1109/TSG.2015.2478278

Dolara, A., Leva, S., & Manzolini, G. (2015). Comparison of different physical models for PV power output prediction. *Solar Energy*, *119*, 83–99. doi: 10.1016/j.solener.2015.06.017

Durán, F., Pavón, W., & Minchala, L. I. (2024). Forecast-Based Energy Management for Optimal Energy Dispatch in a Microgrid. *Energies*, *17*(2), 1–21. doi: 10.3390/en17020486

El-Baz, W., Tzscheutschler, P., & Wagner, U. (2018). Day-ahead probabilistic PV generation forecast for buildings energy management systems. *Solar Energy*, *171*(June), 478–490. doi: 10.1016/j.solener.2018.06.100

Elsir, M., Al-Sumaiti, A. S., & El Moursi, M. S. (2024). Towards energy transition: A novel day-ahead operation scheduling strategy for demand response and hybrid energy storage systems in smart grid. *Energy*, *293*(February), 130623. doi: 10.1016/j.energy.2024.130623

Feng, L., Zhang, X., Li, C., Li, X., Li, B., Ding, J., Zhang, C., Qiu, H., Xu, Y., & Chen, H. (2022). Optimization analysis of energy storage application based on electricity price arbitrage and ancillary services. *Journal of Energy Storage*, *55*(PB), 105508. doi: 10.1016/j.est.2022.105508

Fresia, M., Bordo, L., Delfino, F., & Bracco, S. (2024). Optimal day-ahead active and reactive power management for microgrids with high penetration of renewables. *Energy Conversion and Management: X*, *23*(February), 100598. doi: 10.1016/j.ecmx.2024.100598

Gamil, A., Al-Abadi, A., Schatzl, F., & Schlucker, E. (2018). Theoretical and Empirical-Based Thermal Modelling of Power Transformers. *ICHVE 2018 - 2018 IEEE International Conference on High Voltage Engineering and Application*. doi: 10.1109/ICHVE.2018.8642180

Gandhi, O., Rodríguez-Gallegos, C. D., Gorla, N. B. Y., Bieri, M., Reindl, T., & Srinivasan, D. (2019a). Reactive Power Cost From PV Inverters Considering Inverter Lifetime Assessment. *IEEE Transactions on Sustainable Energy*, *10*(2), 738–747. doi: 10.1109/TSTE.2018.2846544

Gandhi, O., Rodríguez-Gallegos, C. D., Gorla, N. B. Y., Bieri, M., Reindl, T., & Srinivasan, D. (2019b). Reactive Power Cost From PV Inverters Considering Inverter Lifetime Assessment. *IEEE Transactions on Sustainable Energy*, *10*(2), 738–747. doi: 10.1109/TSTE.2018.2846544

Gandhi, O., Rodríguez-Gallegos, C. D., Zhang, W., Reindl, T., & Srinivasan, D. (2022). Levelised cost of PV integration for distribution networks. *Renewable and Sustainable Energy Reviews*, *169*(April), 112922. doi: 10.1016/j.rser.2022.112922

Gandhi, O., Rodríguez-Gallegos, C. D., Zhang, W., Srinivasan, D., & Reindl, T. (2018). Economic and technical analysis of reactive power provision from distributed energy resources in microgrids. *Applied Energy*, *210*(July), 827–841. doi: 10.1016/j.apenergy.2017.08.154

Gandhi, O., Rodríguez-Gallegos, C., Reindl, T., & Srinivasan, D. (2018). Competitiveness of PV inverter as a reactive power compensator considering inverter lifetime reduction. *Energy Procedia*, *150*, 74–82. doi: 10.1016/j.egypro.2018.09.005

Gandhi, O., Zhang, W., Rodriguez-Gallegos, C. D., Srinivasan, D., & Reindl, T. (2016). Continuous optimization of reactive power from PV and EV in distribution system. *IEEE PES Innovative Smart Grid Technologies Conference Europe*, 281–287. doi: 10.1109/ISGT-Asia.2016.7796399

Ghorashi Khalil Abadi, S. A., & Bidram, A. (2021). A distributed rule-based power management strategy in a photovoltaic/hybrid energy storage based on an active compensation filtering technique. *IET Renewable Power Generation*, *15*(15), 3688–3703. doi: 10.1049/rpg2.12263

Gouda, O. E., Amer, G. M., & Salem, W. A. A. (2012). Predicting transformer temperature rise and loss of life in the presence of harmonic load currents. *Ain Shams Engineering Journal*, *3*(2), 113–121. doi: 10.1016/j.asej.2012.01.003

Grab, R., Hans, F., Flores, M. I. R., Schmidt, H., Rogalla, S., & Engel, B. (2022). Modeling of Photovoltaic Inverter Losses for Reactive Power Provision. *IEEE Access*, *10*(September), 108506–108516. doi: 10.1109/ACCESS.2022.3213272

Hartel, F., & Bocklisch, T. (2023). Minimizing Energy Cost in PV Battery Storage Systems using Reinforcement Learning. *IEEE Access*, *11*(March), 39855–39865.

doi: 10.1109/ACCESS.2023.3267978

Hashmi, M. U., Deka, D., Busic, A., Pereira, L., & Backhaus, S. (2020). Arbitrage with Power Factor Correction Using Energy Storage. *IEEE Transactions on Power Systems*, *35*(4), 2693–2703. doi: 10.1109/TPWRS.2020.2969978

Hashmi, M. U., Deka, D., Busic, A., & Van Hertem, D. (2023). Can Locational Disparity of Prosumer Energy Optimization Due to Inverter Rules Be Limited? *IEEE Transactions on Power Systems*, *38*(6), 5726–5739. doi: 10.1109/TPWRS.2022.3223842

Hohne, P. A., Kusakana, K., & Numbi, B. P. (2020). Model validation and economic dispatch of a dual axis pv tracking system connected to energy storage with grid connection: A case of a healthcare institution in South Africa. *Journal of Energy Storage*, *32*, 101986. doi: 10.1016/j.est.2020.101986

Hu, Y., Armada, M., & Jesús Sánchez, M. (2022). Potential utilization of battery energy storage systems (BESS) in the major European electricity markets. *Applied Energy*, *322*(June). doi: 10.1016/j.apenergy.2022.119512

Huaman-Rivera, A., Calloquispe-Huallpa, R., Luna Hernandez, A. C. L., & Irizarry-Rivera, A. (2024). An Overview of Electric Vehicle Load Modeling Strategies for Grid Integration Studies. *Electronics*, *13*(12), 2259. doi: 10.3390/electronics13122259

Technical Data - SUN2000-(196KTL-H0, 200KTL-H2, 215KTL-H0) User Manual - Huawei, (2022). Accessed 1 June 2022 from https://support.huawei.com/enterprise/en/doc/EDOC1100141536/6696534f/technical-data

IEC 60076-7. (2005). "Loading guide for oil-immersed power transformers." *IEC 60076-7*, *4*, 13.

IEEE. (2012). IEEE Guide for Loading Mineral-Oil-Immersed Transformers and Step-Voltage Regulators - Redline. In IEEE Std C57.91™-2011(Revision of C57.91-1995) (Vol. 2011, Issue March).

IEEE. (2018). Ieee Std 1547-2018. In IEEE Standard for Interconnection and Interoperability of Distributed Energy Resources with Associated Electric Power Systems Interfaces.

Javid, Z., Kocar, I., Holderbaum, W., & Karaagac, U. (2024). Future Distribution Networks: A Review. *Energies*, *17*(8), 1–45. doi: 10.3390/en17081822

JRC. 2012. "JRC Photovoltaic Geographical Information System(PVGIS) – European Commission." Accessed 1 June 2022.https://re.jrc.ec.europa.eu/pvg_tools/en/

Kanchev, H., Colas, F., Lazarov, V., & Francois, B. (2014). Emission reduction and economical optimization of an urban microgrid operation including dispatched PV-based active generators. *IEEE Transactions on Sustainable Energy*, *5*(4), 1397–1405. doi: 10.1109/TSTE.2014.2331712

Kang, W., Chen, M., Guan, Y., Wei, B., Vasquez Q., J. C., & Guerrero, J. M. (2022). Event-triggered distributed voltage regulation by heterogeneous BESS in low-voltage distribution networks. *Applied Energy*, *312*(December 2021). doi: 10.1016/j.apenergy.2022.118597

Katiraei, F., & Agüero, J. R. (2011). Solar PV integration challenges. *IEEE Power and Energy Magazine*, *9*(3), 62–71. doi: 10.1109/MPE.2011.940579

Kirthiga, M. V., Daniel, S. A., & Gurunathan, S. (2013). A methodology for transforming an existing distribution network into a sustainable autonomous micro-grid. *IEEE Transactions on Sustainable Energy*, *4*(1), 31–41. doi: 10.1109/TSTE.2012.2196771

Kiss, V. M., Hetesi, Z., & Kiss, T. (2024). The effect of time resolution on energy system simulation in case of intermittent energies. *Renewable and Sustainable Energy Reviews*, *191*(November 2023), 114099. doi: 10.1016/j.rser.2023.114099

Kuss, M., Markel, T., & Kramer, W. (2010). Application of distribution transformer thermal life models to electrified vehicle charging loads using monte-carlo method. *EVS 2010 - Sustainable Mobility Revolution: 25th World Battery, Hybrid and Fuel Cell Electric Vehicle Symposium and Exhibition*, *January*.

Li, S., Li, X., Kang, Y., & Gao, Q. (2022). Load capability assessment and enhancement for transformers with integration of large-scale renewable energy: A brief review. *Frontiers in Energy Research*, *10*(September), 1–6. doi: 10.3389/fenrg.2022.1002973

Li, X., Ma, R., Gan, W., & Yan, S. (2022). Optimal Dispatch for Battery Energy Storage Station in Distribution Network Considering Voltage Distribution Improvement and Peak Load Shifting. *Journal of Modern Power Systems and Clean Energy*, *10*(1), 131–139. doi: 10.35833/MPCE.2020.000183

Li, X., Member, S., Hui, D., & Lai, X. (2013). Battery Energy Storage Station (BESS) -Based Smoothing Control of Photovoltaic (PV) and Wind Power Generation Fluctuations. *IEEE Transactions on Sustainable Energy*, *4*(2), 464–473. doi: 10.1109/TSTE.2013.2247428

Li, Z., Hilber, P., Laneryd, T., Diaz, G. P. N., & Ivanell, S. (2024). Impact of turbine availability and wake effect on the application of dynamic thermal rating of wind farm export transformers. *Energy Reports*, *11*(January), 1399–1411. doi: 10.1016/j.egyr.2023.12.042

Lim, J. Y., Ji, P. S., Lee, J. P., Kim, K. D., Kim, J. H., & Singh, C. (2000). Load modeling for power system analysis software. *Proceedings of the American Power Conference*, *62*, 393–398.

Liu, L., Hu, X., Chen, C., Wu, R., Wu, T., & Huang, H. (2024). Research on day-ahead and intraday scheduling strategy of distribution network based on dynamic partitioning. *International Journal of Electrical Power and Energy Systems*, *160*(March), 110078. doi: 10.1016/j.ijepes.2024.110078

Lu, X., Zhou, K., & Yang, S. (2017). Multi-objective optimal dispatch of microgrid containing electric vehicles. *Journal of Cleaner Production*, *165*, 1572–1581. doi: 10.1016/j.jclepro.2017.07.221

Malekpour, A. R., & Pahwa, A. (2017). A Dynamic Operational Scheme for Residential PV Smart Inverters. *IEEE Transactions on Smart Grid*, *8*(5), 2258–2267. doi: 10.1109/TSG.2016.2521367

Manikanta, G., Mani, A., Singh, H. P., & Chaturvedi, D. K. (2024). Enhancement of

performance indices on realistic load models with distributed generators in radial distribution network. In Energy Systems (Vol. 15, Issue 2). Springer Berlin Heidelberg. doi: 10.1007/s12667-022-00517-4

Maraaba, L., Almuhaini, M., Habli, M., & Khalid, M. (2023). Neural Networks Based Dynamic Load Modeling for Power System Reliability Assessment. *Sustainability (Switzerland) , 15*(6). doi: 10.3390/su15065403

Martins, H. P. (2019). Digital Asset Management: Overload of Power Transformers [UNIVERSIDADE DO PORTO]. In Transformer Technology. Retrieved from https://transformer-technology.com/tt-issues/1687-tt-issue-8.html

Nair, S. P., & Sundari, M. S. S. (2024). Optimizing day-ahead energy management with demand response in a PV-diesel-battery system using a hybrid GOA-SNN strategy. *Journal of Energy Storage*, *76*(April 2023), 109717. doi: 10.1016/j.est.2023.109717

Nguyen Hong, N., & Nguyen Duc, H. (2024). Virtual Power Plant's Optimal Scheduling Strategy in Day-Ahead and Balancing Markets Considering Reserve Provision Model of Energy Storage System. *Applied Sciences (Switzerland)*, *14*(5). doi: 10.3390/app14052175

Notingher, P. V., Stancu, C., Dragan, I., & Bey, M. I. (2021). Calculation of the Temperatures and Lifetimes for Distribution Transformers. *Revue Roumaine Des Sciences Techniques Serie Electrotechnique et Energetique*, *66*(4), 275–284.

Notton, G., Nivet, M. L., Voyant, C., Paoli, C., Darras, C., Motte, F., & Fouilloy, A. (2018). Intermittent and stochastic character of renewable energy sources: Consequences, cost of intermittence and benefit of forecasting. *Renewable and Sustainable Energy Reviews*, *87*(December 2016), 96–105. doi: 10.1016/j.rser.2018.02.007

Osorio, L., Moreno, M., Rivera, M., Tuninetti, V., Chavarria, G. R., Duchêne, L., & Wheeler, P. (2024). A metaheuristic-based method for photovoltaic temperature computation under tropical conditions. *Solar Energy*, *271*(February), 112414. doi: 10.1016/j.solener.2024.112414

Pacific Northwest National Laboratory, & PNNL. (2010). Evaluation of CVR on a National Level. In Report (Issue July). Retrieved from http://www.pnl.gov/main/publications/external/technical_reports/PNNL-19596.pdf

Polat, S., Biyik, E., & Sekerci Oztura, H. (2023). Sensitivity and Cost Analysis of a Microgrid With a Day-Ahead Energy Management System. *Turkish Journal of Electrical Power and Energy Systems*, *3*(1), 47–60. doi: 10.5152/tepes.2023.23001

Prakash, K., & Sydulu, M. (2011). Topological and primitive impedance based load flow method for radial and weakly meshed distribution systems. *Iranian Journal of Electrical and Computer Engineering*, *10*(1), 10–18.

Rafique, S. F., & Jianhua, Z. (2018). Energy management system, generation and demand predictors: A review. *IET Generation, Transmission and Distribution*, *12*(3), 519–530. doi: 10.1049/iet-gtd.2017.0354

Ragab, M. M., Ibrahim, R. A., Desouki, H., & Swief, R. (2023). Optimal energy management applying load elasticity integrating renewable resources. *Scientific Reports*, *13*(1), 1–19. doi: 10.1038/s41598-023-41929-1

Raghavan, A., Maan, P., & Shenoy, A. K. B. (2020). Optimization of day-ahead energy storage system scheduling in microgrid using genetic algorithm and particle swarm optimization. *IEEE Access*, *8*, 173068–173078. doi: 10.1109/ACCESS.2020.3025673

Rezaeimozafar, M., Barrett, E., Monaghan, R. F. D., & Duffy, M. (2024). A stochastic method for behind-the-meter PV-battery energy storage systems sizing with degradation minimization by limiting battery cycling. *Journal of Energy Storage*, *86*(PA), 111199. doi: 10.1016/j.est.2024.111199

Rigo-Mariani, R., & Vai, V. (2022). An iterative linear DistFLow for dynamic optimization in distributed generation planning studies. *International Journal of Electrical Power and Energy Systems*, *138*(February 2021). doi: 10.1016/j.ijepes.2021.107936

Saboori, H., Hemmati, R., & Jirdehi, M. A. (2015). Reliability improvement in radial electrical distribution network by optimal planning of energy storage systems. *Energy*, *93*, 2299–2312. doi: 10.1016/j.energy.2015.10.125

Saleem, M. I., Saha, S., Izhar, U., & Ang, L. (2024). Optimized energy management of a solar battery microgrid: An economic approach towards voltage stability. *Journal of Energy Storage*, *90*(PB), 111876. doi: 10.1016/j.est.2024.111876

Satsangi, S., & Kumbhar, G. B. (2017). Effect of load models on energy loss reduction using volt-VAr optimization. *2016 National Power Systems Conference, NPSC 2016*. doi: 10.1109/NPSC.2016.7858922

Şeker, A. A., Gözel, T., & Hocaoğlu, M. H. (2021). BIBC matrix modification for network topology changes: Reconfiguration problem implementation. *Energies*, *14*(10). doi: 10.3390/en14102738

Sen, P. K., Pansuwan, S., Malmedal, K., Martinoo, O., & Simoes, M. G. (2011). Transformer Overloading and Assessment of Loss-of-Life for Liquid-Filled Transformerss. *Power Systems Engineering Research Center*, 121.

Silva, V. A., Aoki, A. R., & Lambert-Torres, G. (2020). Optimal day-ahead scheduling of microgrids with battery energy storage system. *Energies*, *13*(19), 1–28. doi: 10.3390/en13195188

Singh, S., Kumar, A., Singh, S. K., & Jarial, R. K. (2015). *Dielectric Response Analysis and Diagnosis of Oil-Filled Power Transformers*. 1–4.

Soares, J., Fotouhi Ghazvini, M. A., Vale, Z., & de Moura Oliveira, P. B. (2016). A multi-objective model for the day-ahead energy resource scheduling of a smart grid with high penetration of sensitive loads. *Applied Energy*, *162*, 1074–1088. doi: 10.1016/j.apenergy.2015.10.181

Soares, J., Morais, H., Sousa, T., Vale, Z., & Faria, P. (2013). Day-ahead resource scheduling including demand response for electric vehicles. *IEEE Transactions on Smart Grid*, *4*(1), 596–605. doi: 10.1109/TSG.2012.2235865

Soleimani, A., Vahidinasab, V., & Aghaei, J. (2022). A Linear Stochastic Formulation

for Distribution Energy Management Systems Considering Lifetime Extension of Battery Storage Devices. *IEEE Access*, *10*, 44564–44576. doi: 10.1109/ACCESS.2022.3169480

Srinivasa Rao, R., Narasimham, S. V. L., Ramalinga Raju, M., & Srinivasa Rao, A. (2011). Optimal network reconfiguration of large-scale distribution system using harmony search algorithm. *IEEE Transactions on Power Systems*, *26*(3), 1080–1088. doi: 10.1109/TPWRS.2010.2076839

Stanelytė, D., & Radziukynas, V. (2022). Analysis of Voltage and Reactive Power Algorithms in Low Voltage Networks. *Energies*, *15*(5). doi: 10.3390/en15051843

Surender Reddy, S., & Bijwe, P. R. (2016). Day-Ahead and Real Time Optimal Power Flow considering Renewable Energy Resources. *International Journal of Electrical Power and Energy Systems*, *82*, 400–408. doi: 10.1016/j.ijepes.2016.03.033

Taha, H. A., Alham, M. H., & Youssef, H. K. M. (2022). Multi-Objective Optimization for Optimal Allocation and Coordination of Wind and Solar DGs, BESSs and Capacitors in Presence of Demand Response. *IEEE Access*, *10*, 16225–16241. doi: 10.1109/ACCESS.2022.3149135

Taha, M. S., Abdeltawab, H. H., & Mohamed, Y. A. R. I. (2018). An online energy management system for a grid-connected hybrid energy source. *IEEE Journal of Emerging and Selected Topics in Power Electronics*, *6*(4), 2015–2030. doi: 10.1109/JESTPE.2018.2828803

Taheri, S., Gholami, A., Fofana, I., & Taheri, H. (2012). Modeling and simulation of transformer loading capability and hot spot temperature under harmonic conditions. *Electric Power Systems Research*, *86*, 68–75. doi: 10.1016/j.epsr.2011.12.005

Talluri, G., Lozito, G. M., Grasso, F., Iturrino Garcia, C., & Luchetta, A. (2021). Optimal Battery Energy Storage System Scheduling within Renewable Energy Communities. *Energies*, *14*(24), 8480. doi: 10.3390/en14248480

Tan, M., Li, Z., Su, Y., Ren, Y., Wang, L., & Wang, R. (2024). Dual time-scale robust optimization for energy management of distributed energy community considering source-load uncertainty. *Renewable Energy*, *226*(January), 120435. doi: 10.1016/j.renene.2024.120435

Tewari, T., Mohapatra, A., & Anand, S. (2021). Coordinated control of OLTC and energy storage for voltage regulation in distribution network with high PV penetration. *IEEE Transactions on Sustainable Energy*, *12*(1), 262–272. doi: 10.1109/TSTE.2020.2991017

Tziovani, L., Hadjidemetriou, L., Kolios, P., Astolfi, A., Kyriakides, E., & Timotheou, S. (2022). Energy Management and Control of Photovoltaic and Storage Systems in Active Distribution Grids. *IEEE Transactions on Power Systems*, *37*(3), 1956–1968. doi: 10.1109/TPWRS.2021.3118785

Sunpower SPR-435NE-WHT-D (435W) Solar Panel- User Manual, (2020). Accessed 1 June 2022 http://www.solardesigntool.com/components/module-panel-solar/Sunpower/3169/SPR-435NE-WHT-D/specification-data-sheet.html

Vardhan, B. V. S., Khedkar, M., & Srivastava, I. (2022). Effective energy management and cost effective day ahead scheduling for distribution system with dynamic market participants. *Sustainable Energy, Grids and Networks*, *31*, 100706. doi: 10.1016/j.segan.2022.100706

Vasquez, W. A., & Quilumba, F. L. (2016). Load flow method for radial distribution systems with distributed generation using a dynamic data matrix. *2016 IEEE Ecuador Technical Chapters Meeting, ETCM 2016*, 16–20. doi: 10.1109/ETCM.2016.7750862

Venkatasamy, B., & Kalaivani, L. (2021). Modeling and Power Quality Analysis of Grid-Connected PV Inverter with Active and Reactive Power Injection Mode. *Journal of Electrical Engineering and Technology*, *16*(3), 1375–1387. doi: 10.1007/s42835-021-00693-w

Vita, V. (2017). Development of a Decision-Making Algorithm for the Optimum Size and Placement of Distributed Generation Units in Distribution Networks. *Energies*, *10*(9), 1433. doi: 10.3390/en10091433

Wagle, R., Sharma, P., Sharma, C., & Amin, M. (2024). Optimal power flow based coordinated reactive and active power control to mitigate voltage violations in smart inverter enriched distribution network. *International Journal of Green Energy*, *21*(2), 359–375. doi: 10.1080/15435075.2023.2196324

Wang, C., Wu, J., Wang, J., & Zhao, W. (2016). Reliability analysis and overload capability assessment of oil-immersed power transformers. *Energies*, *9*(1). doi: 10.3390/en9010043

Wang, J., & Azam, W. (2024). Natural resource scarcity, fossil fuel energy consumption, and total greenhouse gas emissions in top emitting countries. *Geoscience Frontiers*, *15*(2), 101757. doi: 10.1016/j.gsf.2023.101757

Wang, Q., Xiao, Y., Tan, H., & Mohamed, M. A. (2024). Day-Ahead scheduling of rural integrated energy systems based on distributionally robust optimization theory. *Applied Thermal Engineering*, *246*(March), 123001. doi: 10.1016/j.applthermaleng.2024.123001

Wang, Z., Chen, B., Wang, J., Begovic, M. M., & Chen, C. (2015). Coordinated Energy Management of Networked Microgrids in Distribution Systems. *IEEE Transactions on Smart Grid*, *6*(1), 45–53. doi: 10.1109/TSG.2014.2329846

Xavier, L. S., Amorim, W. C. S., Cupertino, A. F., Mendes, V. F., do Boaventura, W. C., & Pereira, H. A. (2019). Power converters for battery energy storage systems connected to medium voltage systems: a comprehensive review. *BMC Energy*, *1*(1), 1–15. doi: 10.1186/s42500-019-0006-5

Xiong, L., Zhu, Y., Huang, S., Guo, S., Ban, C., Li, P., Khan, M. W., & Niu, T. (2024). Multi-objective distributed control of WT-PV-BESS integrated weak grid via finite time containment. *International Journal of Electrical Power and Energy Systems*, *156*(PA), 109709. doi: 10.1016/j.ijepes.2023.109709

Xu, B., Zhang, F., Bai, R., Sun, H., & Ding, S. (2023). The energy management strategy of a loop microgrid with wind energy prediction and energy storage system day-ahead optimization. *Frontiers in Energy Research*, *11*(January), 1–11. doi: 10.3389/fenrg.2023.1334588

Yigit, E., & Ucak, C. (2017). Investigation of IEC thermal models of power transformers. *2017 10th International Conference on Electrical and Electronics Engineering, ELECO 2017*, *2018-Janua*, 100–104.

Zaigham Mahmood. (2012). SMART CITIES Development and Governance Frameworks. In Springer (Vol. 44, Issue December, pp. 17–39). Retrieved from https://bibliotecadigital.fgv.br/dspace/handle/10438/18386%0Ahttp://www.smartcities.es/smart-cities/

Zenhom, Z. M., Aleem, S. H. E. A., Zobaa, A. F., & Boghdady, T. A. (2024). A Comprehensive Review of Renewables and Electric Vehicles Hosting Capacity in Active Distribution Networks. *IEEE Access*, *12*(December 2023), 3672–3699. doi: 10.1109/ACCESS.2023.3349235

Zhang, E., Liu, J., Song, B., Zhang, H., Fan, X., Zhang, Y., & Fu, Q. (2023). Influence of Operational Defects and Hotspot Temperature on Methanol Concentration in Transformer Oil. *IEEE Transactions on Power Delivery*, *38*(3), 1859–1867. doi: 10.1109/TPWRD.2022.3228770

Zhang, J., Wu, Y., Guo, Y., Wang, B., Wang, H., & Liu, H. (2016). A hybrid harmony search algorithm with differential evolution for day-ahead scheduling problem of a microgrid with consideration of power flow constraints. *Applied Energy*, *183*, 791–804. doi: 10.1016/j.apenergy.2016.09.035

Zhao, C., Andersen, P. B., Træholt, C., & Hashemi, S. (2023). Grid-connected battery energy storage system: a review on application and integration. *Renewable and Sustainable Energy Reviews*, *182*(May), 113400. doi: 10.1016/j.rser.2023.113400

Zubair Iftikhar, M., Imran, K., Imran Akbar, M., & Ghafoor, S. (2024). Optimal distributed generators allocation with various load models under load growth using a meta-heuristic technique. *Renewable Energy Focus* , *49*(February), 100550. doi: 10.1016/j.ref.2024.100550

APPENDIX

Table A. Electrical parameters of IEEE 33 test system

Line No	Node i	Node j	$R_{ij}(\Omega)$	$X_{ij}(\Omega)$	P_j(kW)	Q_j(kVAr)
1	1	2	0.0922	0.0470	100	60
2	2	3	0.4930	0.2511	90	40
3	3	4	0.3660	0.1864	120	80
4	4	5	0.3811	0.1941	60	30
5	5	6	0.8190	0.7070	60	20
6	6	7	0.1872	0.6188	200	100
7	7	8	0.7114	0.2351	200	100
8	8	9	1.0300	0.7400	60	20
9	9	10	1.0440	0.7400	60	20
10	10	11	0.1966	0.0650	45	30
11	11	12	0.3744	0.1238	60	35
12	12	13	1.4680	1.1550	60	35
13	13	14	0.5416	0.7129	120	80
14	14	15	0.5910	0.5260	60	10
15	15	16	0.7463	0.5450	60	20
16	16	17	1.2890	1.7210	60	20
17	17	18	0.7320	0.5740	90	40
18	2	19	0.1640	0.1565	90	40
19	19	20	1.5042	1.3554	90	40
20	20	21	0.4095	0.4784	90	40
21	21	22	0.7089	0.9373	90	40
22	3	23	0.4512	0.3083	90	50
23	23	24	0.8980	0.7091	420	200
24	24	25	0.8960	0.7011	420	200
25	6	26	0.2030	0.1034	60	25
26	26	27	0.2842	0.1447	60	25
27	27	28	1.0590	0.9337	60	20
28	28	29	0.8042	0.7006	120	70
29	29	30	0.5075	0.2585	200	60
30	30	31	0.9744	0.9630	150	70
31	31	32	0.3105	0.3619	210	100
32	32	33	0.3410	0.5302	60	40